Generation of frequency entanglement with an effective quantum dot-waveguide two-photon quadratic interaction

Mohamed Meguebel, Maxime Federico, Simone Felicetti, Nadia Belabas, Nicolas Fabre

Generation of frequency entanglement with an effective quantum dot-waveguide two-photon quadratic interaction

Mohamed Meguebel,[1] Maxime Federico,[1] Simone Felicetti,[2,3] Nadia Belabas,[4] and Nicolas Fabre[1]

[1] *Telecom Paris, Institut Polytechnique de Paris, 19 Place Marguerite Perey, 91120 Palaiseau, France*
[2] *Institute for Complex Systems, National Research Council (ISC-CNR), Via dei Taurini 19, 00185 Rome, Italy*
[3] *Physics Department, Sapienza University, P.le A. Moro 2, 00185 Rome, Italy*
[4] *Centre for Nanosciences and Nanotechnology, CNRS, Universite Paris-Saclay, UMR 9001, 10 Boulevard Thomas Gobert, 91120, Palaiseau, France*

(Dated: May 25, 2025)

Light–matter interactions with quantum dots have been extensively studied to harness key quantum properties of photons, such as indistinguishability and entanglement. In this theoretical work, we exploit the atomic-like four-level structure of a quantum dot coupled to a waveguide to model a shaping frequency entangling gate (ShaFrEnGa) for single photons. Our approach is based on the identification of input frequencies and an atomic level structure for which frequency-dependent one-photon transitions are adiabatically eliminated, while frequency-dependent two-photon transitions are resonantly enhanced. The frequency entanglement performance of the gate are analyzed using a Schmidt decomposition for continuous variables, revealing a trade-off between entanglement generation efficiency and entanglement quality. We further demonstrate the use of the ShaFrEnGa for the generation of entangled frequency qudit states.

I. INTRODUCTION

Photonic quantum technologies [1, 2] rising from the second quantum revolution [3–5], include a range of application from quantum communication [6, 7] to quantum metrology [8, 9] and computation [10–12]. Quantum information can be encoded into discrete [13, 14] or continuous variables [15, 16], and some encodings pursue an intermediate hybrid approach [17]. Examples of discrete variables for photonic quantum system are polarization [18] or the rail [10, 19] encoding for qubit-based photonic quantum information. For a d-dimensional computational basis defining qudit-based photonic quantum information, frequency-comb [20–22] or orbital angular momentum of light [23–25] encodings can be listed out. When it comes to continuous variables, although the most common form of encoding relies on the electric field quadratures [26, 27], other proposals have been investigated. For instance, continuous variables correspond to transverse spatial degrees of freedom of photons [28] or time-frequency continuous variables [29, 30]. The latter aims at harnessing continuous degrees of freedom of *time-of-arrival* and *frequency* in the single-photon subspace unlike field quadrature-based quantum information which relies on the number of photons statistical distribution in a given mode [27]. The time-frequency continuous variables formalism defines auxiliary modes which are any possible single-photon degrees of freedom that are not the time-frequency variables and do not couple with them. These auxiliary modes act as photon carriers and do not encode any quantum information. Provided that no two photons occupy the same complete set of auxiliary modes – they may share individual modes, but not the entire configuration – the canonical commutation relation (CCR) of the *time-of-arrival* $\hat{\tau}$ and *frequency* $\hat{\omega}$ operators is the same [29] as that of *position* $\hat{x}$ and *momentum* $\hat{p}$ for the position-momentum field quadratures. This entails a Heisenberg algebra for both and the same mathematical descriptions therein – from the phase-space description to the universal set of gates [29, 31]. Notwithstanding these mathematical similarities, it should be emphasized that in these two cases the information is encoded in different physical degrees of freedom. While the quadratures revolve around the photon-number statistical distribution in a given mode, the time-frequency continuous variables encode quantum information continuously in the single-photon subspace. As such, non-Gaussian operations are difficult to implement in the former case [32], particularly for higher-order processes and multimode gates. These implementations typically employ offline measurements [33] or non-linear interactions [34]. In contrast, time-frequency continuous degrees of freedom benefit from the versatility of waveshapers, that allow performing any single photon gate [29, 35]. Nevertheless, while entangling modes within the field quadrature formalism is well-established [36–38], generating time-frequency entanglement — or entanglement in any other degree of freedom — between single photons remains notoriously challenging [39]. A prevalent approach in linear optical quantum computing involves a probabilistic scheme that relies on post-selection, utilizing linear optical elements and measurements of ancillary photons. [11, 40, 41].

In contrast, *measurement-free* – *i.e.* without post-selection – time-frequency entanglement naturally arises in the photon pairs generated via spontaneous parametric down-conversion (SPDC) and spontaneous four-wave mixing (SFWM). However, these processes have significant drawbacks. (i) SPDC and SFWM do not directly entangle preexisting photons but rather produce entangled pairs. (ii) The photon pair generation

rate is inefficient and putting SPDC in cascade is not scalable for generating larger entangled state. (iii) These non-linear processes also generate multiphoton states and are thus imperfect sources of true frequency-correlated photon pairs. To circumvent these pitfalls, other schemes should and have been investigated.
Namely, Le Jeannic *et al.* proposed in [42] an experimental implementation employing a quantum dot (QD) embedded in a photonic crystal waveguide which scatters [43] time-correlated photon pairs. Nonetheless, the light-matter interaction considered in [42] is dictated by a linear Hamiltonian in bosonic creation and annihilation operators, which can limit the gate fidelity of controlled-phase gate [44]. In [45], Alushi *et al.* investigated the frequency photon-pair correlations originating from a general quadratic Hamiltonian in the bosonic creation and annihilation operators. Using scattering theory calculations, the authors demonstrated how this quadratic Hamiltonian allowed to overcome the aforementioned no-go theorem [44]. Although possible physical implementations were suggested, the derivations of the quadratic Hamiltonian were based on a generic toy model, without considering the specific system's requirements. The present work aims at filling this gap.

We design a photonic scheme where a QD is embedded in a single-mode, linear, and nonmagnetic waveguide for which, under certain conditions that permit an adiabatic elimination, the light-matter interaction in the weak coupling regime can be shown to yield an *ab initio* quadratic Hamiltonian identical to the *ad hoc* Hamiltonian considered by Alushi *et al.* [45]. The proposed photonic system can be employed to entangle single photons in their continuously distributed frequencies. The light-matter interaction model is founded upon an adiabatic elimination procedure [46–51]. Adiabatic elimination is typically carried out within either an isolated (closed system) framework or an open system framework. In the isolated system approach [46, 47], states that are far off-resonance – *i.e.*, those with large frequency detunings compared to the states of interest – are effectively discarded from the dynamics. In contrast, the open system derivation [49–51] considers a system coupled to an external bath whose degrees of freedom are adiabatically eliminated, leading to an effective evolution for the system that incorporates dissipation and decoherence. Our approach employs frequency-dependent *joint* transition operators, where atomic transitions are coupled to the continuously defined bosonic creation and annihilation operators of the field. This formalism encapsulates the interplay between the atomic and photonic degrees of freedom in a frequency-resolved manner. Within this framework, frequency-dependent *joint* one-photon transition operators are adiabatically eliminated in favor of frequency-dependent *joint* two-photon transition operators described in the Heisenberg picture. Moreover, the present model notably addresses the requirement of having at most one photon per auxiliary mode configuration–here being the polarization, as mentioned in [29]. Similarly to Le Jeannic *et al.* [42] and Alushi *et al.* [45], the frequency-correlated photon pairs are effectively produced without post-selection [2, 52], i.e. *measurement-free*. By applying a Schmidt decomposition to analyze the frequency continuous entanglement, we further highlight a trade-off between the efficiency of entanglement generation and the quality of the entanglement. Furthermore, we demonstrate that the shaping frequency entangling gate (ShaFrEnGa) can be used for the generation of frequency qudit states [22, 53–60].

The article is organized as follows. In Sec. II, we cover the light-matter interaction system and the calculation of the effective two-photon quadratic Hamiltonian based on the *joint* one-photon operator adiabatic elimination. Then, in Sec. III, we make use of the methods from Alushi *et al.* [45] to show how photon-photon frequency entanglement can be generated without auxiliary photons and measurement-free, effectively outputting a two-photon Gaussian distribution along the sum and difference of frequencies. The entanglement generation and efficiency are scrutinized in Sec. IV before applying our method to frequency qudit states.

II. QUANTUM DOT-WAVEGUIDE EFFECTIVE QUADRATIC TWO-PHOTON INTERACTION MODEL

A. Physical system

1. Waveguide

The physical system that we consider to implement the photonic frequency entangling gate is a QD embedded in a single-mode, linear and nonmagnetic waveguide. The waveguide electric field quantization follows that of [61] and is detailed in Appendix A. We extend the analysis by taking into account the polarization degree of freedom along with the waveguide's time-reversal symmetry, yielding the following expression for the electric field operator

$$\hat{\boldsymbol{E}}(\boldsymbol{r}) = \sum_{\sigma} \sum_{\mu\in\{\pm\}} \int_{\mathbb{R}} d\omega \, (\boldsymbol{\mathcal{E}}_{\sigma\mu}(\boldsymbol{\rho}, \beta(\omega)) e^{i\beta(\omega)\mu z} \hat{a}_{\sigma\mu}(\omega) + \text{h.c}), \tag{1}$$

where σ, μ, $\boldsymbol{\rho}$, $\beta(\omega)$, $\boldsymbol{\mathcal{E}}_{\sigma\mu}(\boldsymbol{r}, \beta) = \boldsymbol{\mathcal{E}}_{\sigma\mu}(\boldsymbol{\rho}, \beta(\omega)) e^{i\beta(\omega)z}$ correspond, respectively, to the polarization, the direction of propagation–either rightward $\mu = +$ or leftward $\mu = -$ along the z-axis aligned with the QD's growth axis -, the transverse coordinate, the wavevector – depending on the frequency ω through the dispersion relation – and the propagating modes, solutions to the wave equation

$$\boldsymbol{\nabla} \times \boldsymbol{\nabla} \times \boldsymbol{\mathcal{E}}_{\sigma\mu}(\boldsymbol{r}, \beta) - \frac{\omega(\beta)^2}{c^2} \epsilon(\boldsymbol{r}, \mu\beta) \boldsymbol{\mathcal{E}}_{\sigma\mu}(\boldsymbol{r}, \beta) = \boldsymbol{0}, \tag{2}$$

where $\epsilon(\boldsymbol{r}, \mu\beta)$ is the permittivity of the material. The operators $\hat{a}_{\sigma\mu}(\omega)$ are bosonic operators fulfilling the standard commutation relation

$$[\hat{a}_{\sigma\mu}(\omega), \hat{a}^\dagger_{\sigma'\mu'}(\omega')] = \delta(\omega - \omega')\delta_{\sigma\sigma'}\delta_{\mu\mu'}. \tag{3}$$

Then, the free Hamiltonian for the waveguide quantized field reads

$$\hat{H}_{\text{free,WG}} = \sum_{\sigma} \sum_{\mu\in\{\pm\}} \int_{\mathbb{R}} d\omega\, \hbar\omega \hat{a}^\dagger_{\sigma\mu}(\omega)\hat{a}_{\sigma\mu}(\omega), \tag{4}$$

discarding the zero-point energy.

2. *Quantum dot*

The QD is modeled as a four-level system with a ground state, two excitonic states and one biexcitonic state (see Fig. 1 (a)). This four-level atomic-like structure can be represented in two different bases – the linear and circular bases – with different optical selection rules [62–64]. In the first basis, identically linearly polarized photons can drive the QD from its ground state to its biexcitonic state. In the circular basis the optical selection rules require the involved photons to be circularly polarized and orthogonal, see Fig. 1 (a). The QD's free Hamiltonian can be expressed in the circular basis as

$$\begin{aligned}\hat{H}_{\text{free, QD}} &= \hbar\omega_{2X} |2X\rangle \langle 2X| \\ &+ \hbar\omega_X \left(|X_+\rangle \langle X_+| + |X_-\rangle \langle X_-|\right) \\ &+ \hbar S \left(|X_+\rangle \langle X_-| + |X_-\rangle \langle X_+|\right),\end{aligned} \tag{5}$$

with S the so-called fine-structure splitting (FSS) due to the QD's asymmetry [62, 65, 66]. The FSS scale typically ranges from 0 to 100 GHz in III–V semiconductor QDs [65, 67] and several strategies to suppress it have been investigated [67–70]. In the linear basis, the FSS lifts the degeneracy of the excitonic levels while it induces a coupling between the two excitonic states in the circular basis [64]. Unless mentioned otherwise, we work in the QD's circular basis throughout.

B. Effective two-photon quadratic Hamiltonian

1. *Jaynes-Cummings Hamiltonian*

The light-matter interaction is described within the Goeppert-Mayer gauge and the dipole approximation in such a way that the interaction Hamiltonian is

$$\begin{aligned}\hat{H}_{\text{int}} = &-\hat{\boldsymbol{d}}_{0X_+} \cdot \hat{\boldsymbol{E}}(\boldsymbol{0}) - \hat{\boldsymbol{d}}_{0X_-} \cdot \hat{\boldsymbol{E}}(\boldsymbol{0}) \\ &- \hat{\boldsymbol{d}}_{X_+2X} \cdot \hat{\boldsymbol{E}}(\boldsymbol{0}) - \hat{\boldsymbol{d}}_{X_-2X} \cdot \hat{\boldsymbol{E}}(\boldsymbol{0}),\end{aligned} \tag{6}$$

in the QD's and field's circular basis with $\hat{\boldsymbol{d}}_{..}$ the dipole moment operators of the different transitions and with the QD's position set at the reference origin of the waveguide $\boldsymbol{r} = \boldsymbol{0}$, without loss of generality. For instance, $\hat{\boldsymbol{d}}_{0X_+} = \boldsymbol{d}_{0X_+} |X_+\rangle \langle 0| + \text{h.c}$ where $|0\rangle$ is the QD's ground state. The first term $-\hat{\boldsymbol{d}}_{0X_+} \cdot \hat{\boldsymbol{E}}(\boldsymbol{0})$ can be expressed as

$$\begin{aligned}&- \hat{\boldsymbol{d}}_{0X_+} \cdot \hat{\boldsymbol{E}}(\boldsymbol{0}) = - \sum_{\sigma\in\{R,L\}} \sum_{\mu\in\{\pm\}} \int_{\mathbb{R}} d\omega \\ &\Big(\boldsymbol{d}_{0X_+} \cdot \boldsymbol{\mathcal{E}}_{\sigma\mu}(\boldsymbol{0}, \beta(\omega)) |X_+\rangle \langle 0| \otimes \hat{a}_{\sigma\mu}(\omega) \\ &+ \boldsymbol{d}_{0X_+} \cdot \boldsymbol{\mathcal{E}}^*_{\sigma\mu}(\boldsymbol{0}, \beta(\omega)) |X_+\rangle \langle 0| \otimes \hat{a}^\dagger_{\sigma\mu}(\omega) + \text{h.c}\Big),\end{aligned} \tag{7}$$

in the field circular basis $\sigma = R, L$ where R and L stand for right-handed and left-handed circular polarizations, respectively. One can define the frequency-dependent coupling terms

$$g^{\sigma\mu}_{0X_+}(\omega) \equiv -\frac{\boldsymbol{d}_{0X_+} \cdot \boldsymbol{\mathcal{E}}_{\sigma\mu}(\boldsymbol{0}, \beta(\omega))}{\hbar} \tag{8}$$

$$f^{\sigma\mu}_{0X_+}(\omega) \equiv -\frac{\boldsymbol{d}_{0X_+} \cdot \boldsymbol{\mathcal{E}}^*_{\sigma\mu}(\boldsymbol{0}, \beta(\omega))}{\hbar}. \tag{9}$$

Up to first order in these coupling terms and in S – which acts as the coupling term in the circular basis – the operators $|X_+\rangle \langle 0| \otimes \hat{a}_{\sigma\mu}(\omega)$ and $|X_+\rangle \langle 0| \otimes \hat{a}^\dagger_{\sigma\mu}(\omega)$ evolve in the Heisenberg picture with frequencies $\omega + \omega_X$ and $|\omega - \omega_X|$, respectively. Assuming the weak coupling regime, where all the coupling terms in Eq. (7) are small compared to $\omega + \omega_X$, one can apply the standard rotating-wave approximation (RWA) and discard the non-resonant terms associated with the coupling term $f^{\sigma\mu}_{0X_+}(\omega)$. Therefore, the first term of the interaction Hamiltonian is:

$$\begin{aligned}&- \hat{\boldsymbol{d}}_{0X_+} \cdot \hat{\boldsymbol{E}}(\boldsymbol{0}) = \sum_{\sigma\in\{R,L\}} \sum_{\mu\in\{\pm\}} \int_{\mathbb{R}} d\omega \\ &\times \left(\hbar g^{\sigma\mu}_{0X_+}(\omega) |X_+\rangle \langle 0| \otimes \hat{a}_{\sigma\mu}(\omega) + \text{h.c}\right).\end{aligned} \tag{10}$$

Following the same procedure for $\hat{\boldsymbol{d}}_{0X_-} \cdot \hat{\boldsymbol{E}}(\boldsymbol{0})$, $\hat{\boldsymbol{d}}_{X_+2X} \cdot \hat{\boldsymbol{E}}(\boldsymbol{0})$ and $\hat{\boldsymbol{d}}_{X_-2X} \cdot \hat{\boldsymbol{E}}(\boldsymbol{0})$, the interaction Hamiltonian reads

$$\begin{aligned}\hat{H}_{\text{int}} = \hbar \sum_{\sigma\in\{R,L\}} \sum_{\mu\in\{\pm\}} \int_{\mathbb{R}} d\omega \Big(&g^{\sigma\mu}_{0X_+}(\omega) |X_+\rangle \langle 0| \otimes \hat{a}_{\sigma\mu}(\omega) \\ &+ g^{\sigma\mu}_{X_+2X}(\omega) |2X\rangle \langle X_+| \otimes \hat{a}_{\sigma\mu}(\omega) \\ &+ g^{\sigma\mu}_{0X_-}(\omega) |X_-\rangle \langle 0| \otimes \hat{a}_{\sigma\mu}(\omega) \\ &+ g^{\sigma\mu}_{X_-2X}(\omega) |2X\rangle \langle X_-| \otimes \hat{a}_{\sigma\mu}(\omega) + \text{h.c}\Big),\end{aligned} \tag{11}$$

which is a sum of four one-photon Hamiltonians. In order to retrieve a quadratic Hamiltonian analogous to that of Alushi *et al.* [45], we would like to have two-photon Hamiltonians instead. With this aim, we resort to an adiabatic elimination to obtain an effective two-level system characterized by frequency-dependent two-photon transitions.

2. Adiabatic elimination

Inspired by the stimulated-Raman adiabatic passage (STIRAP) [71, 72], we perform an adiabatic elimination [46–51, 73–76] to suppress rapidly evolving one-photon processes in favor of two-photon ones. To this end, we invoke the transition operators time-evolution Heisenberg equation as it was done in [74–77]. Nonetheless, unlike [74–77], we manipulate *joint* light-matter operators. In our case, they encompass both matter and light while [75–77] considered bare matter operators only. Puri *et al.* [74] did evoke the physical differences that rise from considering the evolution of the joint transition operators, namely for spontaneous photon-number-dependent Stark shifts. Nevertheless, their work applies to a single-mode cavity and not to a continuum for which the bookkeeping of each frequency-dependent joint one-photon transition operator is paramount. This *joint* operator terminology is not to be confused with *dressed* states from quantum optics' atom-field *dressed* states or polaritons [73] which refers to coherent superpositions of light-matter states. The joint one-photon transition operators are written as $|j\rangle\langle i|\otimes\hat{a}_{\sigma\mu}(\omega)$ depicting a transition from state $|i\rangle$ to $|j\rangle$ by absorbing a photon. For instance, the $\hat{\xi}^{\sigma\mu}_{0X_+}(\omega)\equiv|X_+\rangle\langle 0|\otimes\hat{a}_{\sigma\mu}(\omega)$ joint operator corresponds to the $|0\rangle\rightarrow|X_+\rangle$ QD excitonic transition by annihilation of a field excitation at frequency ω, polarization σ and with a direction of propagation μ. The corresponding Heisenberg picture time-evolution of this joint one-photon transition operator is given by

$$\frac{d\hat{\xi}^{\sigma\mu}_{0X_+}(\omega,t)}{dt}=\frac{[\hat{\xi}^{\sigma\mu}_{0X_+}(\omega,t),\hat{H}]}{i\hbar}. \tag{12}$$

It should be noted that, here, the time t is the dynamical time of the Hamiltonian evolution and not the *time-of-arrival* defined in the time-frequency continuous variables formalism [29, 78]. Up to second order in the FSS parameter S and in the coupling terms $g^{\cdot\cdot}_{\cdot\cdot}(.)$, the effective interaction Hamiltonian can be expressed as

$$\hat{H}_{\text{int}}=\left(\hat{H}_{\text{int}}\right)_{|0\rangle\leftrightarrow|X_+\rangle\leftrightarrow|2X\rangle}+\left(\hat{H}_{\text{int}}\right)_{|0\rangle\leftrightarrow|X_-\rangle\leftrightarrow|2X\rangle}, \tag{13}$$

where we have separated the two interaction branches which read

$$\left(\hat{H}_{\text{int}}\right)_{|0\rangle\leftrightarrow|X_\pm\rangle\leftrightarrow|2X\rangle}=\hbar\sum_{\substack{\sigma'\in\{R,L\}\\ \mu'\in\{\pm\}}}\sum_{\substack{\sigma\in\{R,L\}\\ \mu\in\{\pm\}}}\int_{\mathbb{R}^2}d\omega' d\omega$$
$$\left(g^{\sigma'\mu'\sigma\mu}_{X_\pm}(\omega',\omega)\,|2X\rangle\langle 0|\otimes\hat{a}_{\sigma'\mu'}(\omega')\hat{a}_{\sigma\mu}(\omega)+\text{h.c}\right), \tag{14}$$

and where we have dropped the photon-number-dependent Stark shifts energy renormalization for readability. The calculated two-photon coupling terms are

$$g^{\sigma'\mu'\sigma\mu}_{X_\pm}(\omega',\omega)=g^{\sigma'\mu'}_{X_\pm 2X}(\omega')g^{\sigma\mu}_{0X_\pm}(\omega)\times\left[\frac{1}{\omega-\omega_X}-\frac{1}{\omega'-(\omega_{2X}-\omega_X)}\right], \tag{15}$$

where the one-photon detunings $\delta_e(\omega)\equiv\omega-\omega_X$ and $\delta_b(\omega')\equiv\omega'-(\omega_{2X}-\omega_X)$ arises. The detailed calculations are included in Appendix B. It should be pointed out that the FSS contribution has been eliminated by neglecting coupling terms of third or higher-order in the interaction Hamiltonian. Although a second-order term involving S does emerge from the time-evolution of the joint one-photon transition operator, it is suppressed within the adiabatic elimination. This adiabatic elimination regime is valid as long as: (i) $\delta_e(\omega)$ and $\delta_b(\omega')$ are large in absolute value compared to the $|0\rangle\leftrightarrow|2X\rangle$ two-photon detuning $|\omega+\omega'-\omega_{2X}|$, and to the photons' bandwidths. This condition ensures that the two-photon joint transition operators undergo a considerably slower evolution than the one-photon joint transition operators. (ii) The interaction time t is such that $1/t$ is much smaller than the one-photon detunings and much larger than the photons' bandwidths and two-photon detunings. This guarantees that the one-photon joint transition operators have averaged to zero, whereas the two-photon joint transition operators have undergone minimal evolution and can thus be regarded as constant. The effective interaction Hamiltonian Eq. (13) describes the QD adiabatic passage from its ground to its biexcitonic state by annihilation of two photons at frequencies ω and ω', polarizations σ and σ' and with directions of propagation μ and μ', and reciprocally for the relaxation from the biexcitonic to the ground state. As expected, employing the STIRAP-like method took us from four one-photon interaction Hamiltonians to two two-photon interaction Hamiltonians. Whether one interaction regime or the other occurs depends on the interaction timescale relative to the system spectral characteristics. Therefore, one can use this time criterion to selectively filter the photons that are effectively going to be frequency-entangled with this adiabatic elimination process. This one-photon operators adiabatic elimination is outlined in Fig. 1. The two-photon coupling terms Eq. (15) are non-separable in the two-photon frequencies ω and ω'. As it is discussed in Sec. III, this is paramount for the ShaFrEnGa. One way to fathom this is to think of the two-photon interaction with the QD as a spectral reshaping. Since the two-photon coupling term is non-separable in the two photon frequencies, the reshaping is also non-separable, as is the resulting emitted two-photon distribution. In addition to their non-separability, the coupling terms are also in general non-symmetric, that is to say $g^{\sigma'\mu'\sigma\mu}_{X_\pm}(\omega',\omega)\neq g^{\sigma\mu\sigma'\mu'}_{X_\pm}(\omega',\omega)$. This will become clearer in the next section, which addresses the optical selection rules. At this stage, one can intuitively understand this ordering by observing that the indices are arranged such that the leftmost ones correspond to the biexcitonic photon, while the rightmost ones pertain to

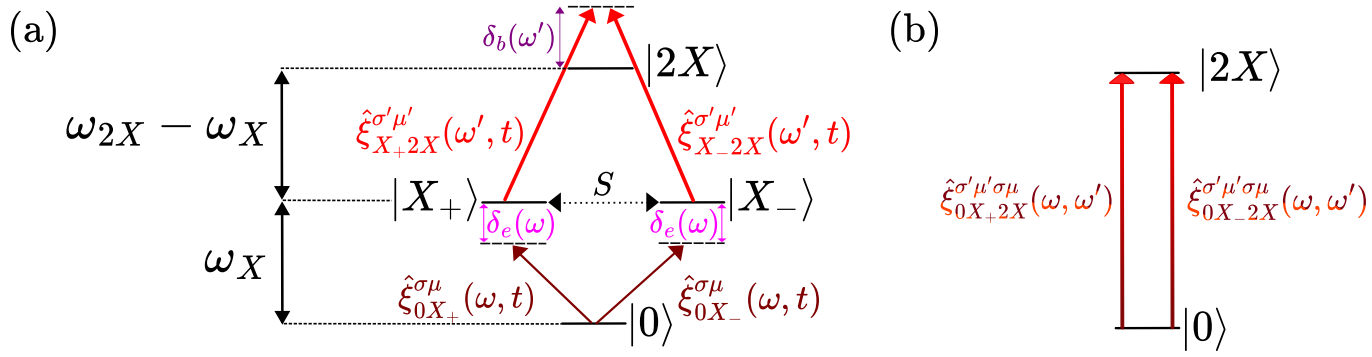

FIG. 1. (a) QD's four-level structure in the circular polarization basis. The energy structure is displayed *before* the one-photon joint operators $\hat{\xi}^{\sigma\mu}_{0X_\pm}(\omega, t) = (|X_\pm\rangle\langle 0| \otimes \hat{a}_{\sigma\mu}(\omega))(t)$ and $\hat{\xi}^{\sigma'\mu'}_{X_\pm 2X}(\omega', t) = (|2X\rangle\langle X_\pm| \otimes \hat{a}_{\sigma\mu}(\omega))(t)$ adiabatic eliminations. The one-photon transition detunings are $\delta_e(\omega) \equiv \omega - \omega_X$ and $\delta_b(\omega') \equiv \omega' - (\omega_{2X} - \omega_X)$. The excitonic transitions $|0\rangle \leftrightarrow |X_\pm\rangle$ can be driven by a right-handed and left-handed circularly polarized photon, respectively. The biexcitonic transitions $|X_\pm\rangle \leftrightarrow |2X\rangle$ can be triggered by a left-handed and right-handed circularly polarized photon, respectively. The fine-structure splitting (FSS) S couples the two excitonic states $|X_\pm\rangle$ together. (b) Effective two-level QD's energy structure *after* the adiabatic elimination. This adiabatic elimination switches from four one-photon joint transitions operators (a) to two two-photon joint transitions operators $\hat{\xi}^{\sigma'\mu'\sigma\mu}_{0X_\pm 2X}(\omega', \omega)$ (b) driving the transition $|0\rangle \to |2X\rangle$ either through $|X_+\rangle$ or $|X_-\rangle$. This effectively results in a two-level atomic system. The two-photon joint transition operators $\hat{\xi}^{\sigma'\mu'\sigma\mu}_{0X_\pm 2X}(\omega', \omega)$ in (b) are time-independent during the interaction time verifying the adiabatic elimination conditions. Note that the additional $X_\pm$ indices in these joint two-photon transition operators were introduced to indicate the origin of $\hat{\xi}^{\sigma'\mu'\sigma\mu}_{0X_\pm 2X}(\omega', \omega)$. They both read $\hat{\xi}^{\sigma'\mu'\sigma\mu}_{0X_\pm 2X}(\omega', \omega) = |2X\rangle\langle 0| \otimes \hat{a}_{\sigma'\mu'}(\omega')\hat{a}_{\sigma\mu}(\omega)$ regardless of the transition path.

the excitonic photon. This follows from the proportionality relation $g^{\sigma'\mu'\sigma\mu}_{\pm}(\omega', \omega) \propto g^{\sigma'\mu'}_{X_\pm 2X}(\omega') g^{\sigma\mu}_{0X_\pm}(\omega)$. Indeed, if the single-photon coupling terms were different, the two-photon coupling terms associated with the two excitation pathways $|0\rangle \leftrightarrow |X_\pm\rangle \leftrightarrow |2X\rangle$ would necessarily differ as well. The retrieved Hamiltonian Eq. (13) constructed from Eq. (14) is exactly of the same form as the one suggested by Alushi *et al.* [45] to perform the frequency-entanglement

$$\hat{H}_{\text{int,Alushi}} = \hbar \sum_{\mu', \mu \in \{\pm\}} \int_{\mathbb{R}^2} d\omega' d\omega \left(g^{\mu'\mu}(\omega', \omega) \hat{\sigma}_+ \otimes \hat{a}_{\mu'}(\omega') \hat{a}_\mu(\omega) + \text{h.c} \right), \tag{16}$$

where $\hat{\sigma}_+$ is a general raising operator associated to the two-level system under consideration and where the polarization has not been taken into account. Unlike Eq. (16), the Hamiltonian Eq. (13) that we derived has been constructed based on a specific photonic system, ensuring a concrete physical foundation thus laying the groundwork for experimental implementations. More specifically, the coupling terms Eq. (15) have an explicit form hence providing greater insights as to how to engineer the light-matter system. Besides, one may notice that we have yet to specify the optical selection rules. The derivations detailed in Appendix B are thus sufficiently general to be applied to photonic systems analogous to the one investigated here with other auxiliary modes and not only the polarization and direction of propagation.

3. *Optical selection rules*

In this section, we restrict the effective interaction Hamiltonian Eq. (13) to fulfill the QD's optical selection rules [62, 65]. Fixing the quantization axis along the photons propagation axis z, σ-polarized photons propagating in the $\mu = -$ direction are seen as $\sigma^\perp$-polarized by the QD. Hence, R-polarized photons can drive the $|0\rangle \leftrightarrow |X_+\rangle$ and $|X_-\rangle \leftrightarrow |2X\rangle$ transitions if they propagate with $\mu = +$ and the $|0\rangle \leftrightarrow |X_-\rangle$ and $|X_+\rangle \leftrightarrow |2X\rangle$ if they travel with $\mu = -$. The reasoning is identical for L-polarized photons. The two interaction paths Eq. (14) thus read

$$\begin{aligned} \left(\hat{H}_{\text{int}}\right)_{|0\rangle \leftrightarrow |X_+\rangle \leftrightarrow |2X\rangle} = \hbar \int_{\mathbb{R}^2} d\omega' d\omega \, |2X\rangle\langle 0| \otimes \\ \Big(g^{L+R+}_{X_+}(\omega', \omega) \hat{a}_{L+}(\omega') \hat{a}_{R+}(\omega) \\ + g^{R-L-}_{X_+}(\omega', \omega) \hat{a}_{R-}(\omega') \hat{a}_{L-}(\omega) \\ + g^{R-R+}_{X_+}(\omega', \omega) \hat{a}_{R-}(\omega') \hat{a}_{R+}(\omega) \\ + g^{L+L-}_{X_+}(\omega', \omega) \hat{a}_{L+}(\omega') \hat{a}_{L-}(\omega) + \text{h.c} \Big) \end{aligned} \tag{17}$$

and

$$\begin{aligned}\left(\hat{H}_{\text{int}}\right)_{|0\rangle\leftrightarrow|X_-\rangle\leftrightarrow|2X\rangle} &= \hbar\int_{\mathbb{R}^2} d\omega' d\omega\, |2X\rangle\langle 0|\otimes \\ &\Big(g_{X_-}^{R+L+}(\omega',\omega)\hat{a}_{R+}(\omega')\hat{a}_{L+}(\omega) \\ &+ g_{X_-}^{L-R-}(\omega',\omega)\hat{a}_{L-}(\omega')\hat{a}_{R-}(\omega) \\ &+ g_{X_-}^{L-L+}(\omega',\omega)\hat{a}_{L-}(\omega')\hat{a}_{L+}(\omega) \\ &+ g_{X_-}^{R+R-}(\omega',\omega)\hat{a}_{R+}(\omega')\hat{a}_{R-}(\omega) + \text{h.c}\Big).\end{aligned} \tag{18}$$

By grouping the two interaction branches Hamiltonian Eq. (17) and Eq. (18) together and by rearranging the ω and ω' dumb indices, one obtains

$$\begin{aligned}\hat{H}_{\text{int}} = \hbar\int_{\mathbb{R}^2} d\omega' d\omega\, |2X\rangle\langle 0|\otimes\Big(&g^{++}(\omega',\omega)\hat{a}_{L+}(\omega')\hat{a}_{R+}(\omega) \\ &+ g^{--}(\omega',\omega)\hat{a}_{R-}(\omega')\hat{a}_{L-}(\omega) + g^{-+}(\omega',\omega)\hat{a}_{R-}(\omega')\hat{a}_{R+}(\omega) \\ &g^{+-}(\omega',\omega)\hat{a}_{L+}(\omega')\hat{a}_{L-}(\omega) + \text{h.c}\Big),\end{aligned} \tag{19}$$

where we have defined the two-photon coupling terms comprising both interaction paths for each pair of propagation directions (μ,μ') as

$$\begin{aligned} g^{++}(\omega',\omega) &= g_{X_+}^{L+R+}(\omega',\omega) + g_{X_-}^{R+L+}(\omega',\omega) \\ g^{--}(\omega',\omega) &= g_{X_+}^{R-L-}(\omega',\omega) + g_{X_-}^{L-R-}(\omega',\omega) \\ g^{-+}(\omega',\omega) &= g_{X_+}^{R-R+}(\omega',\omega) + g_{X_-}^{R+R-}(\omega',\omega) \\ g^{+-}(\omega',\omega) &= g_{X_+}^{L+L-}(\omega',\omega) + g_{X_-}^{L-L+}(\omega',\omega).\end{aligned} \tag{20}$$

We recall that the indices are ordered such that the leftmost ones correspond to the biexciton photon, while the rightmost ones relate to the excitonic photon. For instance, the coupling terms $g_{X_+}^{L+R+}(\omega',\omega)$ depicts a transition where the biexcitonic photon is L-polarized and propagating rightward at frequency ω' and the excitonic photon is R-polarized and propagating rightward at frequency ω. The Eq. (17) and Eq. (18) each contribute eight terms to the total Hamiltonian, whereas the rearranged Hamiltonian in Eq. (19) contains only four. This can be understood by the fact that photons do not carry any information regarding what transitions – excitonic or biexcitonic – they have driven. Their degrees of freedom are solely the frequency, polarization and direction of propagation, as seen in the commutation relation Eq. (3). Whether the transition is $|0\rangle \leftrightarrow |X_\pm\rangle$ or $|X_\pm\rangle \leftrightarrow |2X\rangle$ is imposed by the QD's optical selection rules and is conveyed through the coupling terms. In other words, there is meaning in referring to *excitonic* and *biexcitonic* photons only from the QD's perspective. Therefore, the Hamiltonian in Eq. (19) erased the information regarding the $|0\rangle \leftrightarrow |2X\rangle$ interaction path – $|0\rangle \leftrightarrow |X_+\rangle \leftrightarrow |2X\rangle$ or $|0\rangle \leftrightarrow |X_-\rangle \leftrightarrow |2X\rangle$ and only retains the degrees of freedom relevant from the photons' perspective, namely the frequency, the polarization and the direction of propagation; thus merging the two interaction paths into one.

4. *Two-photon coupling terms*

In this section, we focus on the two-photon coupling terms given in Eq. (20). As explained, the two-photon Hamiltonians Eq. (17) and Eq. (18) for the two interaction paths can be combined into one global Hamiltonian Eq. (19) where the details of the transition branch have been removed. Let us assume that

$$\begin{aligned} g_{X_+2X}^{L+}(\omega')g_{0X_+}^{R+}(\omega) &= g_{X_-2X}^{R+}(\omega)g_{0X_-}^{L+}(\omega') \\ g_{X_+2X}^{R-}(\omega')g_{0X_+}^{L-}(\omega) &= g_{X_-2X}^{L-}(\omega)g_{0X_-}^{R-}(\omega') \\ g_{X_+2X}^{R-}(\omega')g_{0X_+}^{R+}(\omega) &= g_{X_-2X}^{R+}(\omega)g_{0X_-}^{R-}(\omega') \\ g_{X_+2X}^{L+}(\omega')g_{0X_+}^{L-}(\omega) &= g_{X_-2X}^{L-}(\omega)g_{0X_-}^{L+}(\omega'),\end{aligned} \tag{21}$$

meaning that the interaction paths have the same strength. The magnitudes of the electric dipole moments are independent of the excitonic state $|X_\pm\rangle$ [62, 65]: $||\boldsymbol{d}_{0X_+}|| = ||\boldsymbol{d}_{0X_-}||$ and $||\boldsymbol{d}_{X_+2X}|| = ||\boldsymbol{d}_{X_-2X}||$. Therefore, given the expression of the one-photon coupling term Eq. (8), this approximation is legitimate provided that the norm of the propagation mode $\boldsymbol{\mathcal{E}}_{\sigma\mu}(\mathbf{0},\beta(\omega))$ – solution to the wave equation Eq. (2) – does not depend on neither the polarization nor the direction of propagation; this is valid provided there is propagation isotropy. Consequently, the product of the two one-photon coupling terms in Eq. (21) are all considered equal to $D/\hbar^2 \times u(\omega')u(\omega)$ where $D = ||\boldsymbol{d}_{0X_\pm}|| \times ||\boldsymbol{d}_{X_\pm 2X}||$ and $u(\omega)$ is the magnitude of the propagation mode which depends on the frequency. The two-photon coupling terms (20) in the global Hamiltonian (19) are thus equal and read

$$\begin{aligned} g^{\mu'\mu}(\omega',\omega) = \frac{D}{\hbar^2}u(\omega')u(\omega)\times\Bigg[&\frac{1}{\omega-\omega_X} - \frac{1}{\omega'-(\omega_{2X}-\omega_X)} \\ &+ \frac{1}{\omega'-\omega_X} - \frac{1}{\omega-(\omega_{2X}-\omega_X)}\Bigg].\end{aligned} \tag{22}$$

The poles in Eq. (22) can be disregarded because the adiabatic elimination calculation assumed the off-resonance condition for the one-photon transitions. The biexcitonic level has a characteristic frequency equal to $\omega_{2X} = 2\omega_X - \delta_X$ where δ_X denotes the biding frequency which is in general positive and of the order of $10^{-2}\omega_X$ [62]. This energy shift is due to the energy needed to separate an exciton into its individual electron and hole charge carriers. In the telecommunication wavelengths for instance, type III-V QD can be engineered [79–81] to have $\omega_X \approx 2\pi \times 190$ THz, that is a corresponding wavelength $\lambda_X \approx 1550$ nm. The two-photon coupling term can be rewritten as

$$\begin{aligned} g^{\mu'\mu}(\omega',\omega) = \frac{D}{\hbar^2}u(\omega')u(\omega)\times\Bigg[&\frac{1}{\omega-\omega_X} - \frac{1}{\omega'-(\omega_X-\delta_X)} \\ &+ \frac{1}{\omega'-\omega_X} - \frac{1}{\omega-(\omega_X-\delta_X)}\Bigg].\end{aligned} \tag{23}$$

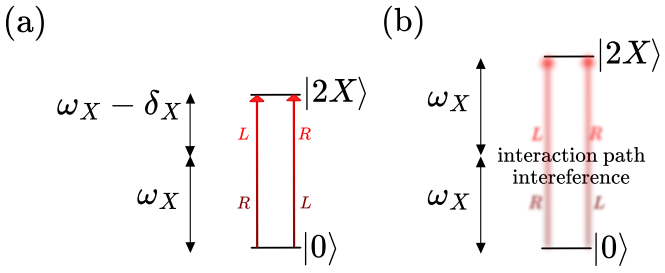

FIG. 2. Effective two-level system where the interaction can be driven through two interaction paths: one where the first photon is R-polarized (respectively L-polarized) with a frequency far-detuned from ω_X and the second photon is L-polarized (respectively R-polarized) with a frequency far-detuned from $\omega_X - \delta_X$. (a) For $\delta_X \neq 0$, the two transition paths are distinguishable and do not interefere leading to a non-zero two-photon coupling term. (b) For $\delta_X = 0$, the two interaction paths are now indistinguishable and destructively interfere. This entails a two-photon coupling term equal to zero thus preventing the $|0\rangle \leftrightarrow |2X\rangle$ transition.

Notably, it appears that the two-photon coupling term vanishes if δ_X is equal to zero, that is to say that the excitonic $|0\rangle \leftrightarrow |X_\pm\rangle$ and biexcitonic $|X_\pm\rangle \leftrightarrow |2X\rangle$ transitions have the same energies. In this case, the two indistinguishable interaction paths $|0\rangle \leftrightarrow |X_\pm\rangle \leftrightarrow |2X\rangle$ interfere destructively, therefore preventing the $|0\rangle \leftrightarrow |2X\rangle$ two-photon interaction emerging from the adiabiatic elimination described previously, see Fig. 2. Two-photon interaction path interferences were described in other photonic systems. For instance, in [82] the pump-driven cavity-cavity photon blockade effect is interpreted as quantum interferences between different excitation paths. Building on the above considerations, the theoretical engineering of the two-photon coupling term in Eq. (23) can be realized by shaping the magnitude of the propagation mode u across the two photons' bandwidths, effectively leveraging the waveguide dispersion properties.

III. SHAPING FREQUENCY ENTANGLING GATE

This section details how the effective two-photon quadratic interaction Hamiltonian – with Eq. (19) or without selection rules Eq. (13) – can be exploited as in [45] to generate frequency correlations between single photons. The overall methodology and computations – based on scattering theory [83, 84] – follow those presented in [45]. The additional time-scale constraints required for the adiabatic elimination regime to hold are discussed.

A. Scattering theory and Markovian approximation

In this section, we employ the scattering theory derivation within the Markovian approximation used in Alushi *et al.* [45]. The main calculation steps are detailed in Appendix C.

1. *Wigner-Weisskopf ansatz*

The present scattering theory calculation is performed within the Schrödinger picture. The Hamiltonian (19) preserves the number of weighted excitations. The matter-field dynamics can thus be encapsulated in a vector state $|\psi(t)\rangle$ with a fixed number of weighted excitations

$$|\psi(t)\rangle = C_{2X}(t)\hat{\xi}_{2X0}\,|\mathbf{0}\rangle + \sum_{\substack{\sigma'\in\{R,L\}\\ \mu'\in\{\pm\}}}\sum_{\substack{\sigma\in\{R,L\}\\ \mu\in\{\pm\}}}\int_{\mathbb{R}^2} d\omega' d\omega\; C^{\sigma'\sigma}_{\mu'\mu}(\omega',\omega;t)\hat{a}^\dagger_{\sigma'\mu'}(\omega')\hat{a}^\dagger_{\sigma\mu}(\omega)\,|\mathbf{0}\rangle\,, \tag{24}$$

where $C_{2X}(t)$ and $C^{\sigma'\sigma}_{\mu'\mu}(\omega',\omega;t)$ are the probability amplitudes to have the system respectively in the QD's biexcitonic state without photons and in the QD's ground state with two photons at frequency ω and ω', polarization σ and σ', and direction of propagation μ and μ', respectively. The latter is also referred to as the joint spectral amplitude (JSA) and its squared modulus as the joint spectral intensity (JSI). The state $|\mathbf{0}\rangle \equiv |0\rangle \otimes |\text{vac}\rangle$ represents the global vacuum state for both light and matter. We define the bare transition operator $\hat{\xi}_{2X0} = \hat{\xi}^\dagger_{02X} \equiv |2X\rangle\langle 0|$. The complete QD-waveguide isolated system is encapsulated within the Wigner-Weisskopf ansatz Eq. (24), whose dynamics is governed by the Schrödinger equation $i\hbar\partial_t|\psi(t)\rangle = \hat{H}|\psi(t)\rangle$ where $\hat{H}$ is the total Hamiltonian.

2. *Markovian and weak coupling approximation*

In the following, we switch to the collective variables $\omega_\Sigma = \omega + \omega'$ and $\omega_\Delta = \omega - \omega'$. This is motivated by the forthcoming Markovian approximation and the action of the ShaFrEnGa which as shown in Sec. III B, effectively reshapes the reference axes of the two-photon distribution from the individual frequencies ω and ω' to the collective frequencies variables ω_Σ and ω_Δ. The expressions of the probability amplitudes $C_{2X}(t)$ and $C^{\sigma'\sigma}_{\mu'\mu}(\omega_\Sigma,\omega_\Delta;t)$ are related to the memory function

$$K(\tau) \equiv \int_{\mathbb{R}} d\omega_\Sigma\, e^{-i\omega_\Sigma\tau}\left(\frac{1}{2}\sum_{\mu',\mu\in\{\pm\}}\int_{\mathbb{R}} d\Delta\,|g^{\mu'\mu}(\omega_\Sigma,\omega_\Delta)|^2\right) \tag{25}$$

of the waveguide seen as a bath which the QD is coupled to. Assuming that the coupling strength is negligible compared to the biexcitonic energy ω_{2X}, the probability amplitude $C_{2X}(\tau)$ can be approximated as $C_{2X}(\tau) = e^{-i\omega_{2X}\tau}S_{2X}(\tau)$. The term $e^{-i\omega_{2X}\tau}$ represents the rapid oscillation due to the biexcitonic energy and $S_{2X}(\tau)$ is a slowly varying function of time. This is the weak coupling approximation. Further, supposing that the the coupling terms $g^{\mu'\mu}(\omega_\Sigma, \omega_\Delta)$ are almost constant with respect to the collective frequency ω_Σ, the memory kernel $K(\tau)$ can be taken as sharply peaked at $\tau = 0$. This implies that the bath does not retain information about the QD's previous states. This is the Markovian approximation. Within these two approximations, the scattered two-photon probability amplitude can be computed as

$$C^{\sigma'\sigma}_{\mu'\mu}(\omega_\Sigma, \omega_\Delta; t_1) = e^{-i\omega_\Sigma(t_1-t_0)}\Bigg[C^{\theta'\theta}_{\nu'\nu}(\omega_\Sigma, \omega_\Delta; t_0)\delta_{\sigma'\theta'}\delta_{\mu'\nu'}\delta_{\sigma\theta}\delta_{\mu\nu} - \frac{\pi\left(g^{\mu'\mu}(\omega_\Sigma, \omega_\Delta)\right)^*}{\frac{\Gamma}{2} + i(\omega_{2X} - \omega_\Sigma)} \sum_{\nu',\nu\in\{\pm\}} \int_{\mathbb{R}} d\omega'_\Delta \; g^{\nu'\nu}(\omega_\Sigma, \omega'_\Delta) C_{\mu'\mu}(\omega_\Sigma, \omega_\Delta; t_0)\Bigg], \tag{26}$$

where Γ labels the QD's decay rate and t_0 and t_1 the scattered times fulfilling $(t_1 - t_0) \gg 1/\Gamma$ for the QD to have fully decayed by the time the two-photon output state is formally reached. The polarization degrees of freedom indices are omitted whenever there is a two-photon coupling term as it implicitly dictates them due to the selection rules. The two-photon output state consists of two contributions: one term represents photons that did not interact with the QD and are only time-shifted, while the other term corresponds to photons that interacted with the QD, as indicated by the coupling terms.

B. Shaping frequency entangling gate

1. *Gaussian input and coupling*

In this section, we outline how to adjust the system's physical parameters to ensure that the scattered output states, described by Eq. (26), exhibit frequency correlations. More specifically, we aim at recovering Gaussian distributions along both collective variable ω_Σ and ω_Δ. Shaping the distribution this way is mainly motivated by the fact that Gaussianity is well-characterized for several quantum information protocols [85, 86]. Let us consider a Gaussian input two-photon state for rightward incoming photons with polarizations R and L and center frequencies ω_e and ω_b

$$C^{\theta'\theta}_{\nu'\nu}(\omega_\Sigma, \omega_\Delta; t_0) = \frac{\delta_{\theta R}\delta_{\nu+}\delta_{\theta' L}\delta_{\nu'+}}{\sqrt{2\pi\alpha^2}} \times e^{-\frac{[\omega_\Sigma - (\omega_e+\omega_b)]^2}{4\alpha^2}} e^{-\frac{[\omega_\Delta - (\omega_e-\omega_b)]^2}{4\alpha^2}}, \tag{27}$$

normalized to one with $C_{2X}(t_0) = 0$. This distribution is isotropic in the two-frequency plane given that the standard deviations along the two collective variables are identical and equal to α. Let us further assume in the same line as [45] that the coupling terms can be engineered as discussed in Sec. II B 4 to a Gaussian of the form

$$g^{\mu'\mu}(\omega_\Delta) = \sqrt{\frac{\gamma^{\mu'\mu}}{\pi}}\left(\frac{1}{2\pi\beta^2}e^{-\frac{(\omega_\Delta - (\omega_e-\omega_b))^2}{\beta^2}}\right)^{1/4}, \tag{28}$$

where $\gamma^{\mu'\mu}$ is an emission rate taken isotropic that is $\gamma^{\mu'\mu} = \Gamma/4$. This coupling-term is therefore assumed to be independent of the sum of frequencies ω_Σ which aligns with the Markovian approximation previously applied. Based on the structure of the two-photon coupling term Eq. (22), we formally discuss in Appendix E the required form of the propagation mode $u(\omega)$ across the two photons' bandwidths to achieve the desired Gaussian coupling Eq. (28) using a standard numerical optimization method. The coupling term is therefore supposed independent of the total frequency $\omega_\Sigma = \omega + \omega'$ in agreement with the Markovian approximation discussed earlier. Putting the input Gaussian two-photon distribution Eq. (27) and the Gaussian two-photon coupling term Eq. (28) together in the expression of the scattered output states for $\{\mu', \mu\} = \{+, +\}$

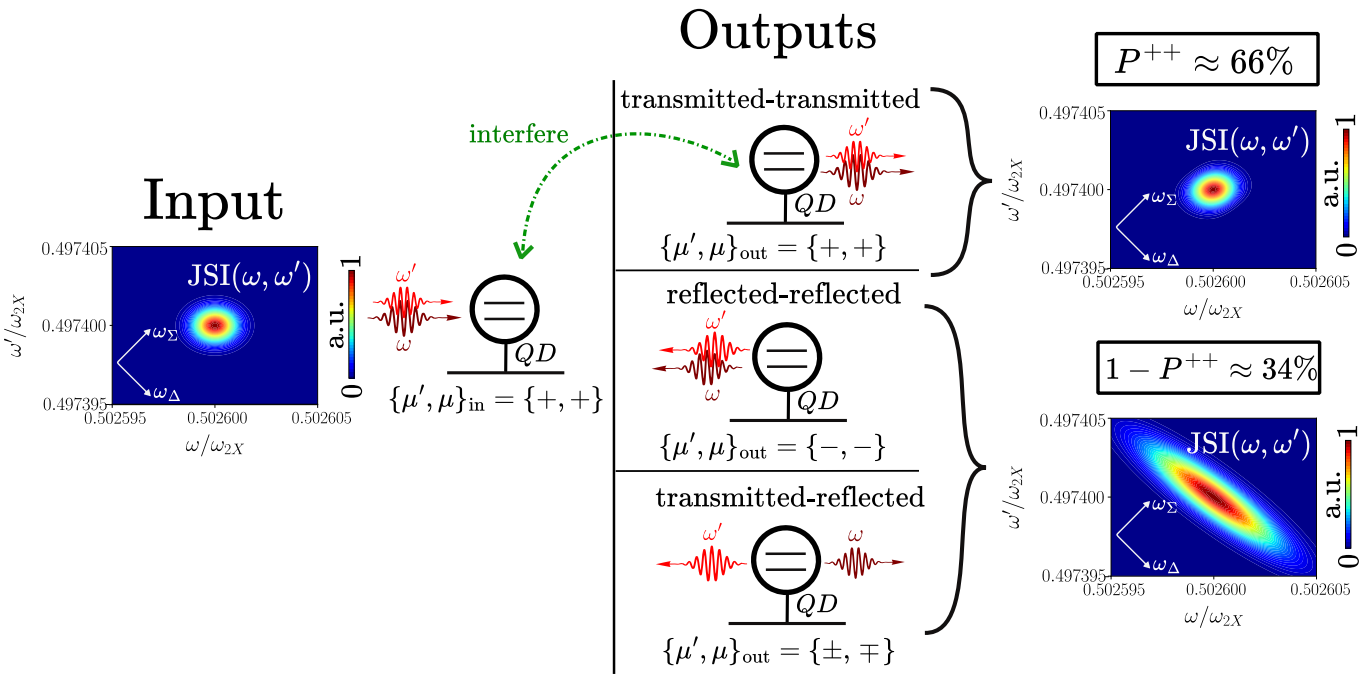

FIG. 3. Scattering channels for the two input photons propagating rightward, i.e.. $\{\mu', \mu\}_{\text{in}} = \{+, +\}$, with an initial Gaussian joint spectral amplitude (left panel) along both collective variables $\omega_\Sigma = \omega + \omega'$ and $\omega_\Delta = \omega - \omega'$ of width $\alpha = 10^{-6}\omega_{2X}$ and centers $\omega_e = 0.5026\omega_{2X}$, $\omega_b = 0.4974\omega_{2X}$. The coupling term is taken as Gaussian of width $\beta = 4\alpha$. The decay rate is chosen as $\Gamma = 10^{-5}\omega_{2X} \gg \alpha$. There are two kinds of outputs (right panels), the one for which the output photons' auxiliary modes are identical to that of the input (upper right panel), i.e.., $\{\mu', \mu\}_{\text{in}} = \{\mu', \mu\}_{\text{out}}$ and those for which they are not (lower right panel), i.e.., $\{\mu', \mu\}_{\text{in}} \neq \{\mu', \mu\}_{\text{out}}$. In the first case, of probability $P^{++} \approx 66\%$ for the chosen physical parameters, the input photons can interfere with the entangled photons scattered out by the QD. This results in an output two-photon distribution that is weakly modified with respect to the input two-photon distribution. In the second case $\{\mu', \mu\}_{\text{in}} \neq \{\mu', \mu\}_{\text{out}}$, which occurs with probability $1 - P^{++} \approx 34\%$ for the chosen physical parameters, only the entangled photons scattered out by the QD contribute to the two-photon distribution. This produces an output two-photon distribution that is reshaped along both collective variables. Along ω_Σ, the JSA is filtered by the Lorentzian profile originating from the Markovian approximation. The two-photon coupling term shapes the JSA along the ω_Δ collective variable. The exact values of the JSIs have been renormalized for readability. They are presented in arbitrary units (a.u.) on a linear scale.

$$C^{LR}_{++}(\omega_\Sigma, \omega_\Delta; t_1) = e^{-i\omega_\Sigma(t_1-t_0)}\Bigg[C^{LR}_{++}(\omega_\Sigma, \omega_\Delta; t_0) - \sqrt{\frac{1}{16\pi(\alpha^2+\beta^2)}}\frac{\Gamma}{\frac{\Gamma}{2} + i(\omega_{2X} - \omega_\Sigma)} e^{-\frac{[\omega_\Sigma - (\omega_e+\omega_b)]^2}{4\alpha^2}} e^{-\frac{(\omega_\Delta - (\omega_e-\omega_b))^2}{4\beta^2}}\Bigg] \tag{29}$$

and for $\{\mu', \mu\} \neq \{+, +\}$

$$C^{\sigma'\sigma}_{\mu'\mu}(\omega_\Sigma, \omega_\Delta; t_1) = -e^{-i\omega_\Sigma(t_1-t_0)}\sqrt{\frac{1}{16\pi(\alpha^2+\beta^2)}}\frac{\Gamma}{\frac{\Gamma}{2} + i(\omega_{2X} - \omega_\Sigma)} e^{-\frac{[\omega_\Sigma - (\omega_e+\omega_b)]^2}{4\alpha^2}} e^{-\frac{(\omega_\Delta - (\omega_e-\omega_b))^2}{4\beta^2}}, \tag{30}$$

where the polarizations σ and σ' match the optical selection rules for each direction of propagation channel. An example of the corresponding squared moduli – or JSI – are plotted in Fig. 3. It appears that while the outputs Eq. (30) exhibit frequency correlations or anticorrelations depending on the ratios of the different widths Γ, α and β, the output Eq. (29) displays a two-photon distribution similar to the input although slightly distorted along the two collective variables ω_Σ and ω_Δ. The latter can be interpreted as an interference pattern arising from the interaction of the photons that did not interact with the QD and those which did. This interference phenomenon does not manifest when considering photons with different auxiliary degrees of freedom as the input photons. The direction of propagation and polarization hence define a coherence condition for the intereferences to manifest in the present scattering derivation.

2. Photon bandwidth limiting filtering

From the scattered output amplitudes' equations (29) and (30), it stands out that the term corresponding to the photons that have interacted with the QD is composed of a Gaussian dependency along the difference of frequencies ω_Δ dictated by the Gaussian form of the coupling term Eq. (28) and two competing dependencies along the sum of frequencies ω_Σ – a Gaussian one imposed by the input two-photon distribution and a Lorentzian one enforced by the Markovian approximation. The latter acts as a frequency filter preventing photons to be emitted by the QD if they do not match the two-photon resonance condition $\omega_\Sigma = \omega_{2X}$ – up to the decay rate Γ. Nonetheless, this resonance condition does not impose any constraint on the difference of frequencies ω_Δ. The Gaussian two-photon input along ω_Σ on the other hand forces the scattered output photons to have the same frequency distribution as the input thus preventing sum of frequencies to be generated by the QD. These two filterings are centered respectively at ω_{2X} and $\omega_e+\omega_b$ with the latter being close to ω_{2X} with respect to the one-photon detunings under the adiabatic elimination we performed in Sec. II B 2. The Lorentzian and Gaussian filterings can be considered centered at the same frequency provided $|\omega_{2X} - (\omega_e + \omega_b)| \ll \Gamma, \alpha$. Therefore, in the limit regime for which $\Gamma \gg \alpha$, the frequency filtering along the collective variable ω_Σ is governed by the input two-photon distribution, resulting in a non-interefered output Eq. (30) two-photon JSI now reading

$$|C^{\sigma'\sigma}_{\mu'\mu}(\omega_\Sigma, \omega_\Delta; t_1)|^2 = \frac{1}{4\pi(\alpha^2+\beta^2)} \times e^{-\frac{(\omega_\Delta-(\omega_e-\omega_b))^2}{2\beta^2}} e^{-\frac{[\omega_\Sigma-(\omega_e+\omega_b)]^2}{2\alpha^2}}, \tag{31}$$

for $\{\mu', \mu\} \neq \{+,+\}$. This two-photon output distribution Eq. (31) is Gaussian in both collective variables ω_Σ and ω_Δ. Remarkably, and unlike Alushi *et al.*, the present photonic microscopic model actually requires this $\Gamma \gg \alpha$ condition to be met. Indeed, for the scattering calculations, especially one considered $(t_1-t_0)\Gamma \gg 1$. In contrast, for the adiabatic elimination resulting in the effective quadratic Hamiltonian Eq. (13) to hold, the interaction time was assumed to be such that $(t_1-t_0)|\overline{\delta_e}| \gg 1$, $(t_1-t_0)|\overline{\delta_b}| \gg 1$ and $(t_1-t_0)\alpha \ll 1$ with $\overline{\delta_e}$ and $\overline{\delta_b}$ the mean value of the one-photon transition detunings previously discussed. This ensures that the one-photon transition operators adiabatically average out while the two-photon transition operators remain constant in time. The $(t_1-t_0)\Gamma \gg 1$ and $(t_1-t_0)\alpha \ll 1$ conditions inevitably entails $\Gamma \gg \alpha$. The different time scales are sketched in Fig. 4. In the telecom band, the decay rate Γ is typically of the order of a few GHz [87, 88] which would require single-photon sources' linewidths in the telecom band to be narrower than a few hundred MHz. Although telecom band single-photon sources' linewidths are generally broader [89–92], several studies have successfully demonstrated devices with narrower linewidths [22, 93, 94]. In that regard, the time (t_1-t_0) should typically be within the $0.1-1$ ns range. Furthermore, the spontaneous emission decay rate may be significantly enhanced by increasing the Purcell factor. The described scattering process thus operates as a frequency reshaping performed by the light-matter interaction coupling term which reshapes the two-photon distribution by modifying its width along the difference of frequencies ω_Δ from α to β. As it will be discussed shortly, the ratio β/α is directly related to the resulting frequency entanglement. Namely, the two photons are maximally frequency-correlated for $\beta/\alpha \to +\infty$ (see Fig. 6, panel (c)) and frequency-anticorrelated for $\beta/\alpha \to 0$ (see Fig. 6, panel (a)). There are no frequency correlations and the two-photon output distribution is separable when $\beta = \alpha$ (see Fig. 6, panel (b)).

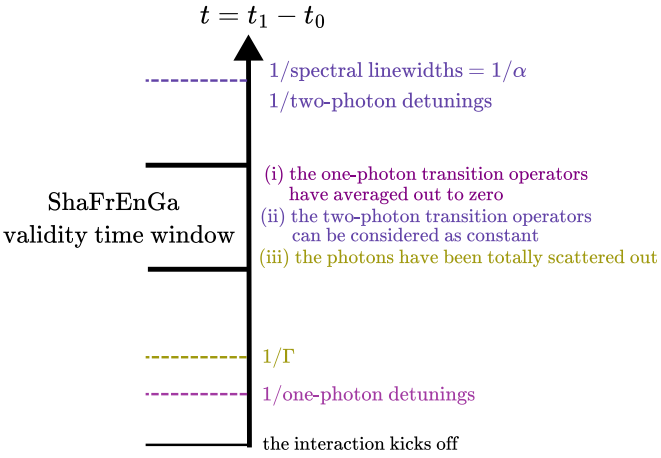

FIG. 4. Time-scale constraints for the ShaFrEnGa gate based on adiabatic elimination in a waveguide-coupled quantum dot. The adiabatic elimination of one-photon transitions requires that the interaction time be much longer than the inverse of the one-photon detunings, ensuring that the corresponding joint operators average out to zero and can be neglected (condition (i)). To treat the two-photon joint operators as effectively time-independent during the scattering process, the time must also remain much shorter than the inverse of the two-photon detunings and the spectral linewidths (condition (ii)). Finally, for the scattering theory approach to be valid, the time must exceed $1/\Gamma$ ensuring that the QD has fully decayed to its ground state by the end of the interaction (condition (iii)).

IV. ENTANGLEMENT AND EFFICIENCY INVESTIGATION OF THE FREQUENCY-ENTANGLEMENT DEVICE

In this section, the entanglement properties are quantitatively analyzed revealing a trade-off between the generation success probability and the entanglement quality. By employing our overall methodology, the ShaFrEnGa is then shown to apply for the generation of frequency-

entangled frequency qudit states.

A. Efficiency of the frequency-entanglement generation

As previously discussed in Sec. III B 1, out of the four scattering outputs depending on the photons' directions of propagation, the one for which the output photons' auxiliary degrees of freedom match that of the input photons exhibits interference patterns that make it unsuitable for the frequency-entanglement generation. Consequently, the efficiency of the entanglement generation is directly given by the probability P^{success} of having the photons scattered out with different auxiliary degrees of freedom as the input photons. Here for instance, since we considered input photons incoming moving to the right, i.e., $\{\mu', \mu\} = \{+, +\}$, $P^{\text{success}} = 1 - P^{++} = P^{--} + P^{+-} + P^{-+}$ where

$$P^{\mu'\mu} = \frac{\int_{\mathbb{R}^2} d\omega_\Sigma d\omega_\Delta \, |C^{\sigma'\mu'\sigma\mu}_{\omega_\Sigma\omega_\Delta}(t_1)|^2}{\int_{\mathbb{R}^2} d\omega_\Sigma d\omega_\Delta \, |C^{LR}_{++}(\omega_\Sigma, \omega_\Delta; t_0)|^2}. \tag{32}$$

The previously discussed frequency filtering imposed by the Lorentzian emission profile also explains why this probability is maximized when $\Gamma \gg \alpha$, as demonstrated by Alushi [45]. For an isotropic process $\gamma^{\mu'\mu} = \Gamma/4$, in the $\Gamma \gg \alpha$ regime and for an input two-photon amplitude normalized to one, the probability of success can be expressed as a function of the ratio β/α using Eq. (31)

$$P^{\text{success}} = \frac{3\beta/\alpha}{2(1 + \beta^2/\alpha^2)}. \tag{33}$$

The success probability of outputting a suitable two-photon distribution – that is to say without interferences – is at most equal to 75% for $\alpha = \beta$. Nevertheless, $\alpha = \beta$ corresponds to a separable two-photon JSI Eq. (31). Indeed, the closer the ratio β/α is to one, the less frequency-entangled the photons are. They are frequency-correlated for $\beta \gg \alpha$ and frequency-anticorrelated for $\alpha \gg \beta$. Subsequently, there is a trade-off between the success probability of producing frequency-entangled photons and the amount of entanglement that is generated. All appears as if the two-photon output distribution opposed the reshaping along ω_Δ to ensure that no frequencies along this collective variable are created – as it does along ω_Σ. This probability of success is achieved without requiring off-line measurements of auxiliary photons, unlike photon entanglement protocols based on the KLM scheme [2, 52]. Note that one could have utilized the QD's spontaneous emission by first pumping it to its biexcetionic state and then let it spontaneously decay. Provided that the photons are collected within the time window in which the adiabatic elimination regime is valid, frequency-entanglement is generated with a Lorentzian dependence of width the decay rate Γ along the sum of frequencies $\omega_\Sigma = \omega + \omega'$ and a Gaussian dependence of width β along the difference of frequencies $\omega_\Delta = \omega - \omega'$. Nevertheless, since there would be no initial Gaussian dependence to draw from, the distribution along ω_Σ will always be Lorentzian and not Gaussian in the Markovian approximation previously discussed.

B. Schmidt decomposition of the output spectral two-photon state

In this subsection, we evaluate the entanglement of the two-photon output state Eq. (30), postselected on scattering events where the auxiliary degrees of freedom differ from those of the input state. To proceed, we perform a Schmidt decomposition for continuous variables bipartite systems [95–97]. Further details are provided in Appendix D. The probability amplitude $C^{\sigma'\sigma}_{\mu'\mu}(\omega', \omega; t_1)$ of the pure renormalized output state

$$\left|\psi^{\sigma'\sigma}_{\mu'\mu}(t_1)\right\rangle = \int_{\mathbb{R}^2} d\omega' d\omega \; C^{\sigma'\sigma}_{\mu'\mu}(\omega', \omega; t_1) \hat{a}^\dagger_{\sigma'\mu'}(\omega') \hat{a}^\dagger_{\sigma\mu}(\omega) \left|\text{vac}\right\rangle \tag{34}$$

is expressed by means of a discrete expansion

$$\left|\psi^{\sigma'\sigma}_{\mu'\mu}(t_1)\right\rangle = \sum_{k=1}^{l} \lambda_k^{\sigma'\mu'\sigma\mu} \hat{b}^{(2)\dagger}_{\sigma'\mu'}(k) \hat{b}^{(1)\dagger}_{\sigma\mu}(k) \left|\text{vac}\right\rangle, \tag{35}$$

where we truncated the number of modes to l to perform the numerical singular-value decomposition. The operators $\hat{b}^{(1)\dagger}_{\sigma\mu}(k)$ and $\hat{b}^{(2)\dagger}_{\sigma'\mu'}(k)$ are bosonic creation operators which can be expressed as

$$\begin{aligned} \hat{b}^{(1)\dagger}_{\sigma\mu}(k) &= \int_{\mathbb{R}} d\omega \; \Theta^{(1)}_k(\omega) \hat{a}^\dagger_{\sigma\mu}(\omega) \\ \hat{b}^{(2)\dagger}_{\sigma'\mu'}(k) &= \int_{\mathbb{R}} d\omega' \; \Theta^{(2)}_k(\omega') \hat{a}^\dagger_{\sigma'\mu'}(\omega'). \end{aligned} \tag{36}$$

These operators create photons in the so-called Schmidt modes labelled by the k index. The functions $\Theta^{(1)}_k(\omega)$ and $\Theta^{(2)}_k(\omega')$ are linear combinations of a set of orthogonal functions. These orthogonal functions are here chosen to be the Hermite-Gauss orthogonal functions because of the Gaussianity of the two-photon distribution. The $\lambda_k^{\sigma'\mu'\sigma\mu}$ Schmidt coefficients are real, non-negative, unique up to reordering and obey $\sum_{k=1}^{\min(m_0,n_0)} \left(\lambda_k^{\sigma'\mu'\sigma\mu}\right)^2 = 1$ provided $C^{\sigma'\sigma}_{\mu'\mu}(\omega', \omega; t_1)$ is normalized to one. From the Schmidt coefficients, two measures of entanglement can be computed [26]: (i) the entanglement entropy $S^{\sigma'\mu'\sigma\mu}_{\text{entropy}} = -\sum_{k=1}^{\min(m_0,n_0)} (\lambda_k^{\sigma'\mu'\sigma\mu})^2 \log\left((\lambda_k^{\sigma'\mu'\sigma\mu})^2\right)$ – corresponding to the von Neumann entropy of the reduced density matrix obtained by tracing out either one of the photons – (ii) the Schmidt number $K^{\sigma'\mu'\sigma\mu} = 1/\sum_{k=1}^{\min(m_0,n_0)} (\lambda_k^{\sigma'\mu'\sigma\mu})^4$. The Schmidt number namely

	$\beta = 10\alpha$	$\beta = 30\alpha$
Entanglement generation probability success	15%	5%
Normalized entanglement entropy	0.4	0.6
Schmidt number	5	12
Ellipticity	98%	99.8%
Frequency bandwidth along ω_Σ	2.4 GHz	790 MHz
Frequency bandwidth along ω_Δ	24 GHz	24 GHz

TABLE I. Characteristic physical values related to the output two-photon distribution for two values of the β/α ratio. The Gaussian coupling term width is fixed at $\beta = 10^{-5}\omega_{2X} \approx 2\pi\times$ 3.8 GHz. These frequency bandwidths along both collective variables can be compared to Le Jeannic *et al.* [42] who found frequency bandwidths of the order of a few GHz.

gives the effective number of modes in the Schmidt decomposition. In the following, we drop the Schmidt number and entropy of entanglement labeling for readability. In Fig. 5, we plot the input and output two-photon joint-spectral intensity (JSI) and the modes structure for $\beta = 10\alpha$ and in the $\Gamma \gg \alpha$ regime. For the input, since the two-photon distribution is separable in the individual frequencies ω and ω', the entanglement entropy is equal to 0 and the Schmidt number to 1. On the other hand, the output two-photon distribution is non-separable in ω and ω' as long as $\beta \neq \alpha$. For $\beta = 10\alpha$, the Schmidt number is approximately equal to 5 and the entanglement entropy is close to 36% of its maximum value. In Fig. 6, we display for ten values of β/α ranging from 0.1 to 10 the evolution of the entanglement generation success probability Eq. (33), the Schmidt number K and the normalized entanglement entropy S_{entropy}. Note that the computed Schmidt number evolution follows its analytical expression for a doubly Gaussian JSA [98]. As previously discussed, a trade-off can be observed between the quality of the entanglement – estimated by the Schmidt number and the entanglement entropy – and success probability of the entanglement generation. An illustrative summary of typical physical values related to the output two-photon distributions is displayed in Tab. I for two different values of the β/α ratio. This section shows how the ShaFrEnGa can produce Gaussian frequency-entangled biphoton states with Gaussian profiles and with high quality and efficiency. The resulting biphoton state can exhibit a Schmidt number of approximately 5, a normalized entanglement entropy of 0.4, and 98% ellipticity, with an entanglement generation efficiency reaching up to 15%—significantly exceeding what is typically achievable with SPDC or SFWM.

C. ShaFrEnGa with frequency qudit states

In this subsection, we cover the action of the ShaFrEnGa when the input state is a two-photon frequency qudit states [22, 53–56, 58, 59, 99–103]. Such frequency grid states are single-photon states characterized by discrete frequency components arranged in a comb-like structure and modulated by an overall envelope. An isotropic frequency grid state in the (ω_s, ω_i) plane can be generated starting with the isotropic Gaussian two-photon distribution $C^{LR}_{++}(\omega_\Sigma, \omega_\Delta; t_0)$ (see Eq. (28)) of standard deviation α and applying a frequency filter such as an optical cavity. This filtering process operates on the individual frequencies ω and ω' shaping the desired grid structure in the frequency domain $C^{LR}_{++}(\omega_\Sigma, \omega_\Delta; t_0) \rightarrow C^{LR}_{++}(\omega_\Sigma, \omega_\Delta; t_0) f_{\text{filter}}(\omega) f_{\text{filter}}(\omega')$ where the filtering function f_{filter} is assumed to be identical for both frequencies. This filtering function is typically a Airy function that can be approximated as a sum of Gaussians in the high-finesse regime of the optical cavity: $f_{\text{filter}}(\omega) = \sum_{n\in\mathbb{Z}} T_n(\omega)$ where $T_n(\omega) = \exp\big(-(\omega - n\overline{\omega})^2/(2\delta\omega^2)\big)$. This high-finesse regime holds for a free spectral range (FSR) much larger than the width of the peaks, *i.e.* $\overline{\omega} \gg \delta\omega$. For the frequency peaks to be distinct, the envelope standard deviation α should be larger than the FSR. Standard frequency comb FSRs [59] below 100 GHz are usually of the order of 10-20 GHz [22, 56, 58, 101] but lower values close to 1 GHz [102, 103] have also been reported. Given the adiabatic elimination constraint imposing the decay rate Γ to be large with respect to α, we take $\overline{\omega} = 10^{-5}\omega_{2X} \approx 2\pi \times 1$ GHz, $\alpha = 2 \times 10^{-5}\omega_{2X} \approx 2\pi\times$ 2 GHz and $\delta\omega = 10^{-6}\omega_{2X} \approx 2\pi \times 100$ MHz $\ll \overline{\omega}$ for the high-finesse regime to hold. This requires Γ to be larger than $2 \times 2\pi \times 10$ GHz which is a bit higher than the standard biexcitonic decay rates [87, 88] but not too far off. The frequency-filtered distribution $C^{LR}_{++}(\omega_\Sigma, \omega_\Delta; t_0) f_{\text{filter}}(\omega) f_{\text{filter}}(\omega')$ can be used as the ShaFrEnGa input. The non-interfered two-photon output distribution can be analytically calculated as

$$C^{\sigma'\sigma}_{\mu'\mu}(\omega', \omega; t_1) = -e^{-i\omega_\Sigma(t_1-t_0)} \sqrt{\frac{\delta\omega^2}{16\pi\left(\alpha^2\beta^2 + \delta\omega^2(\alpha^2+\beta^2)\right)}} e^{-\frac{[\omega_\Delta - (\omega_e - \omega_b)]^2}{4\beta^2}} \frac{\Gamma}{\frac{\Gamma}{2} + i(\omega_{2X} - \omega_\Sigma)} e^{-\frac{[\omega_\Sigma - (\omega_e + \omega_b)]^2}{4\alpha^2}} \sum_{n,m\in\mathbb{Z}} f_{nm}(\omega_\Sigma), \tag{37}$$

for $\{\mu, \mu'\} \neq \{+, +\}$. The computation details are given in Appendix F. The comb structure is now along the sum of frequencies ω_Σ with frequency peaks expressed as

$$f_{nm}(\omega_\Sigma) = e^{D_{nm}} e^{-\frac{1}{4\delta\omega^2}[\omega_\Sigma - \overline{\omega}(n+m)]^2}, \tag{38}$$

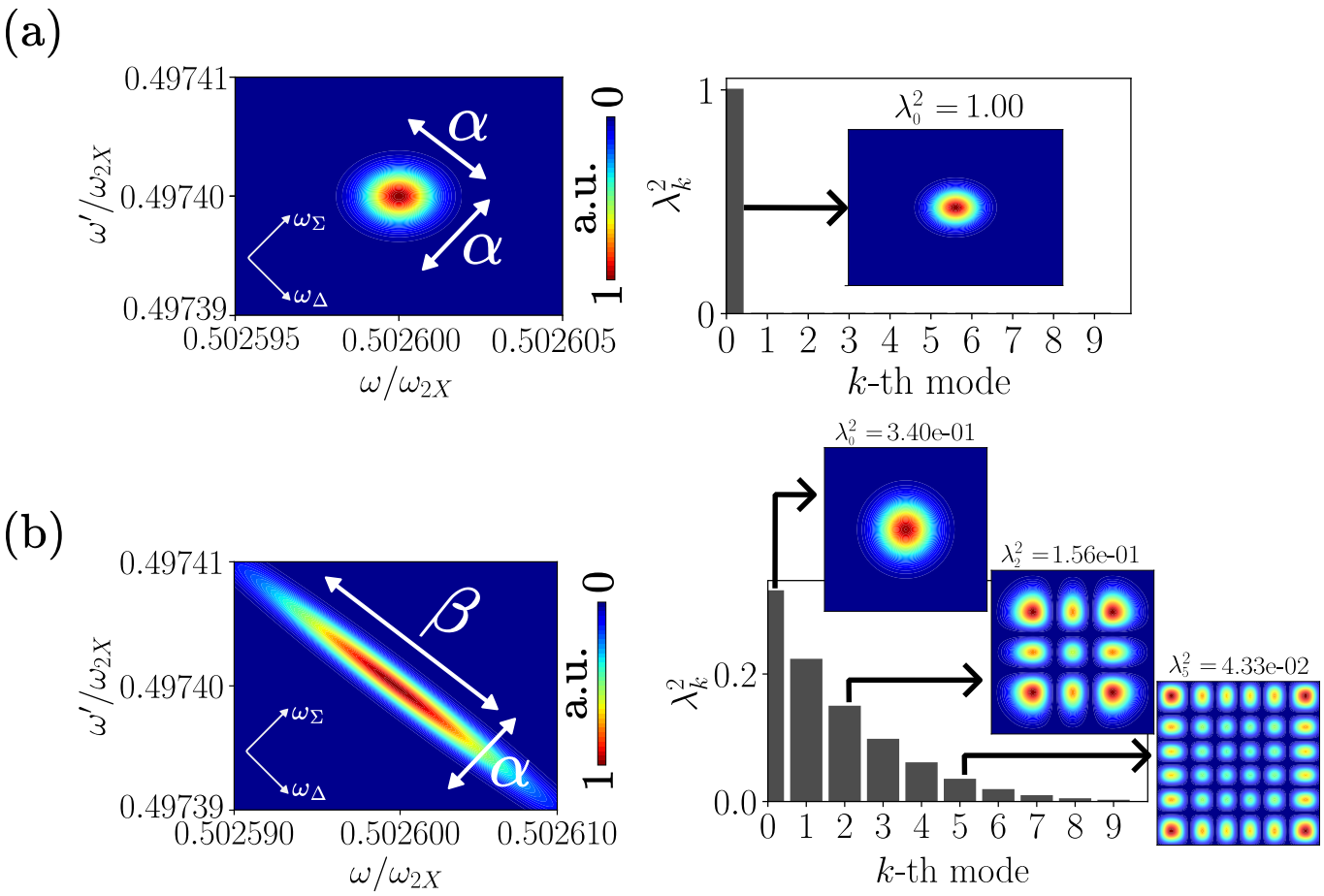

FIG. 5. (a) Modes structure for the input two-photon distribution Gaussian, in both $\omega_\Sigma = \omega + \omega'$ and $\omega_\Delta = \omega - \omega'$ of width $\alpha = 10^{-6}\omega_{2X}$ and centers $\omega_e = 0.5026\omega_{2X}$, $\omega_b = 0.4974\omega_{2X}$. The normalized entanglement entropy and the Schmidt number are computed to be $S_{\text{entropy}} = 0.00$ and $K = 1.00$ respectively. (b) Modes structure for the output two-photon distribution Gaussian in both $\omega_\Sigma = \omega + \omega'$ and $\omega_\Delta = \omega - \omega'$ of width $\alpha = 10^{-6}\omega_{2X}$, centers $\omega_e = 0.5026\omega_{2X}$, $\omega_b = 0.4974\omega_{2X}$ and $\beta = 10\alpha$, respectively. The decay rate is taken as $\Gamma = 10^{-5}\omega_{2X} \gg \alpha$. The normalized entanglement entropy and the Schmidt number are computed to be $S_{\text{entropy}} = 0.39$ and $K = 4.72$ respectively. The first, third and fifth Schmidt modes' JSIs have been plotted. The exact values of the JSIs have been renormalized for readability. They are presented in arbitrary units (a.u.) on the same linear scale in ω/ω_{2X} and ω'/ω_{2X} as the (b) left panel.

where

$$D_{nm} = -\frac{1}{4}\frac{\left(\alpha^2+\beta^2\right)\left((\omega_e-\omega_b)-\overline{\omega}(n-m)\right)^2}{\alpha^2\beta^2+\delta\omega^2(\alpha^2+\beta^2)}. \quad (39)$$

As for Eq. (30), there is a filtering competition along ω_Σ between the input two-photon Gaussian distribution and the Lorentzian emission profile. In the $\Gamma \gg \alpha$ regime enforced by the adiabatic elimination regime and assuming $\Gamma, \alpha \gg |\omega_{2X} - (\omega_e + \omega_b)|$, the two-photon distribution Eq. (37) corresponds to a frequency comb where frequency peaks are approximately $\overline{\omega}$ apart and lie along the ω_Σ collective variable, with a Gaussian envelope of standard deviation α. The frequency peaks standard deviation β along the difference of frequencies ω_Δ is enforced by the Gaussian coupling term. Employing the continuous-variable Schmidt decomposition we display in Fig. 7 the normalized entanglement entropy and the Schmidt number along with the probability Eq. (32) of successfully outputting the non-interfered two-photon state Eq. (37) as functions of the ratio $\beta/\delta\omega$. Our analysis reveals five regimes. The two two-photon states with the lowest Schmidt number and entanglement entropy emerge either due to the separability of the peaks (Fig. 7 (b)) when $\beta = \delta\omega$ or to the apparent separability of the envelope when $\beta = \alpha$ (Fig. 7 (d)). Although these two-photon states exhibit the lowest Schmidt number and entanglement entropy, neither metric reaches the separable limit – Schmidt number equal to 1 and entropy of entanglement equal to 0 –, so they remain partially entangled. These partially-entangled two-photon state have the highest success probability, up to approximately 19% for Fig. 7 (d). Second, when $\beta \ll \delta\omega \ll \alpha$ (Fig. 7 (a)), the two-photon output state is the most frequency-anti-correlated because both the peaks and the envelope are stretched along the ω_Σ variable. For $\beta \gg \alpha \gg \delta\omega$ (Fig. 7 (e)), the two-photon output state appears

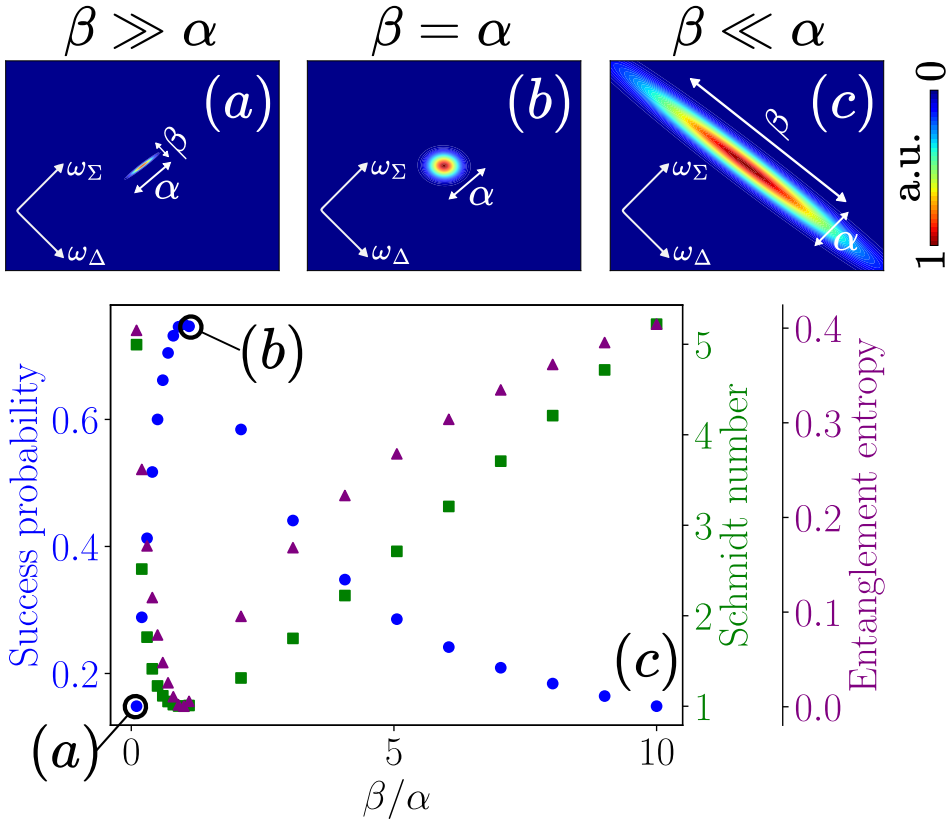

FIG. 6. Trade-off between the probability of successfully outputting a non-interfered entangled two-photon distribution and the quality of the entanglement measured with the Schmidt number and normalized entanglement entropy with respect to the ratio β/α of the Gaussian coupling width β to the two-photon input width α. The normalized entanglement entropy is given with respect to its maximum value. The Gaussian coupling width β varies from 0.1α to 10α with $\alpha = 10^{-6}\omega_{2X}$. The decay rate is taken as $\Gamma = 10^{-5}\omega_{2X} \gg \alpha$. The illustrative JSIs (panels (a), (b), (c)) are all on the same linear scale in ω/ω_{2X} and ω'/ω_{2X}. The panel (a) depicts a regime where $\beta \ll \alpha$ (frequency-anti-correlated photons), the panel (c) where $\beta \gg \alpha$ (frequency-correlated photons) and the panel (b) where $\beta = \alpha$ (no frequency correlations).

as the most frequency-correlated because both the peaks and the envelope are stretched along the ω_Σ variable. In the regime $\beta \gg \alpha \gg \delta\omega$ and for a FSR $\alpha \gtrsim \overline{\omega}$, one can engineer the initial distribution in such a way for the output state to correspond to a cat state with elliptical lobes. The Fig. 7 (a) and Fig. 7 (e) regimes have the lowest success probabilities, dropping to around 1%. Last, the regime where $\alpha > \beta > \delta\omega$ (Fig. 7 (c)) is an intermediate regime where the photons are not as frequency-entangled as in the $\beta \ll \delta\omega \ll \alpha$ and $\beta \gg \alpha \gg \delta\omega$ regimes but exhibit higher frequency correlations than the two other regimes (Fig. 7 (b) and Fig. 7 (d)). Furthermore, this intermediate regime has an intermediate success probabilities as compared to the other regimes, reaching close to 8%. These different regimes show the interplay between the two-photon envelope and frequency peaks' apparent separability. Furthermore, Fig. 7 confirms the trade-off between the generation success probability and the entanglement previously discussed: the higher the Schmidt number and entanglement entropy, the lower the generation success probability.

V. CONCLUSION

The present theoretical work first provides an *ab initio* effective two-level quadratic two-photon Hamiltonian in which the frequency is continuously defined. The derivation is based on a Heisenberg picture adiabatic elimination of frequency-dependent joint one-photon transition operators reducing to frequency-dependent two-photon transition operators. In contrast, adiabatic elimination in atomic physics – for instance in cavity systems – is typically conducted in the interaction-Schrödinger picture, where the populations of irrelevant states are suppressed on average without explicitly keeping track of the frequency dependence of the interaction. Starting from a generic four-level system interacting with a bosonic field continuum, such one-photon transition-operator adiabatic elimination yields a two-photon quadratic Hamiltonian where the field is coupled to an effective two-level atomic-like system, *e.g.* a QD embedded in a waveguide. This Hamiltonian is effective in that it emerges under several

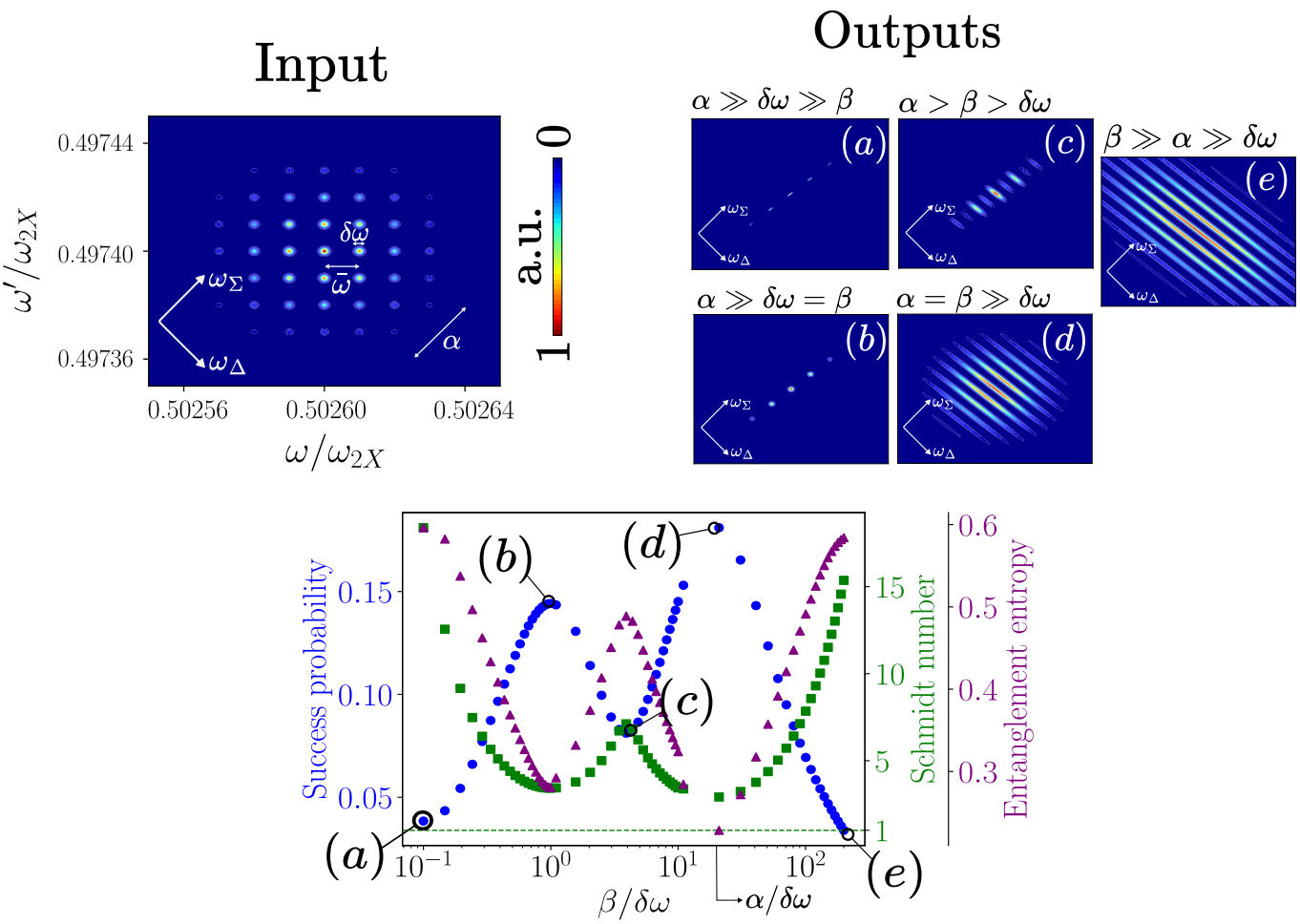

FIG. 7. (bottom) Trade-off between the probability of successfully outputting a non-interfered entangled two-photon distribution and the quality of the entanglement measured with the Schmidt number and normalized entanglement entropy with respect to the ratio $\beta/\delta\omega$ of the Gaussian coupling width β and $\delta\omega$ the input grid state peaks' width. The $\beta/\delta\omega$-axis is displayed in a logarithmic scale. The Gaussian coupling width β varies from $0.1\delta\omega$ to $45\delta\omega$ with $\delta\omega = 10^{-6}\omega_{2X}$. The entanglement entropy is given with respect to its maximum value. The Gaussian envelope input is taken as $\alpha = 2\times10^{-5}\omega_{2X}$ and the FSR as $10^{-5}\omega_{2X}$. The decay rate is taken as $\Gamma = 2\times10^{-5}\omega_{2X} \gg \alpha$. The illustrative output JSIs panels (a), (b), (c), (d) and (e) (top right corner) and the input JSI (top left corner) are all on the same linear scale in ω/ω_{2X} and ω'/ω_{2X}. The input JSA is separable with a normalized entropy of entanglement equal to 0 and a Schmidt number equal to 1.

physical considerations: (i) Provided the one-photon detunings are large compared to the one-photon coupling terms. (ii) The interaction time is large with respect to the inverse of the one-photon detuning, ensuring that the one-photon transition operators have averaged to zero. (iii) The interaction time is small compared to the photon linewidths and two-photon detunings. These hypotheses entail that the two-photon transition operators are roughly constant and can be reinjected in the Schrödinger picture evolution. The computed two-photon coupling terms are frequency-dependent and non-separable in the two photons' frequencies. Alushi *et al.*'s methodology [45] based on a scattering theory computation in the Markovian approximation is then applied to analyze the appearance of frequency-entanglement in the output field. Under the Markovian approximation, the initial two-photon input is reshaped with a Lorentzian-dependence along the collective variables $\omega_\Sigma = \omega + \omega'$ determined by the biexcitonic decay rate Γ. When the frequency-dependent two-photon coupling term is specifically designed along the collective variable ω_Δ, the initial two-photon input distribution follows the profile of the coupling function along this variable. Further, considering a separable, isotropic, Gaussian two-photon input of width α, and assuming a Gaussian two-photon coupling term along ω_Δ, the $\Gamma \gg \alpha$ regime yields a frequency-entangled two-photon output with Gaussian distributions along both collective variables ω_Σ and ω_Δ. A trade-off between the frequency-entanglement generation efficiency and its quality – assessed with the Schmidt number and the entanglement entropy – is showcased using a Schmidt

decomposition for frequency continuous variables. For example, the frequency-entanglement generation efficiency reaches up to 15% for a frequency-entangled biphoton state with a Schmidt number of around 5, a normalized entanglement entropy of 0.4 and an ellipticity of 98%. This frequency-entanglement generation efficiency is much higher than what can be achieved with SPDC [104, 105] or SFWM [106]. The ShaFrEnGa can also be implemented with time–frequency qudit states, where the trade-off between frequency-entanglement and success probability emerges again. Depending on the ratio of the Gaussian coupling's standard deviation to the spacing between spectral peaks, one can identify five distinct regimes of frequency correlation. This versatility shows that the ShaFrEnGa applies equally well in both continuous-variable and discrete-variable (qudit) time–frequency settings.

Importantly, the ShaFrEnGa is *measurement-free* as it does not require any auxiliary photons, post-selection or intense pump for perfoming frequency entanglement, by contrast with fusion-based methods [11] for instance. Nevertheless, in the time-frequency continuous variable framework, the "true" frequency entangling gate has been shown [78, 107] to be quartic in the bosonic creation and annihilation operators, that is *a priori* complicated to carry out experimentally. This quartic Hamiltonian amounts to a rotation of the JSI and acts as a non-linear frequency beam-splitter. This non-linear frequency beam-splitter is a proper unitary gate and is paramount for quantum information protocols, such as universal quantum computing [29]. While obtaining an Hamiltonian which is quartic in the bosonic creation and annihilation operators is particularly relevant within the time-frequency variable framework for time-frequency entanglement, such a Hamiltonian also holds potential for quadrature-based variables. Indeed, quartic operations in bosonic creation and annihilation operators would correspond to non-Gaussian gates, a topic of considerable interest in quantum information processing research. The ShaFrEnGa – a quadratic Hamiltonian in the bosonic creation and annihilation operators – paves the way for both theoretical analyses and experimental realizations of the time–frequency entangling gate in photonic platforms.

ACKNOWLEDGMENT

M. Meguebel acknowledges funding from QuantEduFrance and the Quantum-Saclay Center. M. Federico acknowledges funding from European Union's Horizon Europe research and innovation programme under the project Quantum Secure Network Partnership (QSNP, grant agreement No 101114043). S.F. acknowledges financial support from National Recovery and Resilience Plan (PNRR) Extended Partnership (MUR) project PE0000023-NQSTI, financed by the European Union—Next Generation EU and from the foundation Compagnia di San Paolo, grant vEIcolo no. 121319. We acknowledge discussions with Hélène Ollivier, Eva Maria Gonzalez Ruiz, Hanna le Jeannic, Arne Keller and Pérola Milman for the completion of this manuscript.

Appendix A: Field quantization in a dielectric waveguide

In this appendix, we go over a ready-to-use field quantization in a lossless, nonmagnetic and single mode waveguide inspired from [61] where we additionnaly account for the polarization and the waveguide time-reversal symmetry. Other quantization procedures in a dielectric waveguide [108–110] and more specifically its interaction with an ensemble of point charges [111–113] and a QD [114] can be found in the references therein. A field propagating in a single direction, rightward along the z-axis, the quantized field can be expressed as

$$\hat{\boldsymbol{E}}(\boldsymbol{r}) = \sum_{\sigma} \int_{\mathbb{R}^+} d\beta \; \mathcal{E}_\sigma(\beta) \boldsymbol{E}_\sigma\left(\boldsymbol{r}, \beta\right) \hat{a}_\sigma(\beta) + \text{h.c}, \tag{A1}$$

where σ is the polarization, β the wavenumber, $\mathcal{E}_\sigma(\beta)$ a normalization constant

$$\mathcal{E}_\sigma(\beta) = \sqrt{\frac{\hbar\omega(\beta)}{2\epsilon_0 \int_\Gamma \epsilon(\boldsymbol{\rho}, \beta) |\boldsymbol{E}_\sigma(\boldsymbol{\rho}, \beta)|^2 d^2\boldsymbol{\rho}}} \tag{A2}$$

and $\boldsymbol{E}_\sigma\left(\boldsymbol{r}, \beta\right) = \boldsymbol{E}_\sigma\left(\boldsymbol{\rho}, \beta\right) e^{i\beta z}$ the propagating modes, solution to the wave equation

$$\boldsymbol{\nabla} \times \boldsymbol{\nabla} \times \boldsymbol{E}_\sigma\left(\boldsymbol{r}, \beta\right) - \frac{\omega(\beta)^2}{c^2} \epsilon(\boldsymbol{r}, \beta) \boldsymbol{E}_\sigma\left(\boldsymbol{r}, \beta\right) = \boldsymbol{0}, \tag{A3}$$

where $\boldsymbol{\rho}$ is the transverse coordinate and $\omega(\beta)$ the 1D dispersion relation $\beta^2 = n_{\text{eff}}^2(\omega)\frac{\omega}{c}$ with $n_{\text{eff}}(\omega)$ the effective refractive index. The terme 'effective' encapsulates the idea that the mode propagates as if it were in a homogeneous medium whose refractive index is the average seen by the field. This effective index n_{eff} does not explicity vary with

the transverse coordinate $\boldsymbol{r}$ because all the spatial variations in the dielectric function are contained in the mode profile [115, 116]. These propagating modes constitute an orthogonal basis in such a way that

$$\epsilon_0 \int d^3\boldsymbol{r}\, \epsilon(\boldsymbol{r},\beta)\boldsymbol{E}^*_\sigma(\boldsymbol{r},\beta)\cdot\boldsymbol{E}_{\sigma'}(\boldsymbol{r},\beta') = \delta(\beta-\beta')\delta_{\sigma\sigma'}. \tag{A4}$$

The quantized electric field thus reads

$$\hat{\boldsymbol{E}}(\boldsymbol{r}) = \sum_\sigma \int_{\mathbb{R}^+} d\beta\, \mathcal{E}_\sigma(\beta)\boldsymbol{E}_\sigma(\boldsymbol{\rho},\beta)\, e^{i\beta z}\hat{a}_\sigma(\beta) + \text{h.c.} \tag{A5}$$

From now on, we will group together $\mathcal{E}_\sigma(\beta)$ and $\boldsymbol{E}_\sigma(\boldsymbol{\rho},\beta)$ in a single term $\boldsymbol{\mathcal{E}}_\sigma(\boldsymbol{\rho},\beta)$ for readability. Taking into account the leftward propagating field along the z-axis

$$\hat{\boldsymbol{E}}(\boldsymbol{r}) = \sum_\sigma \int_{\mathbb{R}^+} d\beta \left(\boldsymbol{\mathcal{E}}_\sigma(\boldsymbol{\rho},\beta)e^{i\beta z}\hat{a}_\sigma(\beta) + \boldsymbol{\mathcal{E}}_\sigma(\boldsymbol{\rho},-\beta)e^{-i\beta z}\hat{a}_\sigma(-\beta) + \text{h.c}\right). \tag{A6}$$

From here, we invoke the time-reversal symmetry [117] of the waveguide which enforces

$$\boldsymbol{\mathcal{E}}_\sigma(\boldsymbol{\rho},-\beta) = \boldsymbol{\mathcal{E}}^*_\sigma(\boldsymbol{\rho},\beta), \tag{A7}$$

which entails

$$\hat{\boldsymbol{E}}(\boldsymbol{r}) = \sum_\sigma \sum_{\mu\in\{\pm\}} \int_{\mathbb{R}^+} d\beta\, \boldsymbol{\mathcal{E}}_{\sigma\mu}(\boldsymbol{\rho},\beta)e^{i\beta\mu z}\hat{a}_{\sigma\mu}(\beta) + \text{h.c}, \tag{A8}$$

with

$$\boldsymbol{\mathcal{E}}_{\sigma\mu}(\boldsymbol{\rho},\beta) = \boldsymbol{\mathcal{E}}_\sigma(\boldsymbol{\rho},\mu\beta) \tag{A9}$$

$$\hat{a}_{\sigma\mu}(\beta) = \hat{a}_\sigma(\beta\mu). \tag{A10}$$

The previously introduced bosonic operators fulfill the commutation relations

$$[\hat{a}_{\sigma\mu}(\beta), \hat{a}^\dagger_{\sigma'\mu'}(\beta')] = \delta(\beta-\beta')\delta_{\sigma\sigma'}\delta_{\mu\mu'}. \tag{A11}$$

One can toggle to the frequency $\omega(\beta)$ representation as

$$\hat{\boldsymbol{E}}(\boldsymbol{r}) = \sum_\sigma \sum_{\mu\in\{\pm\}} \int_{\omega_c}^{+\infty} d\omega\, \boldsymbol{\mathcal{E}}_{\sigma\mu}(\boldsymbol{\rho},\beta(\omega))e^{i\beta(\omega)\mu z}\hat{a}_{\sigma\mu}(\omega) + \text{h.c}, \tag{A12}$$

where we have defined

$$\hat{a}_{\sigma\mu}(\omega) = \frac{\hat{a}_{\sigma\mu}(\beta(\omega))}{\sqrt{v_G(\omega)}}, \tag{A13}$$

where $v_G(\omega)$ correspond to the waveguide group velocity at frequency ω and ω_c to the waveguide cutoff frequency respectively. The latter is assumed to be far below the photons' frequency distributions in such a way that one can expand the integral in Eq. (A12) to the entire real line

$$\hat{\boldsymbol{E}}(\boldsymbol{r}) = \sum_\sigma \sum_{\mu\in\{\pm\}} \int_{\mathbb{R}} d\omega\, \boldsymbol{\mathcal{E}}_{\sigma\mu}(\boldsymbol{\rho},\beta(\omega))e^{i\beta(\omega)\mu z}\hat{a}_{\sigma\mu}(\omega) + \text{h.c}, \tag{A14}$$

with the commutation relation expressed with the frequency degree of freedom

$$[\hat{a}_{\sigma\mu}(\omega), \hat{a}^\dagger_{\sigma'\mu'}(\omega')] = \delta(\omega-\omega')\delta_{\sigma\sigma'}\delta_{\mu\mu'}. \tag{A15}$$

The previously defined bosonic operators act as

$$\hat{a}_{\sigma\mu}(\omega)\,|\text{vac}\rangle = 0, \quad \hat{a}_{\sigma\mu}(\omega)\,|\omega'\rangle_{\sigma'\mu'} = \delta_{\sigma\sigma'}\delta(\omega-\omega')\,|\text{vac}\rangle \tag{A16}$$

$$\hat{a}^\dagger_{\sigma\mu}(\omega)\,|\text{vac}\rangle = |\omega\rangle_{\sigma\mu}, \quad \hat{a}^\dagger_{\sigma\mu}(\omega)\,|\omega'\rangle_{\sigma'\mu'} = |\omega',\omega\rangle_{\sigma\mu,\sigma'\mu'}, \tag{A17}$$

where $|\text{vac}\rangle$ is the vacuum state and $|\omega\rangle_{\sigma\mu}$ the state corresponding to one photon at polarization σ traveling in the direction of propagation μ. The field free Hamiltonian reads

$$\hat{H}_{\text{free, field}} = \sum_{\sigma} \sum_{\mu\in\{\pm\}} \int_{\mathbb{R}} d\omega\ \hbar\omega \hat{a}^{\dagger}_{\sigma\mu}(\omega)\hat{a}_{\sigma\mu}(\omega). \tag{A18}$$

For the time-frequency continuous variables framework [29, 30] to mathematically resemble that of electric field quadratures, it is additionally required that no two photons can occupy the same auxiliary modes. For instance, they can share the same propagation direction as long as they have different polarizations.

Appendix B: Transition operators adiabatic elimination

In this appendix, we provide full computation for the adiabatic elimination that leads to the effective interaction Hamiltonian in Sec. II B 2

$$\hat{H}_{\text{int}} = \left(\hat{H}_{\text{int}}\right)_{|0\rangle\leftrightarrow|X_+\rangle\leftrightarrow|2X\rangle} + \left(\hat{H}_{\text{int}}\right)_{|0\rangle\leftrightarrow|X_-\rangle\leftrightarrow|2X\rangle}, \tag{B1}$$

where we divide the two interaction paths

$$\left(\hat{H}_{\text{int}}\right)_{|0\rangle\leftrightarrow|X_\pm\rangle\leftrightarrow|2X\rangle} = \hbar \sum_{\substack{\sigma'\in\{R,L\}\\ \mu'\in\{\pm\}}} \sum_{\substack{\sigma\in\{R,L\}\\ \mu\in\{\pm\}}} \int_{\mathbb{R}^2} d\omega' d\omega \left(g_{X_\pm}^{\sigma'\mu'\sigma\mu}(\omega',\omega)\,|2X\rangle\langle 0|\otimes \hat{a}_{\sigma'\mu'}(\omega')\hat{a}_{\sigma\mu}(\omega) + \text{h.c}\right), \tag{B2}$$

where we incorporate the photon-number-dependent Stark shifts energy renormalization in the natural frequencies. The calculated two-photon coupling terms are shown to be equal to

$$g_{X_\pm}^{\sigma'\mu'\sigma\mu}(\omega',\omega) = g_{X_\pm 2X}^{\sigma'\mu'}(\omega')g_{0X_\pm}^{\sigma\mu}(\omega) \times \left[\frac{1}{\omega-\omega_X} - \frac{1}{\omega'-(\omega_{2X}-\omega_X)}\right]. \tag{B3}$$

In order to demonstrate these results, we consider the Heisenberg picture transition operator $\hat{\xi}_{0X_+}^{\sigma\mu}(\omega,t) \equiv (|X_+\rangle\langle 0|\otimes\hat{a}_{\sigma\mu}(\omega))(t)$ dynamical equation

$$\frac{d\hat{\xi}_{0X_+}^{\sigma\mu}(\omega,t)}{dt} = \frac{1}{i\hbar}\left[\hat{\xi}_{0X_+}^{\sigma\mu}(\omega,t), \hat{H}_H(t)\right], \tag{B4}$$

where the Hamiltonian $\hat{H}_H(t)$ in the Heisenberg picture is equal to the Hamiltonian $\hat{H} = \hat{H}_{\text{free}} + \hat{H}_{\text{int}}$ previously defined

$$\frac{\hat{H}_{\text{free}}}{\hbar} = \omega_{2X}\,|2X\rangle\langle 2X| + \omega_X\left(|X_+\rangle\langle X_+| + |X_-\rangle\langle X_-|\right) + S\left(|X_+\rangle\langle X_-| + |X_-\rangle\langle X_+|\right) + \sum_{\substack{\sigma\in\{R,L\}\\ \mu\in\{\pm\}}} \int_{\mathbb{R}} d\omega\ \omega\hat{a}^{\dagger}_{\sigma\mu}(\omega)\hat{a}_{\sigma\mu}(\omega) \tag{B5}$$

$$\begin{aligned}\frac{\hat{H}_{\text{int}}}{\hbar} = \sum_{\substack{\sigma\in\{R,L\}\\ \mu\in\{\pm\}}} \int_{\mathbb{R}} d\omega \Big(&g_{0X_+}^{\sigma\mu}(\omega)\,|X_+\rangle\langle 0|\otimes\hat{a}_{\sigma\mu}(\omega) + g_{X_+2X}^{\sigma\mu}(\omega)\,|2X\rangle\langle X_+|\otimes\hat{a}_{\sigma\mu}(\omega) + g_{0X_-}^{\sigma\mu}(\omega)\,|X_-\rangle\langle 0|\otimes\hat{a}_{\sigma\mu}(\omega)\\ &+ g_{X_-2X}^{\sigma\mu}(\omega)\,|2X\rangle\langle X_-|\otimes\hat{a}_{\sigma\mu}(\omega) + \text{h.c.}\Big)\end{aligned} \tag{B6}$$

in the Schrödinger picture because the latter is time-independent. This joint operator characterizes the QD transition from its ground state $|0\rangle$ to its excitonic state $|X_+\rangle$ by absorbing a photon of frequency ω, polarization σ and direction of propagation μ. The photons driving the excitonic transitions $|0\rangle\leftrightarrow|X_\pm\rangle$ and the biexcitonic transitions $|X_\pm\rangle\leftrightarrow|2X\rangle$ are referred to as *excitonic* and *biexcitonic* photons respectively. It is important to note that the time t represents the dynamical time in the Hamiltonian evolution and not to the *time-of-arrival* defined in the context of time-frequency continuous variables. Within the free Hamiltonian dynamics, this dynamical time simply amounts

to an offset of the time-of-arrival while its action is *a priori* no longer nontrivial when accounting for the interaction. One can compute the following

$$\hat{\xi}^{\sigma\mu}_{0X_+}(\omega,t)\frac{\hat{H}}{\hbar} = \left(\hat{\xi}^{\sigma\mu}_{0X_+}(\omega)\sum_{\substack{\sigma'\in\{R,L\}\\ \mu'\in\{\pm\}}}\int_{\mathbb{R}} d\omega'\ \omega'\hat{a}^\dagger_{\sigma'\mu'}(\omega')\hat{a}_{\sigma'\mu'}(\omega')\right)(t) + \left(\sum_{\substack{\sigma'\in\{R,L\}\\ \mu'\in\{\pm\}}}\int_{\mathbb{R}} d\omega'\ \left(g^{\sigma'\mu'*}_{0X_+}(\omega')\left|X_+\right\rangle\left\langle X_+\right|\otimes\hat{a}_{\sigma\mu}(\omega)\hat{a}^\dagger_{\sigma'\mu'}(\omega') + g^{\sigma'\mu'*}_{0X_-}(\omega')\left|X_+\right\rangle\left\langle X_-\right|\otimes\hat{a}_{\sigma\mu}(\omega)\hat{a}^\dagger_{\sigma'\mu'}(\omega')\right)\right)(t) \tag{B7}$$

and

$$\frac{\hat{H}}{\hbar}\hat{\xi}^{\sigma\mu}_{0X_+}(\omega,t) = \omega_X\hat{\xi}^{\sigma\mu}_{0X_+}(\omega,t) + S\hat{\xi}^{\sigma\mu}_{0X_-}(\omega,t) + \left(\sum_{\substack{\sigma'\in\{R,L\}\\ \mu'\in\{\pm\}}}\int_{\mathbb{R}} d\omega'\ \omega'\hat{a}^\dagger_{\sigma'\mu'}(\omega')\hat{a}_{\sigma'\mu'}(\omega')\hat{\xi}^{\sigma\mu}_{0X_+}(\omega)\right)(t) \left(\sum_{\substack{\sigma'\in\{R,L\}\\ \mu'\in\{\pm\}}}\int_{\mathbb{R}} d\omega'\ \left(g^{\sigma'\mu'*}_{0X_+}(\omega')\left|0\right\rangle\left\langle 0\right|\otimes\hat{a}^\dagger_{\sigma'\mu'}(\omega')\hat{a}_{\sigma\mu}(\omega) + g^{\sigma'\mu'}_{X_+2X}(\omega')\left|2X\right\rangle\left\langle 0\right|\otimes\hat{a}_{\sigma'\mu'}(\omega')\hat{a}_{\sigma\mu}(\omega)\right)\right)(t), \tag{B8}$$

where as in Eq. (B5) we dropped out the identity operators and therefore the tensor products for readability. The joint operator $\hat{\xi}^{\sigma\mu}_{0X_-}(\omega) \equiv \left|X_-\right\rangle\left\langle 0\right|\otimes\hat{a}_{\sigma\mu}(\omega)$ is defined in the same way as $\hat{\xi}^{\sigma\mu}_{0X_+}(\omega)$. This operator physically represents an optical transition from the ground state to the excitonic state $\left|X_-\right\rangle$ with a σ-polarized photon by means of the fine-structure splitting S coupling – thus bypassing the optical selection rules which do not allow the $\left|0\right\rangle \leftrightarrow \left|X_\pm\right\rangle$ transitions for the same polarization σ and direction of propagation μ. Injecting Eq. (B7) and Eq. (B8) in the transition operator equation of motion Eq. (B4)

$$i\frac{d\hat{\xi}^{\sigma\mu}_{0X_+}(\omega,t)}{dt} = -\omega_X\hat{\xi}^{\sigma\mu}_{0X_+}(\omega,t) + \left(\left|X_+\right\rangle\left\langle 0\right|\otimes\sum_{\substack{\sigma'\in\{R,L\}\\ \mu'\in\{\pm\}}}\int_{\mathbb{R}} d\omega'\ \omega'\left[\hat{a}_{\sigma\mu}(\omega),\hat{a}^\dagger_{\sigma'\mu'}(\omega')\hat{a}_{\sigma'\mu'}(\omega')\right]\right)(t) - S\hat{\xi}^{\sigma\mu}_{0X_-}(\omega,t) + \left(\sum_{\substack{\sigma'\in\{R,L\}\\ \mu'\in\{\pm\}}}\int_{\mathbb{R}} d\omega'\ \left(g^{\sigma'\mu'*}_{0X_+}(\omega')\left|X_+\right\rangle\left\langle X_+\right|\otimes\hat{a}_{\sigma\mu}(\omega)\hat{a}^\dagger_{\sigma'\mu'}(\omega') - g^{\sigma'\mu'*}_{0X_+}(\omega')\left|0\right\rangle\left\langle 0\right|\otimes\hat{a}^\dagger_{\sigma'\mu'}(\omega')\hat{a}_{\sigma\mu}(\omega)\right)\right)(t) + \left(\sum_{\substack{\sigma'\in\{R,L\}\\ \mu'\in\{\pm\}}}\int_{\mathbb{R}} d\omega'\ \left(g^{\sigma'\mu'*}_{0X_-}(\omega')\left|X_+\right\rangle\left\langle X_-\right|\otimes\hat{a}_{\sigma\mu}(\omega)\hat{a}^\dagger_{\sigma'\mu'}(\omega') - g^{\sigma'\mu'}_{X_+2X}(\omega')\left|2X\right\rangle\left\langle 0\right|\otimes\hat{a}_{\sigma'\mu'}(\omega')\hat{a}_{\sigma\mu}(\omega)\right)\right)(t). \tag{B9}$$

The bosonic commutation relations lead to

$$\left[\hat{a}_{\sigma\mu}(\omega),\hat{a}^\dagger_{\sigma'\mu'}(\omega')\hat{a}_{\sigma'\mu'}(\omega')\right] = \delta_{\mu\mu'}\delta_{\sigma\sigma'}\delta(\omega-\omega')\hat{a}_{\sigma'\mu'}(\omega), \tag{B10}$$

in such a way that

$$
\begin{aligned}
i\frac{d\hat{\xi}^{\sigma\mu}_{0X_+}(\omega,t)}{dt} &= (\omega-\omega_X)\,\hat{\xi}^{\sigma\mu}_{0X_+}(\omega,t) - S\hat{\xi}^{\sigma\mu}_{0X_-}(\omega,t) \\
&+ \left(\sum_{\substack{\sigma'\in\{R,L\}\\ \mu'\in\{\pm\}}}\int_{\mathbb{R}} d\omega'\ \left(g^{\sigma'\mu'*}_{0X_+}(\omega')\,|X_+\rangle\langle X_+|\otimes\hat{a}_{\sigma\mu}(\omega)\hat{a}^\dagger_{\sigma'\mu'}(\omega') - g^{\sigma'\mu'*}_{0X_+}(\omega')\,|0\rangle\langle 0|\otimes\hat{a}^\dagger_{\sigma'\mu'}(\omega')\hat{a}_{\sigma\mu}(\omega)\right)\right)(t) \\
&+ \left(\sum_{\substack{\sigma'\in\{R,L\}\\ \mu'\in\{\pm\}}}\int_{\mathbb{R}} d\omega'\ \left(g^{\sigma'\mu'*}_{0X_-}(\omega')\,|X_+\rangle\langle X_-|\otimes\hat{a}_{\sigma\mu}(\omega)\hat{a}^\dagger_{\sigma'\mu'}(\omega') - g^{\sigma'\mu'}_{X_+2X}(\omega')\,|2X\rangle\langle 0|\otimes\hat{a}_{\sigma'\mu'}(\omega')\hat{a}_{\sigma\mu}(\omega)\right)\right)(t).
\end{aligned}
\tag{B11}
$$

A solution to this differential equation is

$$
\hat{\xi}^{\sigma\mu}_{0X_+}(\omega,t) = e^{-i(\omega-\omega_X)t}\hat{\xi}^{\sigma\mu}_{0X_+}(\omega,0) + \hat{l}^{\sigma\mu}_{0X_+}(\omega,t),
\tag{B12}
$$

where the first term $e^{-i(\omega-\omega_X)t}\hat{\xi}^{\sigma\mu}_{0X_+}(\omega,0)$ comes from the homogeneous differential equation

$$
i\frac{d\hat{\xi}^{\sigma\mu}_{0X_+}(\omega,t)_{\text{homogeneous}}}{dt} = (\omega-\omega_X)\,\hat{\xi}^{\sigma\mu}_{0X_+}(\omega,t)_{\text{homogeneous}}
\tag{B13}
$$

and $\hat{l}^{\sigma\mu}_{0X_+}(\omega,t)$ is a particular solution to the differential equation (B11) and is chosen as $\hat{l}^{\sigma\mu}_{0X_+}(\omega,t) = e^{-i(\omega-\omega_X)t}\hat{k}^{\sigma\mu}_{0X+}(\omega,t)$ where $\hat{k}^{\sigma\mu}_{0X_+}(\omega,t)$ is a differentiable operator fulfilling

$$
\begin{aligned}
&ie^{-i(\omega-\omega_X)t}\frac{d\hat{k}^{\sigma\mu}_{0X_+}(\omega,t)}{dt} = -S\hat{\xi}^{\sigma\mu}_{0X_-}(\omega,t) \\
&+ \left(\sum_{\substack{\sigma'\in\{R,L\}\\ \mu'\in\{\pm\}}}\int_{\mathbb{R}} d\omega'\ \left(g^{\sigma'\mu'*}_{0X_+}(\omega')\,|X_+\rangle\langle X_+|\otimes\hat{a}_{\sigma\mu}(\omega)\hat{a}^\dagger_{\sigma'\mu'}(\omega') - g^{\sigma'\mu'*}_{0X_+}(\omega')\,|0\rangle\langle 0|\otimes\hat{a}^\dagger_{\sigma'\mu'}(\omega')\hat{a}_{\sigma\mu}(\omega)\right)\right)(t) \\
&+ \left(\sum_{\substack{\sigma'\in\{R,L\}\\ \mu'\in\{\pm\}}}\int_{\mathbb{R}} d\omega'\ \left(g^{\sigma'\mu'*}_{0X_-}(\omega')\,|X_+\rangle\langle X_-|\otimes\hat{a}_{\sigma\mu}(\omega)\hat{a}^\dagger_{\sigma'\mu'}(\omega') - g^{\sigma'\mu'}_{X_+2X}(\omega')\,|2X\rangle\langle 0|\otimes\hat{a}_{\sigma'\mu'}(\omega')\hat{a}_{\sigma\mu}(\omega)\right)\right)(t).
\end{aligned}
\tag{B14}
$$

Formally integrating Eq. (B14)

$$
\begin{aligned}
\hat{k}^{\sigma\mu}_{0X+}(\omega,t) &= i\int_0^t d\tau\ e^{i(\omega-\omega_X)\tau}S\hat{\xi}^{\sigma\mu}_{0X_-}(\omega,\tau) \\
&- i\int_0^t d\tau\ e^{i(\omega-\omega_X)\tau}\left(\sum_{\substack{\sigma'\in\{R,L\}\\ \mu'\in\{\pm\}}}\int_{\mathbb{R}} d\omega'\ \left(g^{\sigma'\mu'*}_{0X_+}(\omega')\,|X_+\rangle\langle X_+|\otimes\hat{a}_{\sigma\mu}(\omega)\hat{a}^\dagger_{\sigma'\mu'}(\omega') - g^{\sigma'\mu'*}_{0X_+}(\omega')\,|0\rangle\langle 0|\otimes\hat{a}^\dagger_{\sigma'\mu'}(\omega')\hat{a}_{\sigma\mu}(\omega)\right)\right)(\tau) \\
&- i\int_0^t d\tau\ e^{i(\omega-\omega_X)\tau}\left(\sum_{\substack{\sigma'\in\{R,L\}\\ \mu'\in\{\pm\}}}\int_{\mathbb{R}} d\omega'\ \left(g^{\sigma'\mu'*}_{0X_-}(\omega')\,|X_+\rangle\langle X_-|\otimes\hat{a}_{\sigma\mu}(\omega)\hat{a}^\dagger_{\mu'\sigma'}(\omega') - g^{\sigma'\mu'}_{X_+2X}(\omega')\,|2X\rangle\langle 0|\otimes\hat{a}_{\sigma'\mu'}(\omega')\hat{a}_{\sigma\mu}(\omega)\right)\right)(\tau).
\end{aligned}
\tag{B15}
$$

From here, the adiabatic elimination consists in identifying and comparing evolution time scales. The exponential term $e^{i(\omega-\omega_X)\tau}$ oscillates at frequency $|\omega-\omega_X|$ with ω being the frequency of the photon driving the excitonic transition.

On the other hand, up to the zeroth-order in the coupling terms $g_{\cdot\cdot}(.)$ and S – which again drives the $|X_+\rangle \leftrightarrow |X_-\rangle$ transition – in Eq. (B15), the time-dependent two-photon joint transition operators in the Heisenberg picture $\left(|X_+\rangle\langle X_+| \otimes \hat{a}_{\sigma\mu}(\omega)\hat{a}^\dagger_{\sigma'\mu'}(\omega')\right)(\tau)$, $\left(|0\rangle\langle 0| \otimes \hat{a}^\dagger_{\sigma'\mu'}(\omega')\hat{a}_{\sigma\mu}(\omega)\right)(\tau)$ and $\left(|X_+\rangle\langle X_-| \otimes \hat{a}_{\sigma\mu}(\omega)\hat{a}^\dagger_{\sigma'\mu'}(\omega')\right)(\tau)$ evolve according to the time-evolution equation at a frequency $|\omega-\omega'|$ with ω and ω' matching the excitonic photon spectral distribution while $(|2X\rangle\langle 0| \otimes \hat{a}_{\sigma'\mu'}(\omega')\hat{a}_{\sigma\mu}(\omega))(\tau)$ evolves at a frequency $|\omega_{2X}-(\omega+\omega')|$ with ω and ω' matching the excitonic and biexcitonic photons spectral distributions respectively. Subsequently, provided the detuning $\delta_e(\omega) \equiv \omega-\omega_X$ is large in absolute value compared to $|\omega-\omega'|$ – representing the excitonic photon spectral bandwidth $\Delta\omega_e$ – and compared to the two-photon transition $|2X\rangle \leftrightarrow |0\rangle$ detuning $|\omega_{2X}-(\omega+\omega')| \approx |\omega_{2X}-(\omega_e+\omega_b)|$ where ω_e and ω_b denote the central frequencies of the excitonic and biexcitonic photons respectively, the previous solution reads

$$\begin{aligned}
\hat{k}^{\sigma\mu}_{0X_+}(\omega,t) &= i\int_0^t d\tau\, e^{i(\omega-\omega_X)\tau} S\hat{\xi}^{\sigma\mu}_{0X_-}(\omega,\tau) \\
&+ \left(\frac{1-e^{i(\omega-\omega_X)t}}{\omega-\omega_X}\right)\left(\sum_{\substack{\sigma'\in\{R,L\}\\ \mu'\in\{\pm\}}}\int_{\mathbb{R}} d\omega'\ \left(g^{\sigma'\mu'*}_{0X_+}(\omega')\,|X_+\rangle\langle X_+| \otimes \hat{a}_{\sigma\mu}(\omega)\hat{a}^\dagger_{\sigma'\mu'}(\omega') - g^{\sigma'\mu'*}_{0X_+}(\omega')\,|0\rangle\langle 0| \otimes \hat{a}^\dagger_{\sigma'\mu'}(\omega')\hat{a}_{\sigma\mu}(\omega)\right)\right) \\
&+ \left(\frac{1-e^{i(\omega-\omega_X)t}}{\omega-\omega_X}\right)\left(\sum_{\substack{\sigma'\in\{R,L\}\\ \mu'\in\{\pm\}}}\int_{\mathbb{R}} d\omega'\ \left(g^{\sigma'\mu'*}_{0X_-}(\omega')\,|X_+\rangle\langle X_-| \otimes \hat{a}_{\sigma\mu}(\omega)\hat{a}^\dagger_{\sigma'\mu'}(\omega') - g^{\sigma'\mu'}_{X_+2X}(\omega')\,|2X\rangle\langle 0| \otimes \hat{a}_{\sigma'\mu'}(\omega')\hat{a}_{\sigma\mu}(\omega)\right)\right)
\end{aligned} \tag{B16}$$

for a time t such that

$$1/|\delta_e(\omega)| \ll t \ll 1/\Delta\omega_e, 1/|\omega_{2X}-(\omega_e+\omega_b)|, \tag{B17}$$

so that the transition operators are essentially constant during the time of evolution during which the exponential term had had the time to average out to zero. Note that this amounts to a Markovian approximation where memory effects are disregarded [47]. Nonetheless, the last transition operator $\hat{\xi}^{\sigma\mu}_{0X_-}(\omega,t)$ evolves as the same frequency as $\hat{\xi}^{\sigma\mu}_{0X_+}(\omega,t)$ that is to say $|\omega-\omega_X|$ with ω matching the excitonic photon spectral distribution. This operator thus cannot be considered constant during the interaction time t. However, the first term in Eq. (B16) holding the FSS S can – in the similar fashion to Eq. (B12) – be expressed as

$$\begin{aligned}
i\int_0^t d\tau e^{i(\omega-\omega_X)\tau} S\hat{\xi}^{\sigma\mu}_{0X_-}(\omega,\tau) &= i\int_0^t d\tau e^{i(\omega-\omega_X)\tau} S \times \left(e^{-i(\omega-\omega_X)\tau}\hat{\xi}^{\sigma\mu}_{0X_-}(\omega,0) + \hat{l}^{\sigma\mu}_{0X_-}(\omega,\tau)\right) \\
&= iSt\hat{\xi}^{\sigma\mu}_{0X_-}(\omega,0) + iS\int_0^t d\tau e^{i(\omega-\omega_X)\tau}\hat{l}^{\sigma\mu}_{0X_-}(\omega,\tau).
\end{aligned} \tag{B18}$$

As for $\hat{l}^{\sigma\mu}_{0X_+}(t)$, $\hat{l}^{\sigma\mu}_{0X_-}(\tau)$ can be expressed as $e^{-i(\omega-\omega_X)\tau}\hat{k}^{\sigma\mu}_{0X_-}(\omega,\tau)$ with $\hat{k}^{\sigma\mu}_{0X_-}(\omega,\tau)$ fulfilling an equation identical to Eq. (B15)

$$\begin{aligned}
\hat{k}^{\sigma\mu}_{0X_-}(\omega,t) &= i\int_0^t d\tau\, e^{i(\omega-\omega_X)\tau} S\hat{\xi}^{\sigma\mu}_{0X_+}(\omega,\tau) \\
&- i\int_0^t d\tau\, e^{i(\omega-\omega_X)\tau}\left(\sum_{\substack{\sigma'\in\{R,L\}\\ \mu'\in\{\pm\}}}\int_{\mathbb{R}} d\omega'\ \left(g^{\sigma'\mu'*}_{0X_-}(\omega')\,|X_-\rangle\langle X_-| \otimes \hat{a}_{\sigma\mu}(\omega)\hat{a}^\dagger_{\sigma'\mu'}(\omega') - g^{\sigma'\mu'*}_{0X_-}(\omega')\,|0\rangle\langle 0| \otimes \hat{a}^\dagger_{\sigma'\mu'}(\omega')\hat{a}_{\sigma\mu}(\omega)\right)\right)(\tau) \\
&- i\int_0^t d\tau\, e^{i(\omega-\omega_X)\tau}\left(\sum_{\substack{\sigma'\in\{R,L\}\\ \mu'\in\{\pm\}}}\int_{\mathbb{R}} d\omega'\ \left(g^{\sigma'\mu'*}_{0X_+}(\omega')\,|X_-\rangle\langle X_+| \otimes \hat{a}_{\sigma\mu}(\omega)\hat{a}^\dagger_{\mu'\sigma'}(\omega') - g^{\sigma'\mu'}_{X_-2X}(\omega')\,|2X\rangle\langle 0| \otimes \hat{a}_{\sigma'\mu'}(\omega')\hat{a}_{\sigma\mu}(\omega)\right)\right)(\tau).
\end{aligned} \tag{B19}$$

This term is multiplied by S and is therefore a second order term in coupling terms S and $g^{\cdot\cdot}_{\cdot\cdot}(.)$ that we neglect as done above. The fast-oscillating contribution in $\hat{\xi}^{\sigma\mu}_{0X_-}(\omega,\tau)$ can thus be ignored in Eq. (B16) and the particular solution to the differential equation Eq. (B11) $\hat{l}^{\sigma\mu}_{0X_+}(\omega,t) = e^{-i(\omega-\omega_X)t}\hat{k}^{\sigma\mu}_{0X_+}(\omega,t)$ thus yields

$$\begin{aligned}
&\hat{l}^{\sigma\mu}_{0X_+}(\omega,t) = e^{-i(\omega-\omega_X)t} \times iSt\hat{\xi}^{\sigma\mu}_{0X_-}(\omega,0) \\
&\left(\frac{e^{-i(\omega-\omega_X)t}-1}{\omega-\omega_X}\right)\left(\sum_{\substack{\sigma'\in\{R,L\}\\ \mu'\in\{\pm\}}}\int_{\mathbb{R}} d\omega' \ \left(g^{\sigma'\mu'*}_{0X_+}(\omega')\left|X_+\right\rangle\left\langle X_+\right|\otimes\hat{a}_{\sigma\mu}(\omega)\hat{a}^\dagger_{\sigma'\mu'}(\omega') - g^{\sigma'\mu'*}_{0X_+}(\omega')\left|0\right\rangle\left\langle 0\right|\otimes\hat{a}^\dagger_{\sigma'\mu'}(\omega')\hat{a}_{\sigma\mu}(\omega)\right)\right) \\
&+\left(\frac{e^{-i(\omega-\omega_X)t}-1}{\omega-\omega_X}\right)\left(\sum_{\substack{\sigma'\in\{R,L\}\\ \mu'\in\{\pm\}}}\int_{\mathbb{R}} d\omega' \ \left(g^{\sigma'\mu'*}_{0X_-}(\omega')\left|X_+\right\rangle\left\langle X_-\right|\otimes\hat{a}_{\sigma\mu}(\omega)\hat{a}^\dagger_{\sigma'\mu'}(\omega') - g^{\sigma'\mu'}_{X_+2X}(\omega')\left|2X\right\rangle\left\langle 0\right|\otimes\hat{a}_{\sigma'\mu'}(\omega')\hat{a}_{\sigma\mu}(\omega)\right)\right).
\end{aligned} \tag{B20}$$

Putting Eq. (B20) in the solution to the differential equation Eq. (B12) and taking out the $e^{-i(\omega-\omega_X)t}$ fast-oscillating term that averages out to zero over the interaction time t

$$\begin{aligned}
\hat{\xi}^{\sigma\mu}_{0X_+}(\omega,t) = -\frac{1}{\omega-\omega_X}\sum_{\substack{\sigma'\in\{R,L\}\\ \mu'\in\{\pm\}}}\int_{\mathbb{R}} d\omega' \ \Big(&g^{\sigma'\mu'*}_{0X_+}(\omega')\left|X_+\right\rangle\left\langle X_+\right|\otimes\hat{a}_{\sigma\mu}(\omega)\hat{a}^\dagger_{\sigma'\mu'}(\omega') - g^{\sigma'\mu'*}_{0X_+}(\omega')\left|0\right\rangle\left\langle 0\right|\otimes\hat{a}^\dagger_{\sigma'\mu'}(\omega')\hat{a}_{\sigma\mu}(\omega) \\
&+ g^{\sigma'\mu'*}_{0X_-}(\omega')\left|X_+\right\rangle\left\langle X_-\right|\otimes\hat{a}_{\sigma\mu}(\omega)\hat{a}^\dagger_{\sigma'\mu'}(\omega') - g^{\sigma'\mu'}_{X_+2X}(\omega')\left|2X\right\rangle\left\langle 0\right|\otimes\hat{a}_{\sigma'\mu'}(\omega')\hat{a}_{\sigma\mu}(\omega)\Big),
\end{aligned} \tag{B21}$$

which no longer depends on the interaction time t and can therefore be taken as time-independent throughout the evolution. Their Schrödinger and Heisenberg representations are thus identical for this interaction time. With exactly the same reasoning, the biexcitonic transition operator $\hat{\xi}^{\sigma\mu}_{X_+2X}(\omega,t)$ can be shown to read

$$\begin{aligned}
\hat{\xi}^{\sigma\mu}_{X_+2X}(\omega,t) = -\frac{1}{\omega-(\omega_{2X}-\omega_X)}\sum_{\substack{\sigma'\in\{R,L\}\\ \mu'\in\{\pm\}}}\int_{\mathbb{R}} d\omega' \ \Big(&g^{\sigma'\mu'*}_{X_+2X}(\omega')\left|2X\right\rangle\left\langle 2X\right|\otimes\hat{a}_{\sigma\mu}(\omega)\hat{a}^\dagger_{\sigma'\mu'}(\omega') \\
&- g^{\sigma'\mu'*}_{X_+2X}(\omega')\left|X_+\right\rangle\left\langle X_+\right|\otimes\hat{a}^\dagger_{\sigma'\mu'}(\omega')\hat{a}_{\sigma\mu}(\omega) \\
&- g^{\sigma'\mu'*}_{X_-2X}(\omega')\left|X_-\right\rangle\left\langle X_+\right|\otimes\hat{a}^\dagger_{\sigma'\mu'}(\omega')\hat{a}_{\sigma\mu}(\omega) + g^{\sigma'\mu'}_{0X_+}(\omega')\left|2X\right\rangle\left\langle 0\right|\otimes\hat{a}_{\sigma\mu}(\omega)\hat{a}_{\sigma'\mu'}(\omega')\Big),
\end{aligned} \tag{B22}$$

which is again time-independent for an interaction time t such that

$$1/|\delta_b(\omega)| \ll t \ll 1/\Delta\omega_b, 1/|\omega_{2X}-(\omega_e+\omega_b)|, \tag{B23}$$

with $\delta_b(\omega) \equiv \omega-(\omega_{2X}-\omega_X)$ and $\Delta\omega_b$ the biexcitonic photon spectral bandwidth.
Injecting back these two joint operators $\hat{\xi}^{\sigma\mu}_{0X_+}(\omega)$ Eq. (B21) and $\hat{\xi}^{\sigma\mu}_{X_+2X}(\omega)$ Eq. (B22) in the $|0\rangle \leftrightarrow |X_+\rangle \leftrightarrow |2X\rangle$ branch of the interaction Hamiltonian Eq. (B6)

$$\begin{aligned}\left(\hat{H}_{\text{int}}\right)_{|0\rangle\leftrightarrow|X_+\rangle\leftrightarrow|2X\rangle} = \hbar \sum_{\substack{\sigma'\in\{R,L\}\\ \mu'\in\{\pm\}}} \sum_{\substack{\sigma\in\{R,L\}\\ \mu\in\{\pm\}}} \int_{\mathbb{R}^2} d\omega d\omega' \Bigg[-\frac{1}{\omega-\omega_X}\Bigg(g_{0X_+}^{\sigma\mu}(\omega) g_{0X_+}^{\sigma'\mu'*}(\omega') \big[|X_+\rangle\langle X_+| \otimes \hat{a}_{\sigma\mu}(\omega)\hat{a}^\dagger_{\sigma'\mu'}(\omega') \\ - |0\rangle\langle 0| \otimes \hat{a}^\dagger_{\sigma'\mu'}(\omega')\hat{a}_{\sigma\mu}(\omega)\big] + g_{0X_+}^{\sigma\mu}(\omega) g_{0X_-}^{\sigma'\mu'*}(\omega') |X_+\rangle\langle X_-| \otimes \hat{a}_{\sigma\mu}(\omega)\hat{a}^\dagger_{\sigma'\mu'}(\omega') \\ - g_{X_+2X}^{\sigma'\mu'}(\omega') g_{0X_+}^{\sigma\mu}(\omega) |2X\rangle\langle 0| \otimes \hat{a}_{\sigma'\mu'}(\omega')\hat{a}_{\sigma\mu}(\omega)\Bigg) \\ - \frac{1}{\omega-(\omega_{2X}-\omega_X)}\Bigg(g_{X_+2X}^{\sigma\mu}(\omega) g_{X_+2X}^{\sigma'\mu'*}(\omega') \big[|2X\rangle\langle 2X| \otimes \hat{a}_{\sigma\mu}(\omega)\hat{a}^\dagger_{\sigma'\mu'}(\omega') \\ - |X_+\rangle\langle X_+| \otimes \hat{a}^\dagger_{\sigma'\mu'}(\omega')\hat{a}_{\sigma\mu}(\omega)\big] \\ - g_{X_-2X}^{\sigma'\mu'*}(\omega') g_{X_+2X}^{\sigma\mu}(\omega) |X_-\rangle\langle X_+| \otimes \hat{a}^\dagger_{\sigma'\mu'}(\omega')\hat{a}_{\sigma\mu}(\omega) \\ + g_{X_+2X}^{\sigma\mu}(\omega) g_{0X_+}^{\sigma'\mu'}(\omega') |2X\rangle\langle 0| \otimes \hat{a}_{\sigma\mu}(\omega)\hat{a}_{\sigma'\mu'}(\omega')\Bigg)\Bigg] + \text{h.c.}\end{aligned} \tag{B24}$$

These expressions are similar to those found in [75] wherein the derivation was performed for two frequency modes of the electromagnetic field applying a Schrieffer-Wolff transformation [118]. The diagonal terms related to $|X_+\rangle\langle X_+|$, $|0\rangle\langle 0|$ and $|2X\rangle\langle 2X|$ correspond to the intensity- dependent Stark shifts and act as energy renormalization terms in the free Hamiltonian that we thus drop out in the equations for readability. The terms in $|X_+\rangle\langle X_-|$ are two-photon transition terms arising from the excitonic joint transition operator. Indeed, for the terms in $g_{0X_+}^{\sigma\mu}(\omega) g_{0X_-}^{\sigma'\mu'*}(\omega')$ (respectively $g_{X_-2X}^{\sigma'\mu'*}(\omega') g_{X_+2X}^{\sigma\mu}(\omega)$), since $\hat{\xi}_{0X_+}^{\sigma\mu}(\omega,t)$ and $\hat{\xi}_{0X_-}^{\sigma'\mu'\dagger}(\omega',t)$ evolve rapidly in the adiabatic elimination regime, for a QD that goes from its excitonic state $|X_-\rangle$ (respectively $|X_+\rangle$) to its ground state $|0\rangle$ (respectively excited state $|2X\rangle$) before being promoting back up (respectively decaying down to) to its other excitonic state, all appears as if it went from $|X_-\rangle$ to $|X_+\rangle$ (respectively $|X_+\rangle$ to $|X_-\rangle$) by first emitting (respectively absorbing) a photon and then absorbing (respectively emitting) a photon. Nonetheless, this transition only occurs provided one of the two excitonic states is populated which they are not on average over the interaction time t given that the transition operators that promote the QD to these states have been adiabatically eliminated. Therefore, the $|0\rangle \leftrightarrow |X_+\rangle \leftrightarrow |2X\rangle$ branch of the interaction Hamiltonian now yields

$$\begin{aligned}\left(\hat{H}_{\text{int}}\right)_{|0\rangle\leftrightarrow|X_+\rangle\leftrightarrow|2X\rangle} = \hbar \sum_{\substack{\sigma'\in\{R,L\}\\ \mu'\in\{\pm\}}} \sum_{\substack{\sigma\in\{R,L\}\\ \mu\in\{\pm\}}} \int_{\mathbb{R}^2} d\omega d\omega' \Bigg[-\frac{1}{\omega-\omega_X}\Bigg(- g_{0X_+}^{\sigma\mu}(\omega) g_{X_+2X}^{\sigma'\mu'}(\omega') |2X\rangle\langle 0| \otimes \hat{a}_{\sigma'\mu'}(\omega')\hat{a}_{\sigma\mu}(\omega)\Bigg) \\ - \frac{1}{\omega-(\omega_{2X}-\omega_X)}\Bigg(g_{X_+2X}^{\sigma\mu}(\omega) g_{0X_+}^{\sigma'\mu'}(\omega') |2X\rangle\langle 0| \otimes \hat{a}_{\sigma\mu}(\omega)\hat{a}_{\sigma'\mu'}(\omega')\Bigg)\Bigg] + \text{h.c.}\end{aligned} \tag{B25}$$

Reordering the dumb indices ω and ω'

$$\begin{aligned}\left(\hat{H}_{\text{int}}\right)_{|0\rangle\leftrightarrow|X_+\rangle\leftrightarrow|2X\rangle} = \hbar \sum_{\substack{\sigma'\in\{R,L\}\\ \mu'\in\{\pm\}}} \sum_{\substack{\sigma\in\{R,L\}\\ \mu\in\{\pm\}}} \int_{\mathbb{R}^2} d\omega d\omega' \; g_{0X_+}^{\sigma\mu}(\omega) g_{X_+2X}^{\sigma'\mu'}(\omega') \left[\frac{1}{\omega-\omega_X} - \frac{1}{\omega'-(\omega_{2X}-\omega_X)}\right] |2X\rangle\langle 0| \\ \otimes \hat{a}_{\sigma'\mu'}(\omega')\hat{a}_{\sigma\mu}(\omega) + \text{h.c.}\end{aligned} \tag{B26}$$

Adding the $|0\rangle \leftrightarrow |X_-\rangle \leftrightarrow |2X\rangle$ branch, the total effective interaction Hamiltonian reads

$$\hat{H}_{\text{int,eff}} = \hbar \sum_{\substack{\sigma'\in\{R,L\}\\ \mu'\in\{\pm\}}} \sum_{\substack{\sigma\in\{R,L\}\\ \mu\in\{\pm\}}} \int_{\mathbb{R}^2} d\omega' d\omega \;\; |2X\rangle\langle 0| \otimes \left[g_{X_+}^{\sigma'\mu'\sigma\mu}(\omega',\omega)\hat{a}_{\sigma'\mu'}(\omega')\hat{a}_{\sigma\mu}(\omega) + g_{X_-}^{\sigma'\mu'\sigma\mu}(\omega',\omega)\hat{a}_{\sigma'\mu'}(\omega')\hat{a}_{\sigma\mu}(\omega)\right] + \text{h.c,} \tag{B27}$$

with

$$g_{X_\pm}^{\sigma'\mu'\sigma\mu}(\omega',\omega) = g_{X_\pm 2X}^{\sigma'\mu'}(\omega') g_{0X_\pm}^{\sigma\mu}(\omega) \left[\frac{1}{\omega-\omega_X} - \frac{1}{\omega'-(\omega_{2X}-\omega_X)}\right]. \tag{B28}$$

In other words, we obtained an effective two-photon Hamiltonian for which the coupling terms are non-separable in the two photons frequencies ω and ω'. These calculations have been performed up to first order in the coupling terms S and $g^{\cdot}_{\cdot\cdot}(.)$ in the one-photon joint transition operators and to the zeroth-order in the two-photon transition operators. This resulted in a total Hamiltonian Eq. (B27) with up to second order coupling terms. In that regard, within the adiabatic elimination, the fine-structrue splitting S would have contributed to a two-photon interaction if we had considered coupling terms up to the third order in the effective Hamiltonian. This stands to reason because this would be driven by $g^{\sigma\mu}_{0X_\pm}(\omega)$ (respectively $g^{\sigma\mu *}_{X_\pm 2X}(\omega)$) for the transitions $|0\rangle \to |X_\pm\rangle$ (respectively $|2X\rangle \to |X_\pm\rangle$), then a coupling $|X_\pm\rangle \leftrightarrow |X_\mp\rangle$ through S then the transition $|X_\mp\rangle \to |0\rangle$ or $|X_\mp\rangle \to |2X\rangle$ (respectively $|X_\mp\rangle \to |2X\rangle$ or $|X_\mp\rangle \to |0\rangle$) with the coupling term $g^{\sigma\mu *}_{0X_\mp}(\omega)$ or $g^{\sigma\mu}_{X_\mp 2X}(\omega)$ (respectively $g^{\sigma\mu}_{X_\mp 2X}(\omega)$ or $g^{\sigma\mu *}_{0X_\mp}(\omega)$). Considering one-photon joint operators instead of either bare states [46, 47] or bare operators [77] has several key benefits. (i) It is more intuitive to adiabatically eliminate operators rather than states since the goal is to obtain an effective Hamiltonian with effective operators, making operators adiabatic elimination the more natural choice. (ii) Because we are working with transition operators in the uniquely defined Heisenberg picture, frequency detuning naturally arises without requiring a shift to an interaction picture, which is not unique and can lead to different predictions of the system's dynamics [47]. (iii) The light-matter coupling depends on the frequency which is continuously distributed. Tracking the evolution of transitions operator joint for each frequency with the field bosonic operators preserves this frequency dependence throughout and yields effective two-photon coupling terms that are functions of both photons' frequencies. (iv) Using bosonic operators instead of bosonic states allows for the explicit application of the bosonic commutation relation, therefore clearly revealing the photonic processes ordering. Note that the previous derivation was performed without taking into account the optical selection rules. Therefore, the present description can be extended to any four-level system coupled to a bosonic field frequency continuum.

Appendix C: Scattering theory derivation

In this appendix, we present the main computational steps of the scattering theory method employed by Alushi *et al* [45] adapted to our physical system. Further details can be found in [45] and Sec. 7.2 and Appendix B.3 of [119].

a. Wigner-Weisskopf ansatz

Let us first define the bare transition operator $\hat{\xi}_{2X0} = \hat{\xi}^\dagger_{02X} \equiv |2X\rangle\langle 0|$, the following $\hat{N}$ operator

$$\hat{N} = 2\hat{\xi}_{02X}\hat{\xi}_{2X0} + \sum_{\sigma\in\{R,L\}}\sum_{\mu\in\{\pm\}}\int_{\mathbb{R}} d\omega\ \hat{a}^\dagger_{\sigma_\mu}(\omega)\hat{a}_{\sigma_\mu}(\omega), \tag{C1}$$

accounting of the number of weighted excitations in the system, commutes with the total effective Hamiltonian. Consequently, the system's dynamics can be effectively described using a normalized Wigner-Weisskopf ansatz $|\psi(t)\rangle$ with a fixed number of weighted excitations. Given the expression of the effective interaction Hamiltonian Eq. (13), the photonic states are decoupled from the emitter in the vacuum and individual photon sectors. As a result, we can focus on solving the scattering problem for input states consisting either of two photons with the emitter in the ground state or a single excited emitter in the vacuum state

$$|\psi(t)\rangle = C_{2X}(t)\hat{\xi}_{2X0}|\mathbf{0}\rangle + \sum_{\substack{\sigma'\in\{R,L\}\\ \mu'\in\{\pm\}}}\sum_{\substack{\sigma\in\{R,L\}\\ \mu\in\{\pm\}}}\int_{\mathbb{R}^2} d\omega' d\omega C^{\sigma'\sigma}_{\mu'\mu}(\omega',\omega;t)\hat{a}^\dagger_{\sigma'_{\mu'}}(\omega')\hat{a}^\dagger_{\sigma_\mu}(\omega)|\mathbf{0}\rangle, \tag{C2}$$

where $C_{2X}(t)$ and $C^{\sigma'\sigma}_{\mu'\mu}(\omega',\omega;t)$ are the probability amplitudes to have the system respectively in the QD's biexcitonic state without photons and in the QD's ground state with two-photons at frequency ω and ω', polarization σ and σ', and direction of propagation μ and μ'. The state $|\mathbf{0}\rangle \equiv |0\rangle \otimes |\text{vac}\rangle$ denotes the global vacuum state for both light and matter. The entire QD-waveguide isolated system is enclosed within the Wigner-Weisskopf ansatz, whose dynamics is governed by the Schrödinger equation $i\hbar\partial_t|\psi(t)\rangle = \hat{H}|\psi(t)\rangle$ giving rise to a system of linear, coupled ordinary differential equations

$$i\dot{C}_{2X}(t) = \omega_{2X}C_{2X}(t) + \sum_{\mu',\mu\in\{\pm\}}\int_{\mathbb{R}^2} d\omega' d\omega\ g^{\mu'\mu}(\omega',\omega)C^{\sigma'\sigma}_{\mu'\mu}(\omega',\omega;t) \tag{C3a}$$

$$i\dot{C}^{\sigma'\sigma}_{\mu'\mu}(\omega',\omega;t) = (\omega+\omega')C^{\sigma'\sigma}_{\mu'\mu}(\omega',\omega;t) + \left(g^{\mu'\mu}(\omega',\omega)\right)^* C_{2X}(t), \tag{C3b}$$

with the polarization σ and σ' left unspecified but implicitly enforced by the coupling terms selection rules. The two-photon state linear differential equation Eq. (C3b) can be formally integrated as

$$C^{\sigma'\sigma}_{\mu'\mu}(\omega',\omega;t_1) = C^{\sigma'\sigma}_{\mu'\mu}(\omega',\omega;t_0)e^{-i(\omega+\omega')(t_1-t_0)} - i\left(g^{\mu'\mu}(\omega',\omega)\right)^* \int_{t_0}^{t_1} d\tau\; C_{2X}(\tau)e^{-i(\omega+\omega')(t_1-\tau)}, \tag{C4}$$

which can be substituted back into the differential equation for the biexciton probability amplitude

$$\begin{aligned} i\dot{C}_{2X}(t_1) = \omega_{2X}C_{2X}(t_1) + \sum_{\mu',\mu\in\{\pm\}}\int_{\mathbb{R}^2} d\omega' d\omega \left(g^{\mu'\mu}(\omega',\omega)C^{\sigma'\sigma}_{\mu'\mu}(\omega',\omega;t_0)e^{-i(\omega+\omega')(t_1-t_0)} \right. \\ \left. - i\int_{t_0}^{t_1} d\tau\; |g^{\mu'\mu}(\omega',\omega)|^2 C_{2X}(\tau)e^{-i(\omega+\omega')(t_1-\tau)} \right). \end{aligned} \tag{C5}$$

The first term corresponds to the QD's free evolution, the second to the photons absorbed by the QD and the third to the photons emitted by the QD in the past that got reabsorbed.

b. *Markovian and weak coupling approximation*

Let us toggle to the collective variables $\omega_\Sigma = \omega + \omega'$ and $\omega_\Delta = \omega - \omega'$. This choice is driven by the forthcoming Markovian approximation and the nature of the frequency entangling gate , which transforms the reference axes of the two-photon distribution from the individual frequencies ω and ω' to the collective frequencies variables $\omega+\omega'$ and $\omega-\omega'$. The third term in Eq. (C5) can be expressed as

$$F(t) = -i\int_0^{t_1-t_0} d\tau\; C_{2X}(t_1-\tau)K(\tau), \tag{C6}$$

where $K(\tau)$ is the memory kernel

$$K(\tau) \equiv \int_{\mathbb{R}} d\omega_\Sigma\; e^{-i\omega_\Sigma\tau}\left(\frac{1}{2}\sum_{\mu',\mu\in\{\pm\}}\int_{\mathbb{R}} d\Delta\; |g^{\mu'\mu}(\omega_\Sigma,\omega_\Delta)|^2\right) \tag{C7}$$

connected to the spectral function $J(\omega_\Sigma)$ [119] through a Fourier transform

$$J(\omega_\Sigma) = \pi\sum_{\mu',\mu\in\{\pm\}}\int_{\mathbb{R}} d\omega_\Delta\; |g^{\mu'\mu}(\omega_\Sigma,\omega_\Delta)|^2. \tag{C8}$$

The spectral function can be interpreted as a function counting the coupling function contributions in the frequency domain to the term $F(t_1)$ [defined in Eq. (C6)], in particular here with respect to the sum of photons frequencies. This stands to reason given that the resonance condition for this two-photon process is $\omega_\Sigma = \omega + \omega' = \omega_{2X}$. The Markovian and weak coupling approximations now consist in: (i) Assuming that the coupling strength is negligible with respect to the biexcitonic energy ω_{2X} so that the probability amplitude $C_{2X}(\tau)$ can be expressed as the product of a free-evolving term and a slowly time-varying function of time $C_{2X}(\tau) = e^{-i\omega_{2X}\tau}S_{2X}(\tau)$. (ii) Supposing that the spectral function Eq. (C8) – and hence the coupling terms $g^{\mu'\mu}(\omega_\Sigma,\omega_\Delta)$ – has a minimal dependence on the collective frequency ω_Σ, so that the memory kernel $K(\tau)$ is sharply peaked at $\tau = 0$. The term $F(t)$ can thus be approximated as

$$F(t) \approx -iC_{2X}(t)\int_0^{t_1-t_0} d\tau\; e^{i\omega_{2X}\tau}K(\tau), \tag{C9}$$

where the envelope was treated as a constant over the short time interval where the memory kernel is nonzero. From this point, $F(t_1)$ can be directly substituted back into the differential equation Eq. (C5) or can be simplified by expanding the time t_1 in the integral to infinity. This approach is valid as long as the memory kernel closely approximates a Dirac δ function in time and aligns with scattering states, where t_0 and t_1 are extended to $+\infty$ and $-\infty$, respectively. In that case, using the Sokhotski–Plemelj theorem, $F(t_1)$ yields

$$F(t_1) = -i\left(\frac{\Gamma}{2} - i\delta_{\text{Lamb}}\right)C_{2X}(t_1), \tag{C10}$$

with Γ and δ_{Lamb} the decay rate and the frequency Lamb shift respectively

$$\Gamma = J(\omega_{2X}) \tag{C11}$$

$$\delta_{\text{Lamb}} = \mathcal{PV}\int_{\mathbb{R}} d\omega_\Sigma \left(\frac{J(\omega_\Sigma)}{\omega_{2X}-\omega_\Sigma}\right), \tag{C12}$$

where $\mathcal{PV}$ labels the Cauchy principal value. The Lamb shift is recast in the definition of the biexcitonic frequency $\omega_{2X} \to \omega_{2X} + \delta_{\text{Lamb}}$. In most cases, the experimental measurement of the emitter's frequency already accounts for the Lamb shift regardless [119]. The extension $t_1 \to +\infty$ and $t_0 \to -\infty$ can now be clarified by defining the scattering times as $(t_1 - t_0) \gg 1/\Gamma$, that is to say times such that the emitter has fully decayed before the output state is formally established. Writing the second term from the two-photon probability amplitude Eq. (C4)

$$\int_{t_0}^{t_1} d\tau\; C_{2X}(\tau) e^{-i\omega_\Sigma(t_1-\tau)} \approx e^{-i\omega_\Sigma t_1}\widetilde{C}_{2X}(\omega_\Sigma), \tag{C13}$$

with $\widetilde{C}_{2X}(\omega_\Sigma)$ the Fourier transform of $C_{2X}(\tau)$ that can obtained from Eq. (C5) using $\int_{\mathbb{R}} dt\; e^{it(\omega_\Sigma-\omega'_\Sigma)} = 2\pi\delta(\omega_\Sigma-\omega'_\Sigma)$. The two-photon probability amplitude can then be expressed as

$$\begin{aligned} C^{\sigma'\sigma}_{\mu'\mu}(\omega_\Sigma,\omega_\Delta;t_1) = e^{-i\omega_\Sigma(t_1-t_0)}\Bigg[& C^{\theta'\theta}_{\nu'\nu}(\omega_\Sigma,\omega_\Delta;t_0)\delta_{\sigma'\theta'}\delta_{\mu'\nu'}\delta_{\sigma\theta}\delta_{\mu\nu} \\ & - \frac{\pi\left(g^{\mu'\mu}(\omega_\Sigma,\omega_\Delta)\right)^*}{\frac{\Gamma}{2}+i(\omega_{2X}-\omega_\Sigma)} \sum_{\nu',\nu\in\{\pm\}}\int_{\mathbb{R}} d\omega'_\Delta\; g^{\nu'\nu}(\omega_\Sigma,\omega'_\Delta) C_{\mu'\mu}(\omega_\Sigma,\omega_\Delta;t_0)\Bigg], \end{aligned} \tag{C14}$$

where again, the polarization degrees of freedom indices are omitted whenever there is a two-photon coupling term as it implicitly dictates them due to the selection rules. The two-photon output state, given in Eq. (C14), consists of two contributions: one term represents photons that did not interact with the (QD) and are only time-shifted, while the other term corresponds to photons that interacted with the QD, as indicated by the coupling terms.

Appendix D: Schmidt decomposition for continuous variables

In this appendix, we provide additional details on the Schmidt decomposition discussed in the main text. For a comprehensive treatment refer to [95–97]. The pure renomarlized output state

$$\left|\psi^{\sigma'\sigma}_{\mu'\mu}(t_1)\right\rangle = \int_{\mathbb{R}^2} d\omega' d\omega\; C^{\sigma'\sigma}_{\mu'\mu}(\omega',\omega;t_1)\hat{a}^\dagger_{\sigma'\mu'}(\omega')\hat{a}^\dagger_{\sigma\mu}(\omega)\left|\text{vac}\right\rangle \tag{D1}$$

is expressed by means of a discrete expansion

$$C^{\sigma'\sigma}_{\mu'\mu}(\omega',\omega;t_1) = \sum_{n,m\in\mathbb{N}} C^{\sigma'\sigma}_{\mu'\mu}(n,m;t_1) O^{(2)}_n(\omega') O^{(1)}_m(\omega), \tag{D2}$$

where $\{O^{(1)}_m(\omega)\}_{m\in\mathbb{N}}$ and $\{O^{(2)}_n(\omega')\}_{n\in\mathbb{N}}$ are two set of orthogonal $L^2(\mathbb{R})$ functions associated to the first and second photon respectively. These functions verify

$$\int_{\mathbb{R}} d\nu\; O^{(i)}_k(\nu) O^{(i)}_{k'}(\nu) = \delta_{kk'} \tag{D3}$$

$$\sum_{k\in\mathbb{N}} O^{(i)}_k(\nu) O^{(i)}_k(\nu') = \delta(\nu-\nu'), \tag{D4}$$

for $i = 1, 2$. Here for instance, we choose the Hermite-Gauss orthogonal functions given the Gaussianity of the two-photon distribution. The elements $C^{\sigma'\sigma}_{\mu'\mu}(n,m;t_1)$ of the discrete expansion Eq. (D2) are given by

$$C^{\sigma'\sigma}_{\mu'\mu}(n,m;t_1) = \int_{\mathbb{R}^2} d\omega' d\omega\; C^{\sigma'\sigma}_{\mu'\mu}(\omega',\omega;t_1) O^{(2)*}_n(\omega') O^{(1)*}_m(\omega). \tag{D5}$$

By discretizing the continuous problem, we work with the discrete coefficients of the linear combination while preserving the continuous nature of the state through the ω- and ω'-dependence of the set of orthogonal functions

$\{O_m^{(1)}(\omega)\}_{m\in\mathbb{N}}$ and $\{O_n^{(2)}(\omega')\}_{n\in\mathbb{N}}$. The next step consists in performing a numerical matrix singular-value decomposition to the $C_{\mu'\mu}^{\sigma'\sigma}(t_1)$ matrix with elements $C_{\mu'\mu}^{\sigma'\sigma}(n,m;t_1)$. In order to perform the numerical singular value decomposition, we first truncate the discrete sums. Throughout the computations, we ensure that these truncations are sufficiently large to maintain an approximation close to the exact solution. This is assessed by the computation of a distance – *e.g.* the mean squared error – to the actual JSA $C_{\mu'\mu}^{\sigma'\sigma}(\omega',\omega;t_1)$. The amplitude Eq. (D2) can be rewritten as

$$C_{\mu'\mu}^{\sigma'\sigma}(\omega',\omega;t_1) = \sum_{k=1}^{\min(m_0,n_0)} \lambda_k^{\sigma'\mu'\sigma\mu}\Theta_k^{(2)}(\omega')\Theta_k^{(1)}(\omega), \tag{D6}$$

where the discrete expansion has been truncated for the singular-value decomposition to be applied

$$C_{\mu'\mu}^{\sigma'\sigma}(\omega',\omega;t_1) = \sum_{n=1}^{n_0}\sum_{m=1}^{m_0} C_{\mu'\mu}^{\sigma'\sigma}(n,m;t_1)O_n^{(2)}(\omega')O_m^{(1)}(\omega). \tag{D7}$$

The $\Theta_k^{(1)}(\omega)$ and $\Theta_k^{(2)}(\omega')$ functions are linear combinations of the orthogonal functions $\{O_m^{(1)}(\omega)\}_{m\in[\![1,m_0]\!]}$ and $\{O_n^{(2)}(\omega')\}_{n\in[\![1,n_0]\!]}$ respectively. The $\lambda_k^{\sigma'\mu'\sigma\mu}$ Schmidt coefficients are real, non-negative, unique up to reordering and obey $\sum_{k=1}^{\min(m_0,n_0)}\left(\lambda_k^{\sigma'\mu'\sigma\mu}\right)^2 = 1$ provided $C_{\mu'\mu}^{\sigma'\sigma}(\omega',\omega;t_1)$ is normalized to one. The two-photon scattered output state $\left|\psi_{\mu'\mu}^{\sigma'\sigma}(t_1)\right\rangle$ in Eq. (D1) can be expressed as a discrete sum

$$\left|\psi_{\mu'\mu}^{\sigma'\sigma}(t_1)\right\rangle = \sum_{k=1}^{\min(m_0,n_0)} \lambda_k^{\sigma'\mu'\sigma\mu}\hat{b}_{\sigma'\mu'}^{(2)\dagger}(k)\hat{b}_{\sigma\mu}^{(1)\dagger}(k)\left|\text{vac}\right\rangle, \tag{D8}$$

where $\hat{b}_{\sigma\mu}^{(1)\dagger}(k)$ and $\hat{b}_{\sigma'\mu'}^{(2)\dagger}(k)$ are bosonic creation operators which read

$$\begin{aligned}\hat{b}_{\sigma\mu}^{(1)\dagger}(k) &= \int_{\mathbb{R}} d\omega\ \Theta_k^{(1)}(\omega)\hat{a}_{\sigma\mu}^{\dagger}(\omega)\\ \hat{b}_{\sigma'\mu'}^{(2)\dagger}(k) &= \int_{\mathbb{R}} d\omega'\ \Theta_k^{(2)}(\omega')\hat{a}_{\sigma'\mu'}^{\dagger}(\omega').\end{aligned} \tag{D9}$$

These operators create photons in the Schmidt modes, each labeled by the index k.

Appendix E: Optimization of the propagation mode

In this appendix, we offer numerical insights into optimizing the propagation mode $u(\omega)$, which corresponds to the magnitude of the solution to the waveguide wave equation Eq. (2)

$$\boldsymbol{\nabla}\times\boldsymbol{\nabla}\times\boldsymbol{\mathcal{E}}_{\sigma\mu}(\boldsymbol{r},\beta) - \frac{\omega(\beta)^2}{c^2}\epsilon(\boldsymbol{r},\mu\beta)\boldsymbol{\mathcal{E}}_{\sigma\mu}(\boldsymbol{r},\beta) = \boldsymbol{0}, \tag{E1}$$

in such a way for the two-photon coupling term Eq. (22)

$$g^{\mu'\mu}(\omega',\omega) = \frac{D}{\hbar^2}u(\omega')u(\omega)\times\left[\frac{1}{\omega-\omega_X} - \frac{1}{\omega'-(\omega_X-\delta_X)} + \frac{1}{\omega'-\omega_X} - \frac{1}{\omega-(\omega_X-\delta_X)}\right] \tag{E2}$$

to be as Eq. (28) a non-separable Gaussian function of width β and defined along the collective variable $\omega_\Delta = \omega-\omega'$

$$g^{\mu'\mu}(\omega_\Delta) = \sqrt{\frac{\gamma^{\mu'\mu}}{\pi}}\left(\frac{1}{2\pi\beta^2}e^{-\frac{(\omega_\Delta-(\omega_e-\omega_b))^2}{\beta^2}}\right)^{1/4}. \tag{E3}$$

Injecting the constants $D/\hbar^2$ in the definition of the products $u(\omega')u(\omega)$, this problem can be formulated as $u(\omega')u(\omega)h(\omega',\omega) = g(\omega',\omega)$ where $h(\omega',\omega)$ is the non-separable part of Eq. (E2) and $g(\omega',\omega)$ the target two-variable functions Eq. (E3). Since $g(\omega',\omega)$ is non-separable in the two variables ω and ω', i.e.. it cannot be written as a

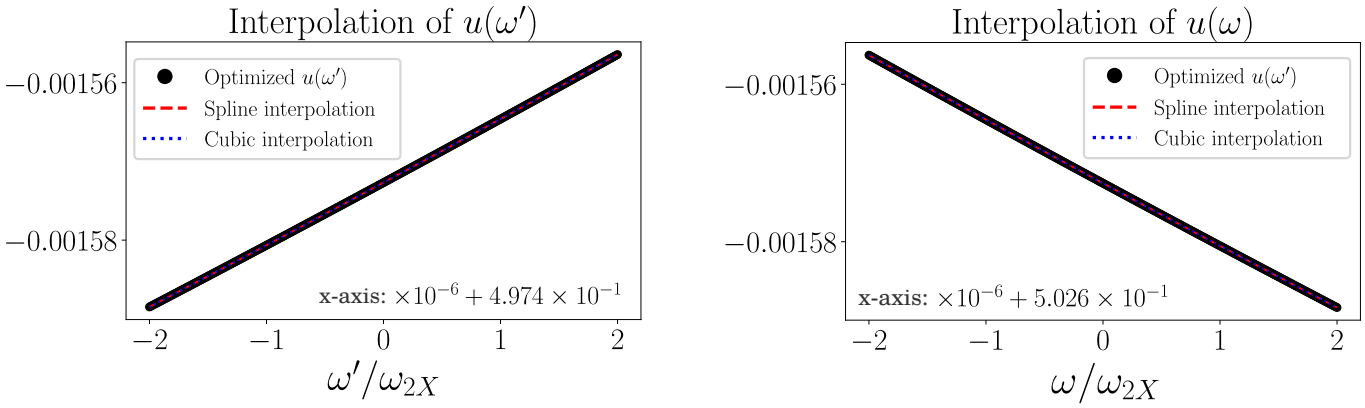

FIG. 8. Spline and cubic interpolation of the propagation mode u over the excitonic range ω and biexcitonic range ω' normalized to the biexcitonic transition frequency ω_{2X} for $\alpha = 10^{-6}\omega_{2X}$, $\Gamma = 10^{-5}\omega_{2X}$ and $\beta \approx 10^{-4}\omega_{2X}$, $\omega_X = 0.5025\omega_{2X}$, $\delta_X = 0.005\omega_{2X}$, $\omega_e = 0.5026\omega_{2X}$, $\omega_b = 0.4974\omega_{2X}$.

product $g(\omega', \omega) = g_1(\omega)g_2(\omega')$ with g_1 and g_2 two functions, the importance of $h(\omega', \omega)$ non-separability becomes apparent. In order to optimize the function u over the ranges of definition of ω and ω', let us write

$$u(\omega)u(\omega') = \frac{g(\omega', \omega)}{h(\omega', \omega)} \tag{E4}$$

and express this equation in a matrix form $\boldsymbol{U} = \boldsymbol{T}$ with

$$\boldsymbol{U} \equiv \begin{bmatrix} u(\omega_1)u(\omega'_1) & u(\omega_2)u(\omega'_1) & \dots & u(\omega_n)u(\omega'_1) \\ \vdots & \vdots & \vdots & \vdots \\ u(\omega_1)u(\omega'_n) & u(\omega_2)u(\omega'_n) & \dots & u(\omega_n)u(\omega'_n) \end{bmatrix} \tag{E5}$$

(E6)

$$\boldsymbol{T} \equiv \begin{bmatrix} \frac{g(\omega_1,\omega'_1)}{h(\omega_1,\omega'_2)} & \frac{g(\omega_2,\omega'_1)}{h(\omega_2,\omega'_2)} & \dots & \frac{g(\omega_n,\omega'_1)}{h(\omega_n,\omega'_1)} \\ \vdots & \vdots & \vdots & \vdots \\ \frac{g(\omega_1,\omega'_n)}{h(\omega_1,\omega'_n)} & \frac{g(\omega_2,\omega'_n)}{h(\omega_2,\omega'_n)} & \dots & \frac{g(\omega_n,\omega'_n)}{h(\omega_n,\omega'_n)} \end{bmatrix}, \tag{E7}$$

where we discretize the frequencies $\boldsymbol{\omega} = [\omega_1 \dots \omega_N]^T$ and $\boldsymbol{\omega'} = [\omega'_1 \dots \omega'_N]^T$. The frequencies ranges are chosen to match the initial two-photon distribution Eq. (27). The optimization problem is thus equivalent to optimizing the entries of two column vectors $\boldsymbol{u} \equiv [u(\omega_1) \dots u(\omega_N)]^T$ and $\boldsymbol{u'} \equiv [u(\omega'_1) \dots u(\omega'_N)]^T$ by minimizing a distance $||.||$ between $\boldsymbol{U}$ and $\boldsymbol{T}$. The optimization loop starts with an initial guess that starkly determines the extent of the optimization's reach and must be carefully chosen. A guess motivated by the previous $\boldsymbol{U} = \boldsymbol{T}$ matrix formulation of the optimization can be chosen by noticing that $\boldsymbol{U} = \boldsymbol{u}^T\boldsymbol{u'}$, and by extension $\boldsymbol{T}$, should be a rank-1 matrix. Indeed, each row (respectively column) of $\boldsymbol{U}$ is a multiple of $\boldsymbol{u'}^T$ (respectively $\boldsymbol{u}$) so all rows (respectively columns) are linearly dependent. Let us now perform the singular value decomposition of $\boldsymbol{T}$

$$\boldsymbol{T} = \boldsymbol{V}\boldsymbol{S}\boldsymbol{W}^T, \tag{E8}$$

where $\boldsymbol{V}$ and $\boldsymbol{W}^T$ orthogonal matrix contain the left and right singular vectors respectively and $\boldsymbol{S}$ is the diagonal matrix of singular values. Any column (respectively row) of $\boldsymbol{T}$ can be expressed as linear combination of the columns (respectively rows) of $\boldsymbol{V}$ and $\boldsymbol{W}^T$. The columns (respectively rows) of $\boldsymbol{V}$ (respectively $\boldsymbol{W}^T$) form an orthonormal basis of the column (respectively row) space of $\boldsymbol{T}$. The leading singular vectors are the first column and row of $\boldsymbol{V}$ and $\boldsymbol{W}^T$ respectively and because $\boldsymbol{U} = \boldsymbol{T}$ is supposed to be a rank-1 matrix, $\boldsymbol{T} \approx \boldsymbol{S}[1]\boldsymbol{V}[0,:]\boldsymbol{W}^T[0,:]$ therefore a good initial guess for $\boldsymbol{u}$ and $\boldsymbol{u'}$ is

$$\boldsymbol{u} = \boldsymbol{W}^T[0,:] \quad \boldsymbol{u'} = \boldsymbol{V}[0,:]. \tag{E9}$$

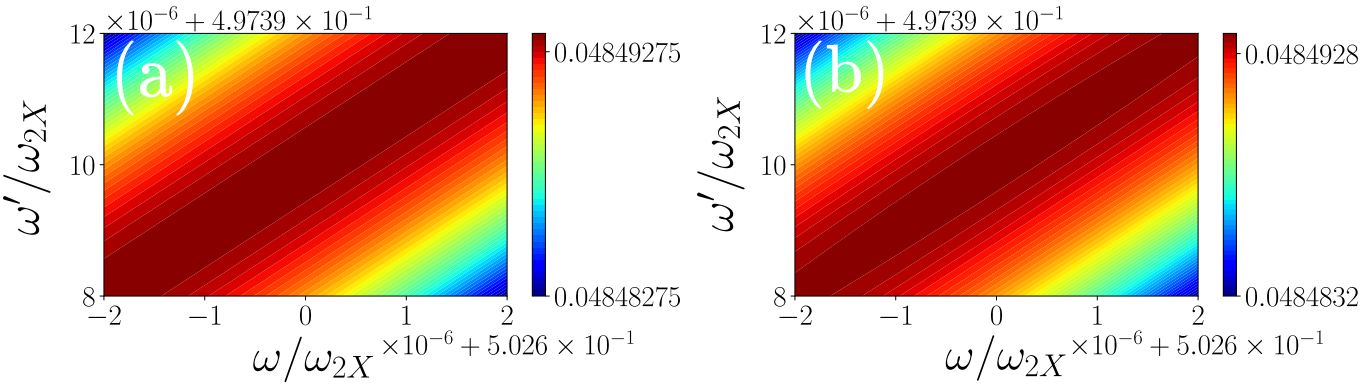

FIG. 9. (a) Target Gaussian non-separable coupling Eq. (E3). (b) Approximated Gaussian non-separable coupling drawn from the optimization of u over the two frequencies ranges, see Fig. 8.

After retrieving the optimized vectors $\boldsymbol{u}$ and $\boldsymbol{u'}$, we interpolate the functional form of u over the ranges of ω and ω' with a spline and cubic interpolation, see Fig. 8. Remarkably, a form of anticorrelation emerges between the values of u over the two frequency ranges, aligning with the anticorrelations in the target coupling term Eq. (E3). In Fig. 9, the target Gaussian non-separable coupling Eq. (E3) and approximated solution to the optimization problem $u(\omega)u(\omega')h(\omega',\omega)$ are plotted. They demonstrate strong agreement, validating the effectiveness of the previous optimization method. It is important to note that the optimization critically depends on the frequency ranges, which are determined by the two-photon input distribution, the Gaussian coupling width β, the one-photon detunings and the binding energy δ_X. The parameters that we consider here follow those used in the main text for the output two-photon distribution to be frequency-entangled with Gaussian distributions along both collective variables $\omega_\Sigma = \omega + \omega'$ and $\omega_\Delta = \omega - \omega'$. All the preceding optimization was carried out in Python. The present optimization scheme is mostly illustrative. Precisely tailoring the propagation mode $u(\omega)$ starkly depends on the different physical parameters at play, and precise waveguide engineering is paramount to experimentally manufacture the required propagation mode $u(\omega)$.

Appendix F: Frequency qudit states computation details

In this section, we provide the computation details leading to the output distribution for the cavity-filtered input $C^{LR}_{++}(\omega_\Sigma,\omega_\Delta;t_0)f_{\text{filter}}(\omega)f_{\text{filter}}(\omega')$. For a non-interefered output, that is an output with auxiliary degrees of freedom $\{\mu,\mu'\} \neq \{+,+\}$, the scattered two-photon distribution reads

$$C^{\sigma'\sigma}_{\mu'\mu}(\omega_\Sigma,\omega_\Delta;t_1) = -e^{-i\omega_\Sigma(t_1-t_0)}\frac{\pi\left(g^{\mu'\mu}(\omega_\Sigma,\omega_\Delta)\right)^*}{\frac{\Gamma}{2}+i(\omega_{2X}-\omega_\Sigma)}\int_{\mathbb{R}} d\omega'_\Delta\, g^{++}(\omega_\Sigma,\omega'_\Delta)C^{LR}_{++}(\omega_\Sigma,\omega'_\Delta;t_0)f_{\text{filter}}(\omega)f_{\text{filter}}(\omega'), \tag{F1}$$

with

$$g^{\mu'\mu}(\omega_\Delta) = \sqrt{\frac{\gamma^{\mu'\mu}}{\pi}}\left(\frac{1}{2\pi\beta^2}e^{-\frac{(\omega_\Delta-(\omega_e-\omega_b))^2}{\beta^2}}\right)^{1/4}, \tag{F2}$$

and

$$C^{LR}_{++}(\omega_\Sigma,\omega_\Delta;t_0) = \frac{1}{\sqrt{2\pi\alpha^2}}e^{-\frac{[\omega_\Sigma-(\omega_e+\omega_b)]^2}{4\alpha^2}}e^{-\frac{[\omega_\Delta-(\omega_e-\omega_b)]^2}{4\alpha^2}}. \tag{F3}$$

Let us focus now on the integral terms. Given that $f_{\text{filter}}(\omega) = \sum_{n\in\mathbb{Z}} T_n(\omega)$ where $T_n(\omega) = \exp\left(-(\omega-n\overline{\omega})^2/(2\delta\omega^2)\right)$, the integral can be expressed as a sum of the following integrals

$$\sqrt{\frac{\gamma^{\mu'\mu}}{\pi}}\left(\frac{1}{2\pi\beta^2}\right)^{1/4}\frac{1}{\sqrt{2\pi\alpha^2}}e^{\frac{[\omega_\Sigma-(\omega_e+\omega_b)]^2}{4\alpha^2}}\int_{\mathbb{R}} d\omega'_\Delta e^{-\left[\omega'_\Delta-(\omega_e-\omega_b)\right]^2\left(\frac{1}{4\alpha^2}+\frac{1}{4\beta^2}\right)}e^{-\frac{1}{4\delta\omega^2}\left(\left[\frac{\omega_\Sigma+\omega'_\Delta}{2}-n\overline{\omega}\right]^2+\left[\frac{\omega_\Sigma-\omega'_\Delta}{2}-m\overline{\omega}\right]^2\right)}. \tag{F4}$$

Rewriting the argument of the second exponential of the integral as

$$-\frac{1}{2\delta\omega^2}\left(\left[\frac{\omega_\Sigma+\omega'_\Delta}{2}-n\overline{\omega}\right]^2+\left[\frac{\omega_\Sigma-\omega'_\Delta}{2}-m\overline{\omega}\right]^2\right)=-\frac{1}{2\delta\omega^2}\left(A_\Sigma\left[\omega_\Sigma-c_{\Sigma,nm}\right]^2+A'_\Delta\left[\omega'_\Delta-c'_{\Delta,nm}\right]^2+B_{nm}\right), \tag{F5}$$

with $A_\Sigma, A'_\Delta, c_{\Sigma,nm}, c'_{\Delta,nm}$ and B which can be determined

$$A_\Sigma = A'_\Delta = \frac{1}{2} \tag{F6}$$
$$c_{\Sigma,nm} = \overline{\omega}(n+m) \tag{F7}$$
$$c_{\Delta',nm} = \overline{\omega}(n-m) \tag{F8}$$
$$B_{nm} = 0, \tag{F9}$$

the term in $A_\Sigma\left[\omega_\Sigma - c_{\Sigma,nm}\right]^2$ can be taken out of the previous integral, which now reads

$$\int_{\mathbb{R}} d\omega'_\Delta e^{-\left(\frac{1}{4\alpha^2}+\frac{1}{4\beta^2}\right)\left[\omega'_\Delta-(\omega_e-\omega_b)\right]^2} e^{-\frac{1}{2\delta\omega^2}\left[\omega'_\Delta-\overline{\omega}(n-m)\right]^2}. \tag{F10}$$

The argument of the exponential can be expressed as

$$-\left(\frac{1}{4\alpha^2}+\frac{1}{4\beta^2}\right)\left[\omega'_\Delta-(\omega_e-\omega_b)\right]^2-\frac{1}{4\delta\omega^2}\left[\omega'_\Delta-\overline{\omega}(n-m)\right]^2=-\frac{\left[\omega'_\Delta-\mu'_{\Delta,nm}\right]^2}{\sigma'^2_\Delta}+D_{nm} \tag{F11}$$

with

$$\sigma'^2_\Delta = \frac{4\alpha^2\beta^2\delta\omega^2}{\alpha^2\beta^2+\delta\omega^2(\alpha^2+\beta^2)} \tag{F12}$$
$$\mu'_{\Delta,nm} = \frac{\delta\omega^2(\alpha^2+\beta^2)(\omega_e-\omega_b)+\alpha^2\beta^2\overline{\omega}(n-m)}{\alpha^2\beta^2+(\alpha^2+\beta^2)\,\delta\omega^2} \tag{F13}$$
$$D_{nm} = -\frac{1}{4}\frac{\left(\alpha^2+\beta^2\right)\left((\omega_e-\omega_b)-\overline{\omega}(n-m)\right)^2}{\alpha^2\beta^2+(\alpha^2+\beta^2)\delta\omega^2}. \tag{F14}$$

The integral can then readily be calculated as

$$\int_{\mathbb{R}} d\omega'_\Delta e^{-\left(\frac{1}{4\alpha^2}+\frac{1}{4\beta^2}\right)\left[\omega'_\Delta-(\omega_e-\omega_b)\right]^2} e^{-\frac{1}{4\delta\omega^2}\left[\omega'_\Delta-\overline{\omega}(n-m)\right]^2} = e^{D_{nm}}\sqrt{\pi\sigma'^2_\Delta}. \tag{F15}$$

One can therefore compute

$$\begin{aligned}\int_{\mathbb{R}} d\omega'_\Delta\; g^{++}(\omega_\Sigma,\omega'_\Delta)C^{LR}_{++}(\omega_\Sigma,\omega'_\Delta;t_0)f_{\text{filter}}(\omega)f_{\text{filter}}(\omega') = \sum_{n,m\in\mathbb{Z}}\sqrt{\frac{\gamma^{\mu'\mu}}{\pi}}\left(\frac{1}{2\pi\beta^2}\right)^{1/4}\sqrt{\frac{\sigma'^2_\Delta}{2\alpha^2}}e^{D_{nm}} \\ \times e^{-\frac{\left[\omega_\Sigma-(\omega_e+\omega_b)\right]^2}{4\alpha^2}}e^{-\frac{1}{4\delta\omega^2}\left[\omega_\Sigma-\overline{\omega}(n+m)\right]^2}.\end{aligned} \tag{F16}$$

All in all, for an isotropic emission $\gamma^{\mu'\mu} = \Gamma/4$, the scattered output two-photon distribution is

$$C^{\sigma'\sigma}_{\mu'\mu}(\omega_\Sigma,\omega_\Delta;t_1) = -e^{-i\omega_\Sigma(t_1-t_0)}e^{-\frac{\left[\omega_\Delta-(\omega_e-\omega_b)\right]^2}{4\beta^2}}\frac{\Gamma}{\frac{\Gamma}{2}+i(\omega_{2X}-\omega_\Sigma)}e^{-\frac{\left[\omega_\Sigma-(\omega_e+\omega_b)\right]^2}{4\alpha^2}}\sqrt{\frac{\sigma'^2_\Delta}{64\pi\alpha^2\beta^2}}\sum_{n,m\in\mathbb{Z}}f_{nm}(\omega_\Sigma), \tag{F17}$$

with

$$f_{nm}(\omega_\Sigma) = e^{D_{nm}}e^{-\frac{1}{4\delta\omega^2}\left[\omega_\Sigma-\overline{\omega}(n+m)\right]^2}, \tag{F18}$$

where

$$D_{nm} = -\frac{1}{4}\frac{\left(\alpha^2+\beta^2\right)\left((\omega_e-\omega_b)-\overline{\omega}(n-m)\right)^2}{\alpha^2\beta^2+(\alpha^2+\beta^2)\delta\omega^2}. \tag{F19}$$

Numerically, one cannot extend the sums to infinity and has to truncate the number of peaks. Nonetheless, if the width α is too small, the frequency-filtering function cannot properly scan the one-photon distribution. Thus, we artificially displace the frequency-filtering as $f_{\text{filter}}(\omega) \to f_{\text{filter}}(\omega - \omega_e)$ and $f_{\text{filter}}(\omega') \to f_{\text{filter}}(\omega' - \omega_b)$. This changes the different computed coefficients as follows

$$A_\Sigma = A'_\Delta = \frac{1}{2}, \tag{F20}$$

$$c_{\Sigma,nm} = \overline{\omega}(n+m) + (\omega_e + \omega_b), \tag{F21}$$

$$c_{\Delta',nm} = \overline{\omega}(n-m) + (\omega_e - \omega_b), \tag{F22}$$

$$B = 0, \tag{F23}$$

$$\mu'_{\Delta,nm} = \frac{(\omega_e - \omega_b)\left[\delta\omega^2(\alpha^2+\beta^2) + \alpha^2\beta^2\right] + \alpha^2\beta^2\overline{\omega}(n-m)}{\alpha^2\beta^2 + \delta\omega^2(\alpha^2+\beta^2)} \tag{F24}$$

$$\sigma'^2_\Delta = \frac{4\alpha^2\beta^2\delta\omega^2}{\alpha^2\beta^2 + \delta\omega^2(\alpha^2+\beta^2)} \tag{F25}$$

$$D_{nm} = -\frac{1}{4}\frac{(\alpha^2+\beta^2)\overline{\omega}^2(n-m)^2}{\alpha^2\beta^2 + (\alpha^2+\beta^2)\delta\omega^2}, \tag{F26}$$

effectively shifting off the center frequency in D_{nm}. The scattered output two-photon distribution can be expressed as

$$C^{\sigma'\sigma}_{\mu'\mu}(\omega_\Sigma, \omega_\Delta; t_1) = -e^{-i\omega_\Sigma(t_1-t_0)} e^{-\frac{[\omega_\Delta - (\omega_e-\omega_b)]^2}{4\beta^2}} \frac{\Gamma}{\frac{\Gamma}{2} + i(\omega_{2X} - \omega_\Sigma)} e^{-\frac{[\omega_\Sigma - (\omega_e+\omega_b)]^2}{4\alpha^2}} \sqrt{\frac{\sigma'^2_\Delta}{64\pi\alpha^2\beta^2}} \sum_{n,m\in\mathbb{Z}} f_{nm}(\omega_\Sigma) \tag{F27}$$

with

$$f_{nm}(\omega_\Sigma) = e^{D_{nm}} e^{-\frac{1}{4\delta\omega^2}[\omega_\Sigma - (\omega_e+\omega_b) - \overline{\omega}(n+m)]^2}. \tag{F28}$$

[1] S. Slussarenko and G. J. Pryde, Photonic quantum information processing: A concise review, Applied Physics Reviews **6** (2019).
[2] J. L. O'brien, A. Furusawa, and J. Vučković, Photonic quantum technologies, Nature Photonics **3**, 687 (2009).
[3] J. P. Dowling and G. J. Milburn, Quantum technology: the second quantum revolution, Philosophical Transactions of the Royal Society of London. Series A: Mathematical, Physical and Engineering Sciences **361**, 1655 (2003).
[4] A. Acín, I. Bloch, H. Buhrman, T. Calarco, C. Eichler, J. Eisert, D. Esteve, N. Gisin, S. J. Glaser, F. Jelezko, *et al.*, The quantum technologies roadmap: a european community view, New Journal of Physics **20**, 080201 (2018).
[5] I. H. Deutsch, Harnessing the power of the second quantum revolution, PRX Quantum **1**, 020101 (2020).
[6] N. Gisin and R. Thew, Quantum communication, Nature photonics **1**, 165 (2007).
[7] D. A. Vajner, L. Rickert, T. Gao, K. Kaymazlar, and T. Heindel, Quantum communication using semiconductor quantum dots, Advanced Quantum Technologies **5**, 2100116 (2022).
[8] V. Giovannetti, S. Lloyd, and L. Maccone, Quantum metrology, Physical review letters **96**, 010401 (2006).
[9] V. Giovannetti, S. Lloyd, and L. Maccone, Advances in quantum metrology, Nature photonics **5**, 222 (2011).
[10] P. Kok, W. J. Munro, K. Nemoto, T. C. Ralph, J. P. Dowling, and G. J. Milburn, Linear optical quantum computing with photonic qubits, Rev. Mod. Phys. **79**, 135 (2007).
[11] S. Bartolucci, P. Birchall, H. Bombin, H. Cable, C. Dawson, M. Gimeno-Segovia, E. Johnston, K. Kieling, N. Nickerson, M. Pant, *et al.*, Fusion-based quantum computation, Nature Communications **14**, 912 (2023).
[12] J. Romero and G. Milburn, Photonic quantum computing, arXiv preprint arXiv:2404.03367 (2024).
[13] M. A. Nielsen, Quantum information theory, arXiv preprint quant-ph/0011036 (2000).
[14] R. Horodecki, Quantum information, Acta Phys. Pol. A **139**, 197 (2021).
[15] C. Weedbrook, S. Pirandola, R. García-Patrón, N. J. Cerf, T. C. Ralph, J. H. Shapiro, and S. Lloyd, Gaussian quantum information, Reviews of Modern Physics **84**, 621 (2012).
[16] A. Serafini, *Quantum continuous variables: a primer of theoretical methods* (CRC press, 2023).
[17] U. L. Andersen, J. S. Neergaard-Nielsen, P. v. Loock, and A. Furusawa, Hybrid quantum information processing, Nature Phys **11**, 713 (2015), 1409.3719 [quant-ph].
[18] L. Sansoni, *Integrated devices for quantum information with polarization encoded qubits* (Springer, 2014).
[19] L.-A. Wu, P. Walther, and D. A. Lidar, No-go theorem for passive single-rail linear optical quantum computing, Scientific reports **3**, 1394 (2013).

[20] C. Bernhard, B. Bessire, T. Feurer, and A. Stefanov, Shaping frequency-entangled qudits, Physical Review A—Atomic, Molecular, and Optical Physics **88**, 032322 (2013).

[21] H.-H. Lu, A. M. Weiner, P. Lougovski, and J. M. Lukens, Quantum information processing with frequency-comb qudits, IEEE Photonics Technology Letters **31**, 1858 (2019).

[22] A. Henry, D. A. Fioretto, L. M. Procopio, S. Monfray, F. Boeuf, L. Vivien, E. Cassan, C. Alonzo-Ramos, K. Bencheikh, I. Zaquine, *et al.*, Parallelization of frequency domain quantum gates: manipulation and distribution of frequency-entangled photon pairs generated by a 21 ghz silicon microresonator, Advanced Photonics **6**, 036003 (2024).

[23] J. C. García-Escartín and P. Chamorro-Posada, Universal quantum computation with the orbital angular momentum of a single photon, Journal of Optics **13**, 064022 (2011).

[24] C. Perumangatt, N. Lal, A. Anwar, S. G. Reddy, and R. Singh, Quantum information with even and odd states of orbital angular momentum of light, Physics Letters A **381**, 1858 (2017).

[25] D. L. Andrews, *Structured light and its applications: An introduction to phase-structured beams and nanoscale optical forces* (Academic press, 2011).

[26] S. L. Braunstein and P. Van Loock, Quantum information with continuous variables, Reviews of modern physics **77**, 513 (2005).

[27] C. Fabre and N. Treps, Modes and states in quantum optics, Reviews of Modern Physics **92**, 035005 (2020).

[28] D. S. Tasca, R. M. Gomes, F. Toscano, P. H. Souto Ribeiro, and S. P. Walborn, Continuous-variable quantum computation with spatial degrees of freedom of photons, Phys. Rev. A **83**, 052325 (2011).

[29] N. Fabre, A. Keller, and P. Milman, Time and frequency as quantum continuous variables, Physical Review A **105**, 052429 (2022).

[30] É. Descamps, A. Keller, and P. Milman, Gottesman-kitaev-preskill encoding in continuous modal variables of single photons, Physical Review Letters **132**, 170601 (2024).

[31] S. L. Braunstein and P. Van Loock, Quantum information with continuous variables, Reviews of modern physics **77**, 513 (2005).

[32] M. Walschaers, Non-gaussian quantum states and where to find them, PRX Quantum **2**, 030204 (2021).

[33] F. Hanamura, W. Asavanant, H. Nagayoshi, A. Sakaguchi, R. Ide, K. Fukui, P. van Loock, and A. Furusawa, Implementing arbitrary multimode continuous-variable quantum gates with fixed non-gaussian states and adaptive linear optics, Phys. Rev. A **110**, 022614 (2024).

[34] A. Zavatta, S. Viciani, and M. Bellini, Quantum-to-classical transition with single-photon-added coherent states of light, science **306**, 660 (2004).

[35] Z. Mazzotta, S. Cialdi, D. Cipriani, S. Olivares, and M. G. A. Paris, High-order dispersion effects in two-photon interference, Phys. Rev. A **94**, 063842 (2016).

[36] J.-i. Yoshikawa, S. Yokoyama, T. Kaji, C. Sornphiphatphong, Y. Shiozawa, K. Makino, and A. Furusawa, Generation of one-million-mode continuous-variable cluster state by unlimited time-domain multiplexing, APL Photonics **1**, 060801 (2016), number: 6, 1606.06688.

[37] W. Asavanant, Y. Shiozawa, S. Yokoyama, B. Charoensombutamon, H. Emura, R. N. Alexander, S. Takeda, J. ichi Yoshikawa, N. C. Menicucci, H. Yonezawa, and A. Furusawa, Generation of time-domain-multiplexed two-dimensional cluster state, Science **366**, 373 (2019), https://www.science.org/doi/pdf/10.1126/science.aay2645.

[38] M. V. Larsen, X. Guo, C. R. Breum, J. S. Neergaard-Nielsen, and U. L. Andersen, Deterministic generation of a two-dimensional cluster state, Science **366**, 369 (2019), https://www.science.org/doi/pdf/10.1126/science.aay4354.

[39] D. E. Chang, V. Vuletić, and M. D. Lukin, Quantum nonlinear optics—photon by photon, Nature Photonics **8**, 685 (2014).

[40] E. Knill, R. Laflamme, and G. J. Milburn, A scheme for efficient quantum computation with linear optics, Nature **409**, 46 (2001).

[41] P. Kok, W. J. Munro, K. Nemoto, T. C. Ralph, J. P. Dowling, and G. J. Milburn, Linear optical quantum computing with photonic qubits, Rev. Mod. Phys. **79**, 135 (2007).

[42] H. Le Jeannic, A. Tiranov, J. Carolan, T. Ramos, Y. Wang, M. H. Appel, S. Scholz, A. D. Wieck, A. Ludwig, N. Rotenberg, *et al.*, Dynamical photon–photon interaction mediated by a quantum emitter, Nature Physics **18**, 1191 (2022).

[43] S. Fan, Ş. E. Kocabaş, and J.-T. Shen, Input-output formalism for few-photon transport in one-dimensional nanophotonic waveguides coupled to a qubit, Physical Review A—Atomic, Molecular, and Optical Physics **82**, 063821 (2010).

[44] A. Nysteen, D. P. McCutcheon, M. Heuck, J. Mørk, and D. R. Englund, Limitations of two-level emitters as nonlinearities in two-photon controlled-phase gates, Physical review A **95**, 062304 (2017).

[45] U. Alushi, T. Ramos, J. J. García-Ripoll, R. Di Candia, and S. Felicetti, Waveguide qed with quadratic light-matter interactions, PRX Quantum **4**, 030326 (2023).

[46] E. Brion, L. H. Pedersen, and K. Mølmer, Adiabatic elimination in a lambda system, Journal of Physics A: Mathematical and Theoretical **40**, 1033 (2007).

[47] V. Paulisch, H. Rui, H. K. Ng, and B.-G. Englert, Beyond adiabatic elimination: A hierarchy of approximations for multi-photon processes, The European Physical Journal Plus **129**, 1 (2014).

[48] P. Maity, Adiabatic elimination in the presence of multiphoton transitions in atoms inside a cavity, International Journal of Modern Physics B , 2450439 (2024).

[49] F.-M. Le Régent and P. Rouchon, Heisenberg formulation of adiabatic elimination for open quantum systems with two timescales, in *2023 62nd IEEE Conference on Decision and Control (CDC)* (IEEE, 2023) pp. 7208–7213.

[50] C. Gonzalez-Ballestero, Tutorial: projector approach to master equations for open quantum systems, Quantum **8**, 1454 (2024).
[51] D. Finkelstein-Shapiro, D. Viennot, I. Saideh, T. Hansen, T. Pullerits, and A. Keller, Adiabatic elimination and subspace evolution of open quantum systems, Physical Review A **101**, 042102 (2020).
[52] E. Knill, R. Laflamme, and G. J. Milburn, A scheme for efficient quantum computation with linear optics, nature **409**, 46 (2001).
[53] C. Bernhard, B. Bessire, T. Feurer, and A. Stefanov, Shaping frequency-entangled qudits, Physical Review A—Atomic, Molecular, and Optical Physics **88**, 032322 (2013).
[54] C. Reimer, M. Kues, P. Roztocki, B. Wetzel, F. Grazioso, B. E. Little, S. T. Chu, T. Johnston, Y. Bromberg, L. Caspani, *et al.*, Generation of multiphoton entangled quantum states by means of integrated frequency combs, Science **351**, 1176 (2016).
[55] M. Kues, C. Reimer, P. Roztocki, L. R. Cortés, S. Sciara, B. Wetzel, Y. Zhang, A. Cino, S. T. Chu, B. E. Little, *et al.*, On-chip generation of high-dimensional entangled quantum states and their coherent control, Nature **546**, 622 (2017).
[56] H.-H. Lu, J. M. Lukens, N. A. Peters, B. P. Williams, A. M. Weiner, and P. Lougovski, Quantum interference and correlation control of frequency-bin qubits, Optica **5**, 1455 (2018).
[57] G. Maltese, M. I. Amanti, F. Appas, G. Sinnl, A. Lemaître, P. Milman, F. Baboux, and S. Ducci, Generation and symmetry control of quantum frequency combs, npj Quantum Inf **6**, 13 (2020).
[58] N. Fabre, G. Maltese, F. Appas, S. Felicetti, A. Ketterer, A. Keller, T. Coudreau, F. Baboux, M. I. Amanti, S. Ducci, and P. Milman, Generation of a time-frequency grid state with integrated biphoton frequency combs, Phys. Rev. A **102**, 012607 (2020).
[59] H.-H. Lu, M. Liscidini, A. L. Gaeta, A. M. Weiner, and J. M. Lukens, Frequency-bin photonic quantum information, Optica **10**, 1655 (2023).
[60] T. Yamazaki, T. Arizono, T. Kobayashi, R. Ikuta, and T. Yamamoto, Linear optical quantum computation with frequency-comb qubits and passive devices, Phys. Rev. Lett. **130**, 200602 (2023).
[61] R. Trivedi, K. A. Fischer, J. Vučković, and K. Müller, Generation of non-classical light using semiconductor quantum dots, Advanced Quantum Technologies **3**, 1900007 (2020).
[62] O. Gywat, H. J. Krenner, and J. Berezovsky, *Spins in optically active quantum dots: concepts and methods* (John Wiley & Sons, 2010).
[63] F. T. Østfeldt, E. M. González-Ruiz, N. Hauff, Y. Wang, A. D. Wieck, A. Ludwig, R. Schott, L. Midolo, A. S. Sørensen, R. Uppu, *et al.*, On-demand source of dual-rail photon pairs based on chiral interaction in a nanophotonic waveguide, PRX quantum **3**, 020363 (2022).
[64] E. M. González-Ruiz, F. T. Østfeldt, R. Uppu, P. Lodahl, and A. S. Sørensen, Entanglement properties of a quantum-dot biexciton cascade in a chiral nanophotonic waveguide, Physical Review A **108**, 013507 (2023).
[65] P. Lodahl, S. Mahmoodian, and S. Stobbe, Interfacing single photons and single quantum dots with photonic nanostructures, Reviews of Modern Physics **87**, 347 (2015).
[66] H. Ollivier, *Quantum purity and symmetry control of single-photon sources based on semiconductor quantum dots*, Ph.D. thesis, Université Paris-Saclay (2021).
[67] A. Fognini, A. Ahmadi, S. Daley, M. Reimer, and V. Zwiller, Universal fine-structure eraser for quantum dots, Optics express **26**, 24487 (2018).
[68] T. Mano, M. Abbarchi, T. Kuroda, B. McSkimming, A. Ohtake, K. Mitsuishi, and K. Sakoda, Self-assembly of symmetric gaas quantum dots on (111) a substrates: Suppression of fine-structure splitting, Applied physics express **3**, 065203 (2010).
[69] J. Wang, M. Gong, G.-C. Guo, and L. He, Eliminating the fine structure splitting of excitons in self-assembled inas/gaas quantum dots via combined stresses, Applied Physics Letters **101** (2012).
[70] T. Lettner, S. Gyger, K. D. Zeuner, L. Schweickert, S. Steinhauer, C. Reuterskiöld Hedlund, S. Stroj, A. Rastelli, M. Hammar, R. Trotta, *et al.*, Strain-controlled quantum dot fine structure for entangled photon generation at 1550 nm, Nano letters **21**, 10501 (2021).
[71] U. Gaubatz, P. Rudecki, S. Schiemann, and K. Bergmann, Population transfer between molecular vibrational levels by stimulated raman scattering with partially overlapping laser fields. a new concept and experimental results, The Journal of Chemical Physics **92**, 5363 (1990).
[72] B. W. Shore, Picturing stimulated raman adiabatic passage: a stirap tutorial, Advances in Optics and Photonics **9**, 563 (2017).
[73] J. Larson and T. Mavrogordatos, *The Jaynes–Cummings model and its descendants: modern research directions* (IoP Publishing, 2021).
[74] R. Puri and R. Bullough, Quantum electrodynamics of an atom making two-photon transitions in an ideal cavity, Journal of the Optical Society of America B **5**, 2021 (1988).
[75] M. Alexanian and S. K. Bose, Unitary transformation and the dynamics of a three-level atom interacting with two quantized field modes, Physical Review A **52**, 2218 (1995).
[76] Y. Wu, Effective raman theory for a three-level atom in the λ configuration, Physical Review A **54**, 1586 (1996).
[77] C. C. Gerry and J. Eberly, Dynamics of a raman coupled model interacting with two quantized cavity fields, Physical Review A **42**, 6805 (1990).
[78] N. Fabre, *Quantum information in time-frequency continuous variables*, Ph.D. thesis, Université Paris Cité (2020).
[79] A. Kors, J. P. Reithmaier, and M. Benyoucef, Telecom wavelength single quantum dots with very small excitonic fine-structure splitting, Applied Physics Letters **112** (2018).

[80] T. Müller, J. Skiba-Szymanska, A. Krysa, J. Huwer, M. Felle, M. Anderson, R. Stevenson, J. Heffernan, D. A. Ritchie, and A. Shields, A quantum light-emitting diode for the standard telecom window around 1,550 nm, Nature communications **9**, 862 (2018).

[81] Y. Arakawa and M. J. Holmes, Progress in quantum-dot single photon sources for quantum information technologies: A broad spectrum overview, Applied Physics Reviews **7** (2020).

[82] M. Bamba, A. Imamoğlu, I. Carusotto, and C. Ciuti, Origin of strong photon antibunching in weakly nonlinear photonic molecules, Phys. Rev. A **83**, 021802 (2011).

[83] S. Fan, Ş. E. Kocabaş, and J.-T. Shen, Input-output formalism for few-photon transport in one-dimensional nanophotonic waveguides coupled to a qubit, Physical Review A—Atomic, Molecular, and Optical Physics **82**, 063821 (2010).

[84] J. J. Sakurai and J. Napolitano, *Modern quantum mechanics* (Cambridge University Press, 2020).

[85] C. Weedbrook, S. Pirandola, R. García-Patrón, N. J. Cerf, T. C. Ralph, J. H. Shapiro, and S. Lloyd, Gaussian quantum information, Reviews of Modern Physics **84**, 621 (2012).

[86] F. Laudenbach, C. Pacher, C.-H. F. Fung, A. Poppe, M. Peev, B. Schrenk, M. Hentschel, P. Walther, and H. Hübel, Continuous-variable quantum key distribution with gaussian modulation—the theory of practical implementations, Advanced Quantum Technologies **1**, 1800011 (2018).

[87] J. Kettler, M. Paul, F. Olbrich, K. Zeuner, M. Jetter, P. Michler, M. Florian, C. Carmesin, and F. Jahnke, Neutral and charged biexciton-exciton cascade in near-telecom-wavelength quantum dots, Physical Review B **94**, 045303 (2016).

[88] K. D. Zeuner, K. D. Jons, L. Schweickert, C. Reuterskiöld Hedlund, C. Nuñez Lobato, T. Lettner, K. Wang, S. Gyger, E. Scholl, S. Steinhauer, *et al.*, On-demand generation of entangled photon pairs in the telecom c-band with inas quantum dots, ACS photonics **8**, 2337 (2021).

[89] K. Takemoto, M. Takatsu, S. Hirose, N. Yokoyama, Y. Sakuma, T. Usuki, T. Miyazawa, and Y. Arakawa, An optical horn structure for single-photon source using quantum dots at telecommunication wavelength, Journal of applied physics **101** (2007).

[90] J. Belhassen, F. Baboux, Q. Yao, M. Amanti, I. Favero, A. Lemaître, W. Kolthammer, I. Walmsley, and S. Ducci, On-chip iii-v monolithic integration of heralded single photon sources and beamsplitters, Applied Physics Letters **112** (2018).

[91] Y. Yu, S. Liu, C.-M. Lee, P. Michler, S. Reitzenstein, K. Srinivasan, E. Waks, and J. Liu, Telecom-band quantum dot technologies for long-distance quantum networks, Nature nanotechnology **18**, 1389 (2023).

[92] A. N. Craddock, Y. Wang, F. Giraldo, R. Sekelsky, M. Flament, and M. Namazi, High-rate subgigahertz-linewidth bichromatic entanglement source for quantum networking, Phys. Rev. Appl. **21**, 034012 (2024).

[93] T. Müller, J. Skiba-Szymanska, A. Krysa, J. Huwer, M. Felle, M. Anderson, R. Stevenson, J. Heffernan, D. A. Ritchie, and A. Shields, A quantum light-emitting diode for the standard telecom window around 1,550 nm, Nature communications **9**, 862 (2018).

[94] PsiQuantum team, K. Alexander, A. Benyamini, D. Black, D. Bonneau, S. Burgos, B. Burridge, H. Cable, G. Campbell, G. Catalano, A. Ceballos, C.-M. Chang, S. S. Choudhury, C. J. Chung, F. Danesh, T. Dauer, M. Davis, E. Dudley, P. Er-Xuan, J. Fargas, A. Farsi, C. Fenrich, J. Frazer, M. Fukami, Y. Ganesan, G. Gibson, M. Gimeno-Segovia, S. Goeldi, P. Goley, R. Haislmaier, S. Halimi, P. Hansen, S. Hardy, J. Horng, M. House, H. Hu, M. Jadidi, V. Jain, H. Johansson, T. Jones, V. Kamineni, N. Kelez, R. Koustuban, G. Kovall, P. Krogen, N. Kumar, Y. Liang, N. LiCausi, D. Llewellyn, K. Lokovic, M. Lovelady, V. R. Manfrinato, A. Melnichuk, G. Mendoza, B. Moores, S. Mukherjee, J. Munns, F.-X. Musalem, F. Najafi, J. L. O'Brien, J. E. Ortmann, S. Pai, B. Park, H.-T. Peng, N. Penthorn, B. Peterson, G. Peterson, M. Poush, G. J. Pryde, T. Ramprasad, G. Ray, A. V. Rodriguez, B. Roxworthy, T. Rudolph, D. J. Saunders, P. Shadbolt, D. Shah, A. Bahgat Shehata, H. Shin, J. Sinsky, J. Smith, B. Sohn, Y.-I. Sohn, G. Son, M. C. M. M. Souza, C. Sparrow, M. Staffaroni, C. Stavrakas, V. Sukumaran, D. Tamborini, M. G. Thompson, K. Tran, M. Triplett, M. Tung, A. Veitia, A. Vert, M. D. Vidrighin, I. Vorobeichik, P. Weigel, M. Wingert, J. Wooding, and X. Zhou, A manufacturable platform for photonic quantum computing, Nature 10.1038/s41586-025-08820-7 (2025).

[95] S. Parker, S. Bose, and M. B. Plenio, Entanglement quantification and purification in continuous-variable systems, Phys. Rev. A **61**, 032305 (2000).

[96] L. Lamata and J. León, Dealing with entanglement of continuous variables: Schmidt decomposition with discrete sets of orthogonal functions, Journal of Optics B: Quantum and Semiclassical Optics **7**, 224 (2005).

[97] A. Y. Bogdanov, Y. I. Bogdanov, and K. A. Valiev, Schmidt modes and entanglement in continuous-variable quantum systems, Russ Microelectron **35**, 7 (2006).

[98] K. Zielnicki, K. Garay-Palmett, D. Cruz-Delgado, H. Cruz-Ramirez, M. F. O'Boyle, B. Fang, V. O. Lorenz, A. B. U'Ren, and P. G. Kwiat, Joint spectral characterization of photon-pair sources, Journal of Modern Optics **65**, 1141 (2018).

[99] C. Reimer, L. Caspani, M. Clerici, M. Ferrera, M. Kues, M. Peccianti, A. Pasquazi, L. Razzari, B. E. Little, S. T. Chu, *et al.*, Integrated frequency comb source of heralded single photons, Optics express **22**, 6535 (2014).

[100] Z. Xie, T. Zhong, S. Shrestha, X. Xu, J. Liang, Y.-X. Gong, J. C. Bienfang, A. Restelli, J. H. Shapiro, F. N. Wong, *et al.*, Harnessing high-dimensional hyperentanglement through a biphoton frequency comb, Nature Photonics **9**, 536 (2015).

[101] Y.-S. Jang, S. Eom, J. Park, and J. Jin, Programmable spectral shaping for nanometric precision of frequency comb mode-resolved spectral interferometric ranging, Optics & Laser Technology **170**, 110324 (2024).

[102] D. Chao, G. Chang, J. L. Morse, F. X. Kärtner, and E. P. Ippen, Octave-spanning supercontinuum generation for an er-doped fiber laser frequency comb at a 1 ghz repetition rate, in *CLEO/QELS: 2010 Laser Science to Photonic Applications* (IEEE, 2010) pp. 1–2.

[103] D. Rieländer, A. Lenhard, O. J. Farìas, A. Máttar, D. Cavalcanti, M. Mazzera, A. Acín, and H. de Riedmatten, Frequency-bin entanglement of ultra-narrow band non-degenerate photon pairs, Quantum Science and Technology **3**, 014007 (2017).

[104] M. Bock, A. Lenhard, C. Chunnilall, and C. Becher, Highly efficient heralded single-photon source for telecom wavelengths based on a ppln waveguide, Optics express **24**, 23992 (2016).
[105] X. Shi, S. S. Mohanraj, V. Dhyani, A. A. Baiju, S. Wang, J. Sun, L. Zhou, A. Paterova, V. Leong, and D. Zhu, Efficient photon-pair generation in layer-poled lithium niobate nanophotonic waveguides, Light: Science & Applications **13**, 282 (2024).
[106] H. Wang, Q. Zeng, H. Ma, and Z. Yuan, Progress on chip-based spontaneous four-wave mixing quantum light sources, Advanced Devices & Instrumentation **5**, 0032 (2024).
[107] N. Fabre and U. Chabaud, Photonic quantum information processing using the frequency continuous-variable of single photons, arXiv,2402.06962 (2024).
[108] B. Huttner and S. M. Barnett, Quantization of the electromagnetic field in dielectrics, Physical Review A **46**, 4306 (1992).
[109] T. Gruner and D.-G. Welsch, Green-function approach to the radiation-field quantization for homogeneous and inhomogeneous kramers-kronig dielectrics, Physical Review A **53**, 1818 (1996).
[110] H. T. Dung, L. Knöll, and D.-G. Welsch, Three-dimensional quantization of the electromagnetic field in dispersive and absorbing inhomogeneous dielectrics, Physical Review A **57**, 3931 (1998).
[111] H. T. Dung, L. Knöll, and D.-G. Welsch, Intermolecular energy transfer in the presence of dispersing and absorbing media, Physical Review A **65**, 043813 (2002).
[112] H. T. Dung, L. Knöll, and D.-G. Welsch, Resonant dipole-dipole interaction in the presence of dispersing and absorbing surroundings, Physical Review A **66**, 063810 (2002).
[113] M. Wubs, L. Suttorp, and A. Lagendijk, Multiple-scattering approach to interatomic interactions and superradiance in inhomogeneous dielectrics, Physical Review A—Atomic, Molecular, and Optical Physics **70**, 053823 (2004).
[114] P. Yao, V. Manga Rao, and S. Hughes, On-chip single photon sources using planar photonic crystals and single quantum dots, Laser & Photonics Reviews **4**, 499 (2010).
[115] M. C. Teich and B. Saleh, *Fundamentals of photonics*, Vol. 2 (Wiley New Jersey, 2007).
[116] H. Benisty, J.-J. Greffet, and P. Lalanne, *Introduction to nanophotonics* (Oxford university press, 2022).
[117] F. Arntzenius and H. Greaves, Time reversal in classical electromagnetism, The British Journal for the Philosophy of Science (2009).
[118] S. Bravyi, D. P. DiVincenzo, and D. Loss, Schrieffer–wolff transformation for quantum many-body systems, Annals of physics **326**, 2793 (2011).
[119] J. J. G. Ripoll, *Quantum information and quantum optics with superconducting circuits* (Cambridge University Press, 2022).